Dissertation

submitted to the

Combined Faculties for the Natural Sciences and for Mathematics

of the Ruperto-Carola University of Heidelberg, Germany

for the degree of

Doctor of Natural Sciences

presented by

M.Sc. Linda Elisabeth Klauss

born in Dordrecht (the Netherlands)

oral examination date: 23.06.2017

Molecular mechanism of chromosome segregation by the *E. coli* Min system

Dissertation referees:

Prof. Dr. Roland Eils

Prof. Dr. Andres Jaeschke

Acknowledgements

First of all, I want to thank Dr. Barbara Di Ventura for giving me the chance of obtaining my PhD in her lab and the daily supervision. Your endless enthusiasm and curiosity to explore undiscovered sometimes bumpy roads were a motivation to me. Furthermore, I highly appreciated the input that guided me through the process of writing my thesis.

I also would like to thank Prof. Roland Eils, for accepting me as an e*ilslabs* member despite being Dutch (and very good at soccer). I enjoyed the time within this diverse group of people and learned a lot during the scientific retreats, not only regarding science.

Besides Prof. Roland Eils, I would also like to thank the other members of my thesis advisory committee (TAC); Dr. Thomas Hofmann and Prof. Andres Jäschke, I appreciated the input during the TAC meetings.

I am grateful to the (ex) members of the Di Ventura group and the *eilslabs* for the support, for creating such a pleasant atmosphere in the lab and for the scientific discussions and feedback during the weekly group meetings. Thanks to cloning queen Sabine Aschenbrenner, Enoch Antwi, Anna Degen, Joel Beaudouin, Roman Kurilov, Clarissa Liesche, Stefan Kallenberger, Dominik Niopek, Navaneethan Palanisamy, Julia Roensch, Edoardo Romano, Pierre Wehler and Daniel Weis.

Anna Degen, thanks for translating my abstract into German.

Navaneethan Palanisamy, my partner in crime, I am grateful for the big help that you were to me while I was doing my 'final' experiments. I wish you all the best in the future.

A lot of the experiments in this work could not have been realised without the help and input of others. I therefore thank every person that is mentioned in the Contributions section from the bottom of my heart.

To all my peers that became friends, people I met outside the academic world, friends and family members from far away or the Netherlands, you know who you are! Thanks for just being there for me.

Last but not least, I want to express my gratitude especially to my parents and Willem Lijmbach, but also to my brother and sister, for the unconditional support while going through all aspects of the university of life.

Contributions

Yuho Kida, a former student assistant of the Di Ventura lab, designed the primers and cloned the desired mutants of MinD in the pET-28a plasmid.

Prof. Jaeschke allowed access to the Typhoon™ scanner that I used frequently to scan the EMSA gels.

Derek Lau and Thomas Bernhardt provided me with the strains TB28, TB43 and TB115, used for the microscopy experiments to study chromosome segregation, and for the reporter gene assays used to follow up the microarray results.

I performed Microscale Thermophoresis measurements to study DNA-binding of ^{His}MinD and ^{His}MinE at the DKFZ Genomics and Proteomics Core Facility. Frank Schwartz introduced me to the Microscale Thermophoresis device and provided very useful advice wherever needed.

I performed surface plasmon resonance (SPR) experiments in the lab of Prof. Haberkorn. Sabine Weiß shared the tips and tricks for the use of the instrument.

The ChIP-Seq experiments are the results of extensive collaborations. I designed the experiments and carried out the immunoprecipitation to enrich for genomic sequences associated with the His-tagged proteins. David Ibberson (CellNetworks Deep Sequencing Core Facility) prepared the sequencing library and did the actual sequencing. Naveed Ishaque aligned the obtained reads to the reference genome and used the MACS algorithm for the identification of DNA-binding peaks. Roman Kurilov performed the supplementary peak calling analysis using the SICER algorithm. The motif analysis of the first ChIP-Seq dataset was done by Suda Parimala Ravindran and Carl Herrmann. The second ChIP-Seq dataset with the lower expression levels has been completely analyzed by Sebastian Steinhauser while being in the lab of Carl Herrmann.

The DKFZ Genomics and Proteomics Core Facility carried out the microarray experiment to analyze the transcriptome of *E. coli* cells with or without a Min system. After I grew the *E. coli* cells and isolated the RNA, all subsequent steps were done by the Core Facility including the RNA quality control, preparation of the cDNA library and the statistical analysis of the results (Students *t*-test). Tobias Bauer performed the KEGG pathway analysis and additionally analyzed the data with SAM and ROTS statistical analysis.

Navaneethan Palanisamy cloned the following pET-28a constructs ^{His}MBP-MinC^{C}, MinC^{K66A}, MinC^{R133A}, MinC$^{N\text{-}G10D}$ and FtsZ. He additionally purified those proteins in addition to wild type MinC, MinD and MinE. He allowed me to use his proteins stocks for many biochemical experiments which are shown in Results 3.4.4 and 3.4.7-13. The plasmid DNA (mEos3.2) used for the co-sedimentation assays was a kind gift of Sabine Aschenbrenner.

The circular dichroism (CD) experiments with MinC^{N} and MinC^{NG10D} and the size exclusion chromatography run prior to CD analysis, were done by the EMBL Protein Purification and Expression Core Facility.

Abstract

Cell division is one of the most essential processes underlying life. Of importance is certainly the equal partitioning of the genetic material into the two daughter cells termed chromosome segregation. It is still debated if entropic forces alone are sufficient to fulfill this task, or whether additional dedicated protein machineries play an active role in this process.

The *E. coli* Min system, consisting of the proteins MinC, MinD and MinE, is well known for its function in defining mid-cell and directing there the FtsZ-ring, which marks the position of the future division site. The Min system is characterized by a pole-to-pole oscillation, corresponding to a time-averaged bipolar protein distribution. It has been discovered in our lab that MinD is able to directly bind DNA *in vitro* and *in vivo*. This led to the proposal of a Brownian Ratchet-like model for chromosome segregation, in which membrane-bound MinD provides DNA tethering sites and biases the diffusion of the duplicated chromosomes in the direction of the poles. However, the molecular details of this mechanism were still lacking.

Here I used several *in vitro* and *in vivo* assays to understand better how MinD binds to the DNA and to clarify what the role of other proteins, such as MinC, MinE and FtsZ, is.

Specifically, I performed ChIP-Seq to study the genome-wide binding of MinD in cells with and without the endogenous Min system and found that MinD does not associate to specific chromosomal macrodomains. This supports the notion that the Min system assists the segregation of the chromosomal bulk. Furthermore, analysis of the transcriptome revealed that the Min system does not function as a global transcriptional regulator.

Using electrophoretic mobility shift assays (EMSAs) with purified proteins, I established that the MinC-MinD complex has a much higher affinity for DNA than the individual proteins. Lipid vesicles coated with MinC-MinD complexes could tether plasmid DNA to the lipid-associated pellet in co-sedimentation assays. These findings advocate for a refined model in which the "working unit" in chromosome segregation *in vivo* is not MinD alone, but rather the MinC-MinD complex. MinE is able to dissociate the DNA from the MinC-MinD complex, suggesting a role for this protein in the termination of the transient membrane tethering of the DNA by the Min system *in vivo*.

Using rational mutagenesis of MinC and MinD, I could pinpoint several residues that are important for the binding and discovered the critical role of the N-terminal domain of MinC.

To clarify whether the recently reported MinC-MinD co-polymers are needed for DNA-binding, I performed *in vitro* assays mixing wild type MinC with the $MinC^{R133A}$ mutant that allows complex

formation between a MinD dimer and a MinC-MinC^{R133A} heterodimer, but not the formation of the co-polymers. Interestingly, in this case, DNA-binding was reduced by 75%.

Finally, since *in vivo* the Min system interacts with FtsZ for its function in mid-cell placement, I studied whether FtsZ could interfere with DNA-binding by MinC-MinD using *in vitro* assays. I found that the binding is not affected unless FtsZ is present at very high concentrations. These data suggest that the presence of FtsZ in the cell, away from the Z-ring, does not interfere with DNA-binding by the MinC-MinD complex.

Taken together, the data I collected during my doctoral work contributed to our understanding of the molecular mechanism of DNA-binding by the Min system. More comprehensive studies in live cells are required to study this mechanism *in vivo* in more detail. Future work is needed to unambiguously determine the surface of the MinC-MinD complex used for direct DNA-binding.

Zusammenfassung

Zellteilung ist einer der wichtigsten Prozesse des Lebens. Während der Zellteilung ist es essentiell, dass das genetische Material gleichmäßig auf die beiden Tochterzellen aufgeteilt wird. Dieser Vorgang heißt Chromosomensegregation. Unklar ist, ob entropische Kräfte alleine ausreichend sind, diese Aufgabe zu erfüllen, oder ob es bestimmte, proteingesteuerte Mechanismen gibt, die eine aktive Rolle in der Chromosomensegregation spielen.

Das *E. coli* Min System besteht aus den Proteinen MinC, MinD und MinE und bestimmt während der Zellteilung die Zellmitte, wohin es die Teilungsmachinerie dirigiert. Dieser Effekt wird erreicht durch das abgestimmte Oszillieren der drei Min Proteine zwischen den beiden Zellpolen. Dabei ist die Aufenthaltswahrscheinlichkeit in der Zellmitte am geringsten, wodurch FtsZ an die Membran binden kann und die Bildung des Septums initiiert. Zusätzlich kann MinD direkt an die DNA binden, was in unserem Labor *in vivo* und *in vitro* gezeigt wurde. Daher schlagen wir das Brownsche Ratsche Model für die Chromosomensegregation vor. In diesem Model dient membrangebundenes MinD als DNA Bindestelle und beeinflusst die Diffusion der duplizierten Chromosomen in Richtung der Zellpole. Allerdings sind die Details dieses Mechanismus auf der molekularen Ebene noch ungeklärt.

In der vorliegenden Arbeit wurde mittels *in vitro* und *in vivo* Analysen untersucht, wie MinD an die DNA bindet und was die Aufgaben der anderen Proteine wie MinC, MinE und FtsZ sind. Im Einzelnen wurde ChIP-Seq in Zellen mit und ohne endogenem Min System angewandt, um genomweit Bindestellen von MinD zu identifizieren. Dabei wurde festgestellt, dass MinD nicht an eine bestimmte Macrodomäne im Genom bindet. Diese Feststellung stützt die Theorie, dass das Min System unspezifisch zur Teilung des gesamten Genoms beiträgt. Außerdem konnte durch die Analyse des Transkriptoms gezeigt werden, dass das Min System nicht als globaler Regulator der Transkription agiert.

Durch elektrophoretische Mobilitäts-Shiftassays (EMSAs) mit aufgereinigten Proteinen konnte nachgewiesen werden, dass der MinC-MinD Komplex eine weitaus größere Affinität zu DNA hat als die einzelnen Proteine an sich. Auch konnten Lipidvesikel, die mit MinC-MinD Komplexen beschichtet sind, Plasmid-DNA zusammen mit dem Lipid assoziierten Pellet sedimentieren. Anhand dieser Ergebnisse wird deutlich, dass die „Arbeitseinheit“ in der Chromosomensegregation *in vivo* aus dem MinC-MinD Komplex besteht und nicht wie bisher angenommen aus MinD alleine. MinE wiederum kann die DNA vom MinC-MinD Komplex entfernen, wodurch MinE vermutlich die Auflösung der transienten Bindung der DNA an die Zellmembran durch das Min System *in vivo* übernimmt.

Durch rationale Mutagenese von MinC und MinD konnte ich einige Aminosäuren bestimmen, die eine wichtige Rolle in der DNA Bindung spielen. Außerdem konnte die entscheidende Rolle der N-terminalen Domäne von MinC aufgedeckt werden.

Um aufzuklären, ob die kürzlich beschriebenen MinC-MinD Kopolymere gebraucht werden um die DNA zu binden, haben wir *in vitro* wild-typ MinC mit der $MinC^{R133A}$ Mutante gemischt, sodass Komplexbildung zwischen einem MinD Dimer und einem MinC-$MinC^{R133A}$ Heterodimer möglich war, nicht jedoch die Ausbildung von Kopolymeren. Interessanterweise wurde dadurch die DNA Bindung um 75% reduziert.

Abschließend untersuchten wir, ob FtsZ die DNA Bindung durch MinC-MinD *in vitro* beeinträchtigen kann, da es *in vivo* mit dem Min System interagiert um die Zellmitte festzulegen. Die Untersuchungsergebnisse zeigen, dass die DNA Bindung nicht beeinträchtigt wird, außer FtsZ liegt in hohen Konzentrationen vor. Diese Daten weisen darauf hin, dass zelluläres FtsZ die DNA Bindung des MinC-MinD Komplex nicht behindert.

Zusammenfassend tragen die während meiner Doktorarbeit gesammelten Erkenntnisse zum Verständnis der molekularen Mechanismen der DNA Bindung durch das Min System bei. Weitere Experimente waeren sinnvoll, um die DNA-bindende Oberfläche des MinC-MinD Komplexes eindeutig zu bestimmen. Detailliertere Studien an lebenden Zellen waeren erforderlich, um den Einfluss des Min-Systems auf die Chromosomensegregation *in vivo* zu erforschen.

Index

1 Introduction

Cell division is one of the most important processes underlying life. The basic rules are the same for every organism, regardless of cellular architecture. To split into two (equally sized) viable daughter cells, the cell must coordinate the place of the division site accordingly. Since *E. coli* is a rod-shaped bacterium, a division that yields two equally sized daughter cells is "simply" accomplished by placing the division machinery exactly in the cell middle. The genetic material should be replicated and evenly distributed among the progeny, in such a way that each cell half contains one full chromosome, a process called chromosome segregation.

1.1 *E. coli* cell cycle, replication and division

The bacterial cell cycle is divided in three stages that are executed one after the other in slow growing cells (Figure 1). The B period is a waiting period right after cell birth preceding initiation of replication. Chromosome replication occurs in the so-called C period, defined as the time needed to complete one replication round. Replication of the circular chromosome is initiated at the origin of replication (Ori) and proceeds bidirectionally along the left and right arms of the circular chromosome. The terminus (Ter) is the endpoint of replication.

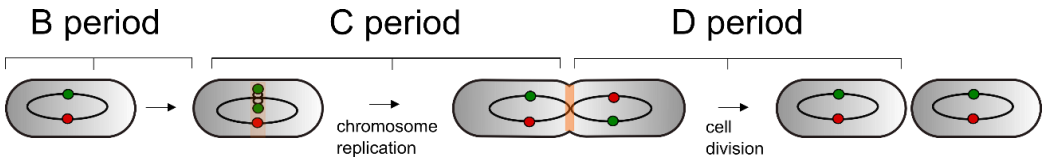

Figure 1| Schematic representation of the *E. coli cell* cycle. The chromosome is depicted as a circle with the Ori marked in green and the Ter in red. The division plane marked by the FtsZ ring is indicated with an orange plane. This image is based on (Wang and Levin 2009).

In nutrient rich conditions, the generation of biomass is faster than the replication (and division) period. High growth rates are maintained by allowing multiple replication events on one chromosome, so called multifork replication (Figure 2). Therefore, finished copies of the chromosomes must be segregated while replication is still ongoing. The principles and mechanisms underlying chromosome segregation are still highly debated and will be discussed later in the introduction. The division (D) period is characterized by the complete closure of the septum, dividing the mother cell into two daughter cells (Wang & Levin 2009).

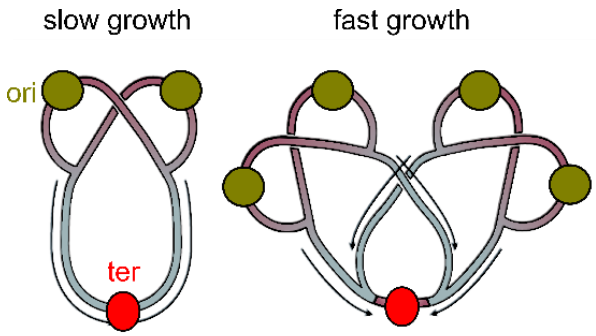

Figure 2| Chromosome replication during slow and fast growth. During slow growth, the chromosome is replicated once per cell cycle leading to the presence of two Ori copies versus one Ter. Cells undergoing rapid growth (with overlapping C and D periods) undergo multiple replications events simultaneously, which described as multifork replication. In these cells, the Ori can be present in a multiple of 2. The direction in which replication proceeds is indicated with arrows. Adapted from (Wang and Levin 2009).

Placement of the septum is coordinated by FtsZ, a conserved GTPase that shares structural similarity with eukaryotic tubulin (Erickson 1995; De Pereda et al. 1996). FtsZ forms a ring (Z-ring) in the cell middle which is anchored to the cell membrane by its protein partners ZipA and FtsA (Bi & Lutkenhaus, 1991; Wang et al. 1997).

In the GTP-bound state, FtsZ forms polar filaments which *in vitro* vary highly in size and stability depending on the buffer conditions (Figure 3A). These protofilaments can interact laterally with each other and have been shown to assemble in a variety of higher order structures including sheets, rings, tubules and bundles (Bramhill & Thompson 1994; Erickson et al. 1996; Rivas et al. 2000; Ahijado-Guzmán et al. 2013). The most recent mechanism that describes the dynamic nature of FtsZ assembly is shown in Figure 3B (Arumugam, Petrašek & Schwille 2014). FtsZ-GTP attaches to the polymeric structure with rate k_a. After binding, the GTP is hydrolyzed with rate k_h, followed by dissociation (k_D).

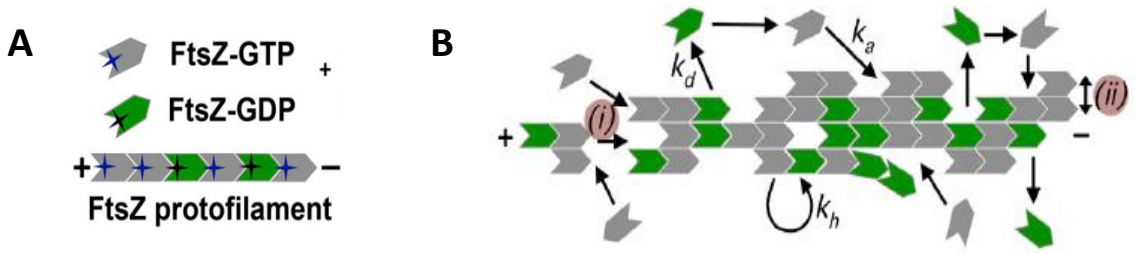

Figure 3| Schematic representation of structures formed by FtsZ. A | In the presence of GTP, FtsZ assembles into protofilaments with the individual proteins arranged in a head to tail manner. **B|** These protofilaments (i) can assemble into sheets via lateral interactions (ii). The intrinsic GTPase activity of FtsZ results in hydrolysis of GTP to GDP (k_h) and subsequent dissociation (k_d). Association of FtsZ-GTP (k_a) occurs simultaneously, making the FtsZ bundles dynamic structures. Figure adapted from (Arumugam, Petrašek & Schwille 2014).

The exchange of FtsZ proteins between the cytoplasm and the ring occurs on a timescale of seconds, making the Z-ring a very dynamic structure (Stricker et al. 2002; Anderson, Gueiros-Filho & Erickson 2004). Photoactivated Localization Microscopy (PALM) revealed that the ring structure *in vivo* is a loose bundle of protofilaments that overlap randomly in all directions at midcell (Fu et al. 2010).

In an early stage of the cell cycle, FtsZ recruits proteins partners that mainly stabilize the ring (Rico, Krupka & Vicente 2013). A plethora of proteins is recruited subsequently which leads to the formation of a multiprotein complex: the divisome. This structure reaches from the cytoplasm through the plasma membrane and is in contact with the outer membrane as well. (reviewed in: Aarsman et al. 2005; Ortiz, Natale, Cueto & Vicente 2015). The mature divisome contains enzymes that digest or remodel the stiff peptidoglycan cell wall. This allows constriction of the FtsZ ring simultaneously with the invagination of the membranes and cell wall (Egan & Vollmer 2013). In the final stage of cell division, components of the septum can aid to properly segregate the chromosomal terminus region (for more details, see 1.4.3, Ter MD organization and segregation).

1.2 The Min system

In the absence of FtsZ regulators, cell division is not restricted to the cell middle and polar divisions lead to the production of small a-nucleate cells. In the 60's, the observation of this minicell phenotype led to the description of a mechanism that prevents polar divisions and guides the divisome to the cell middle (Adler, 1967). The system responsible for mid-cell placement of the FtsZ ring is encoded by the *minB* operon and is called the Min system. The individual players MinC, MinD and MinE were only described in more detail 20 years later (De Boer, Crossley & Rothfield 1992; Raskin & de Boer 1997; Hu & Lutkenhaus 1999).

MinD forms ATP-dependent dimers that are capable of stably binding to the membrane by insertion of a membrane targeting sequence (MTS) (Szeto et al. 2003; Hu & Lutkenhaus 2003). Binding of MinD to the membrane is cooperative, most likely due to a change of membrane properties as a result of the insertion of this amphipathic helix (Shirley Mazor et al. 2008; Renner & Weibel 2012). MinE is recruited by membrane-bound MinD and binds itself to the membrane through a cryptic membrane targeting helix whose exposure is triggered by the binding to MinD (Hsieh et al. 2010). Subsequently, MinE stimulates the ATPase activity of MinD, which leads to the dissociation of te MinD dimer and to the subsequent release of MinD from the membrane (Hu & Lutkenhaus 2001; Lutkenhaus & Sundaramoorthy 2003). After the exchange of ADP for ATP in the cytoplasm, MinD rebinds to the membrane at locations where the MinE concentrations are the lowest. This reaction-diffusion mechanism leads to oscillations of MinD/MinE from one cell pole to the other (Figure 4, A and B) (Hu & Lutkenhaus 1999; Raskin & de Boer 1999). Over the years, many mathematical models have been

used to explain the behavior of the Min system and it self-organizational properties (Kruse, Howard & Margolin 2007; Loose et al. 2011; Di Ventura & Sourjik 2011).

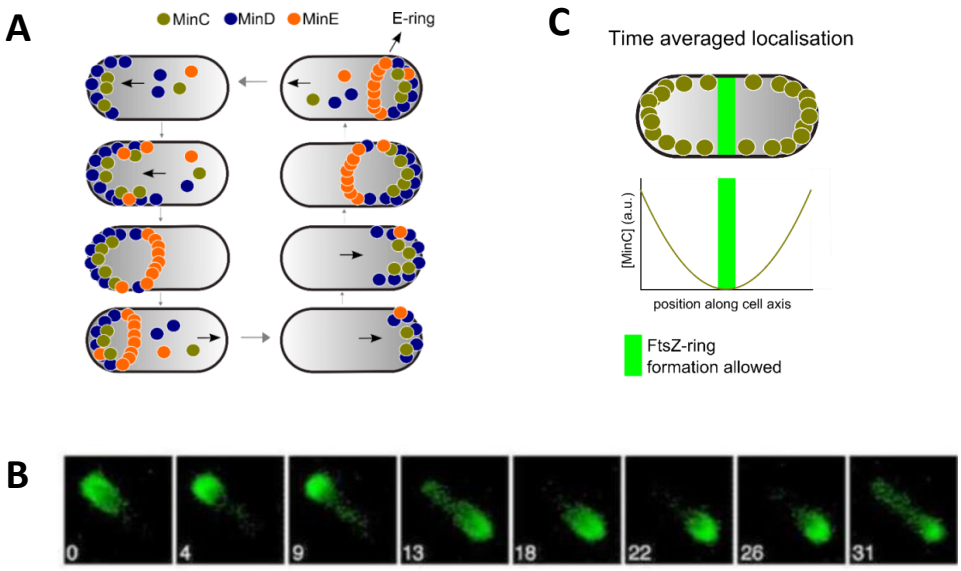

Figure 4|Mid-cell determination by the oscillating *E. coli* Min system. **A|** MinD forms stable dimers on the membrane in the ATP state and recruits MinC there. The topological specificity factor MinE assembles into a ring structure (E-ring) that competes away MinC. Then, it stimulates the intrinsic ATPase activity of MinD which results in dissociation of the MinD dimer and subsequent membrane release. MinD rebinding is favoured at places where the MinE concentration is low, resulting in a pole to pole oscillation. The direction in which the Min proteins oscillate is indicated with a black arrow. Modified from (Rothfield, Taghbalout, and Shih 2005). **B|** Time-lapse microscopy of GFP-MinD expressed in *E. coli.* The time in seconds is indicated in each image frame, and the characteristic pole to pole oscillation is clearly visible. Adapted from (Raskin and de Boer 1999a).**C|** Averaged over time, the Min proteins are enriched at the poles and depleted in the cell middle. This distribution allows the Z-ring to assemble in the cell middle, but not at the poles.

Averaged over time, the MinD protein distribution displays maxima at the poles and a minimum in the cell middle (Figure 4C). MinC binds to MinD and therefore follows this distribution and blocks polar divisions by a direct interaction with FtsZ (Bi & Lutkenhaus 1990; Hu et al. 1999). This allows the Z-ring to form only at mid-cell where the MinC concentration is minimal (De Boer, Crossley & Rothfield 1992; Hu & Lutkenhaus 1999; Raskin & De Boer 1999). The individual Min proteins and their role in the selection of the division site have been extensively studied over the years. The function of the Min system in chromosome segregation is less well-characterised and will be discussed in Introduction, 1.7.

1.2.1 MinC

MinC forms a tight dimer and is a potent inhibitor of FtsZ polymerization. However, this depends highly on the presence of MinD. In the absence of the latter, a 25-50 times higher cellular concentration of MinC is needed to antagonize FtsZ efficiently (De Boer, Crossley & Rothfield 1992). MinC is composed of two functional domains, a N-terminal domain $MinC^{1-115}$ ($MinC^{N}$) and a C-terminal domain $MinC^{116-232}$ ($MinC^{C}$) which are connected by an unstructured linker allowing flexibility in the orientation of $MinC^{N}$ (Hu & Lutkenhaus 2000; Cordell, Anderson & Löwe 2001).

$MinC^{C}$ contains a dimerization domain and interacts directly with MinD (Szeto, Rowland & King 2001). Mutagenic screens showed that residues R133 and S134 are essential for the interaction with MinD. Both of these residues are located in the RSGQ motif, which is highly conserved in MinC from different bacterial species (Zhou & Lutkenhaus 2005). When in complex with MinD, $MinC^{C}$ has a weak interaction with the C-terminal tail of FtsZ (Pazos et al. 2014). This promiscuous part of FtsZ also contains the interaction sites for its membrane anchors FtsA and ZipA (Shiomi and Margolin 2007; Shen & Lutkenhaus 2009; Okuno et al. 2009). The mutant $MinC^{R172A}$ lost this interaction with FtsZ, and is therefore less efficient in blocking the Z-ring (Zhou and J. Lutkenhaus 2005).

The N-terminal domain is also dimeric due to a so called domain swap (Hu & Lutkenhaus 2000). The first beta-strand of each monomer belongs to a beta-sheet located on the other monomer which promotes dimer formation (An et al. 2013). The N-terminal domain is a stronger FtsZ antagonist. It binds to the - end of a the polar FtsZ-filament, after GTP is being hydrolysed into GDP. There it prevents assembly of new FtsZ-GTP, without affecting the GTPase activity (Shen & Lutkenhaus 2010). The mutant $MinC^{G10D}$ has a reduced interaction with FtsZ and causes therefore a minicell phenotype (Labie, Bouche & Bouche 1990; Z Hu et al. 1999).

MinC and MinD were recently shown to form copolymers *in vitro* (Figure 10) (Ghosal et al. 2014; Conti, Viola & Camberg 2015). It was proposed that this could be needed *in vivo* for more efficient disruption of FtsZ filament formation, due to the higher binding avidity provided by such a MinC-MinD co-polymer. However, mutants of MinC and MinD that could interact with each other on only one side of their dimeric interface were capable of proper Z-ring placement (Park, Du & Lutkenhaus 2015). This would argue that the copolymers are not needed per se to perform this specific task.

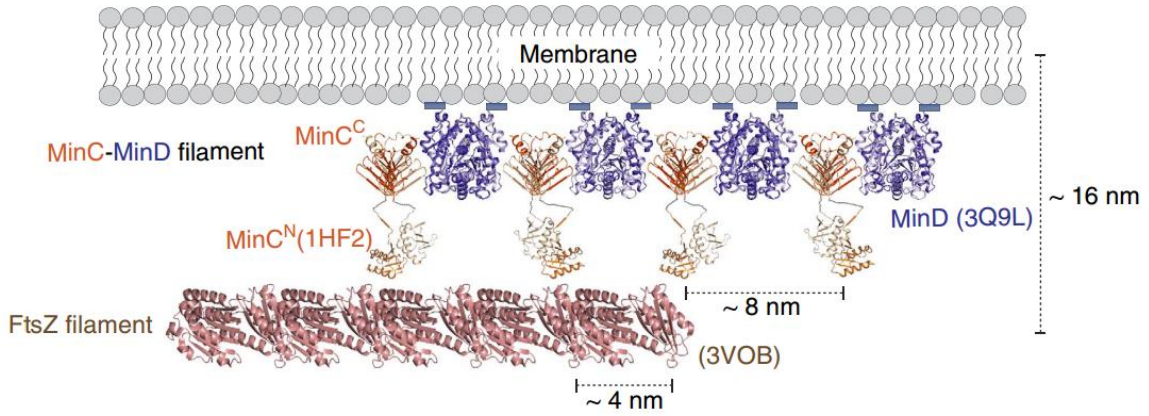

Figure 5| Structural model of membrane-bound MinC-MinD copolymers interacting with a FtsZ protofilament. Taken from (Ghosal et al. 2014). Dimeric crystal structure of $MinD^{D40A\Delta10}$ (PDB: 3Q9L, *E. Coli*), MinC (PDB:1HF2, *T. maritima)* and FtsZ (PDB:3VOB, *S. aureus*).

1.2.2 MinE

MinE is with 88 amino acids the smallest Min protein and is responsible for the proper localization of MinD and indirectly of MinC (de Boer et al. 1989; Pichoff et al. 1995). Expression of $MinE^{1-31}$ (α-CD domain) is sufficient to abrogate the division block induced by MinC-MinD complexes, but is not able to complement a minicell phenotype (Zhao, de Boer & Rothfield 1995). Upon binding MinD, a cryptic membrane targeting sequence (MTS) is released from the hydrophobic core of the protein (Hsieh et al. 2010). Positive residues surrounding this region enhance membrane binding, but are also involved in probing the MinD binding surface to prepare for binding. (Zheng et al. 2014). In solution, the MinD binding interface is completely buried in a six-stranded β-sheet, covered by the N-terminal helix. Binding of MinD results in release of the amphipathic helix and a formation of 4 α-helixes that mirror the binding surface of MinD (Park et al. 2012). Introduction of mutations like in $MinE^{L22D}$, $MinE^{I25V}$ or the truncated $MinE^{1-32}$ leads to constitutive membrane localization of MinE (Hsieh et al., 2010; Zheng et al., 2014).

The C-terminal domain of MinE (amino acid 32-88) is referred to as the topological specificity domain (de Boer et al. 1989). It contains an oligomerization domain and is essential for the formation of the E-ring. This is a dynamic ring (Figure 4A) which is independent of FtsZ and needed for proper septum placement. The basis for this ring formation is first the recruitment of MinE to membrane-bound MinD (Raskin & de Boer, 1997) followed by oligomerization of membrane-bound MinE. Self-interaction of the αCD domain is essential for the formation of this higher order structure (Zheng et al. 2014).

1.2.3 MinD

MinD belongs to the deviant Walker type A ATPases, a protein family that contains functionally diverse members including ParF and the partitioning protein Soj from *B. subtilus* (Lutkenhaus & Sundaramoorthy 2003). In the presence of ATP, a symmetric dimer is formed that interacts with MinC and MinE using a binding surface that comprises the dimeric interface (Wu et al., 2011). It became clear from early studies that MinE and MinC compete for overlapping binding surfaces on MinD. Mutations in helix 7 or 8 of MinD affected the binding to either one or both of its binding partners (Ma, King & Rothfield 2003; H Zhou et al. 2005). A comparison of the crystal structures of MinD in complex with $MinE^{12-31}$ (Park et al. 2011) and MinD in complex with $MinC^{C}$ (Ghosal et al. 2014) supported those early findings.

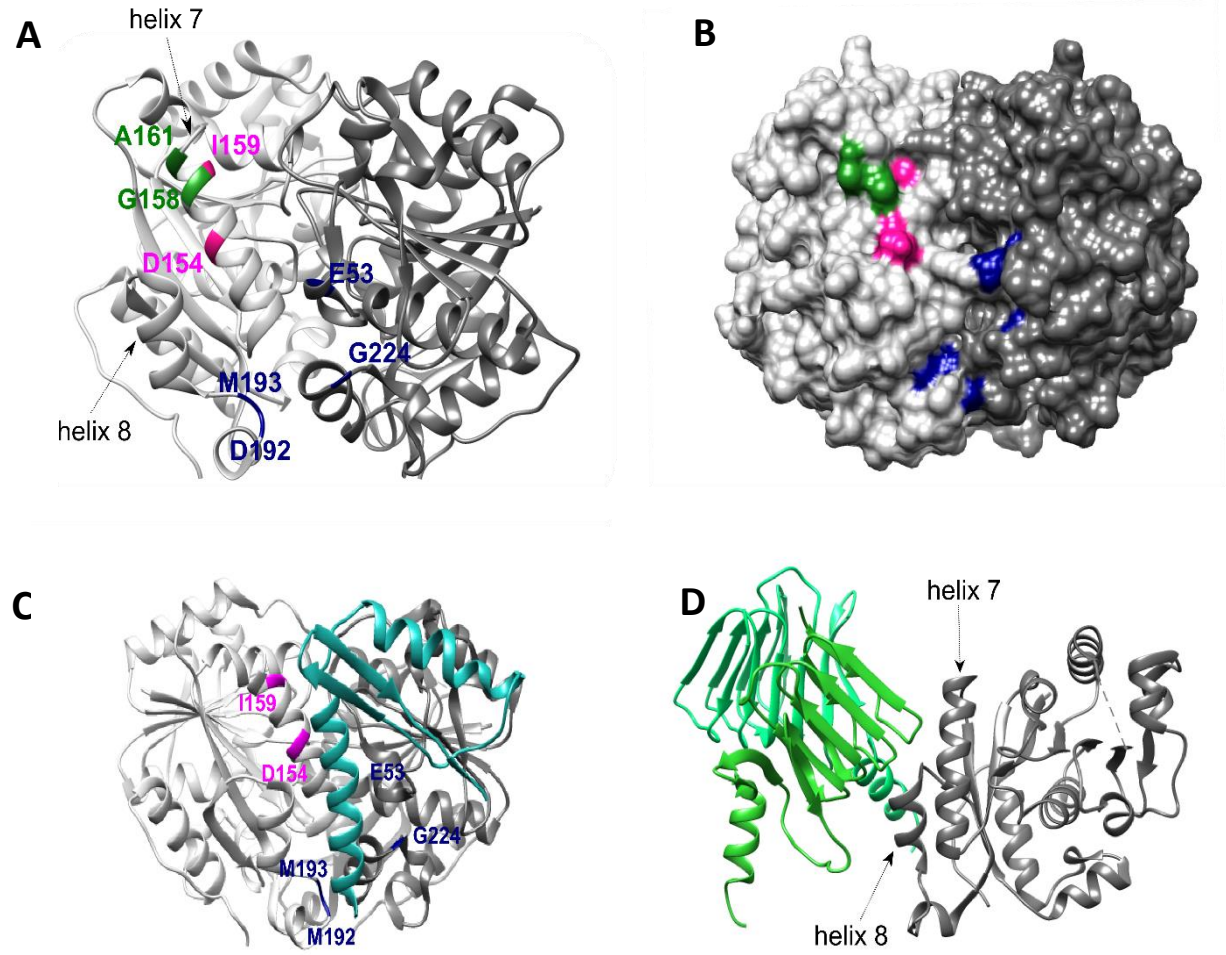

Figure 6| MinE and MinC binding regions overlap on the MinD dimer. A| Ribbon structure of dimeric $MinD^{D40A\Delta10}$ (PDB: 3Q9L, Wu et al., 2011). Residues involved in binding to protein partners are shown in blue (MinE), green (MinC) and magenta (MinE and MinC). Individual MinD monomers are colored light and dark grey respectively. The figure was constructed using Chimera. **B|** Surface view of the same structure as depicted in A. **C|** Dimeric $MinD^{D40A\Delta10}$ in complex with $MinE^{12-88\ (I24N)}$ (cyan), PDB: 3R9J. **D|** $MinD^{D40A\Delta10}$ (monomer visualised) in complex with dimeric $MinC^{C}$ (green), both proteins from *Aquifex Aeolicus* PDB:4V02. (Ghosal et al. 2014).

MinD contains a MTS that is formed by the last ten C-terminal amino acids. This amphipathic helix interacts with the membrane via insertion of hydrophobic residues into the lipid bilayer (Szeto et al. 2003; Hu & Lutkenhaus, 2003). This interaction is so weak, that MinD is only membrane associated dimeric state. Removal of the MTS ($MinD^{\Delta 10}$) leads to a more soluble version of the protein. Membrane association of this mutant is obviously strongly reduced, but binding to MinC (and $MinE^{1-31}$) is still intact, indicating that the protein is properly folded (Taghbalout, Ma & Rothfield 2006). Alteration of the residues involved in ATP binding, produces mutants that fail to self-interact (K11, K16, D38, D120, S121) (Zhou et al. 2005), or are not sensitive for the stimulation of the ATPase activity by MinE (D40 and N45) (Hayashi, Oyama, & Morikawa, 2001; Zhou & Lutkenhaus 2004; Zhou et al. 2005)

1.3 Other regulators of Z ring formation

A random screen for FtsZ regulators in a Min system deficient *E. coli* strain (*ΔminB*), led to the discovery of another negative regulator: SlmA (Synthetic lethal without Min) (Bernhardt and De Boer 2005). This protein prevents Z-ring placement in regions of the cell that contain chromosomal DNA,by binding to the nucleoid and disrupting FtsZ filamentation simultaneously (Tonthat et al. 2011). SlmA-binding sites are scattered over the genome, except for a region spanning the chromosomal terminus (Tonthat et al. 2011). Since this is the last chromosomal region to be segregated, this mechanism already allows onset of septum formation before chromosome segregation is finished.

Together, the Min system and SlmA ensure a narrow range where the Z-ring can assemble. It was observed that the septum still has a bias towards formation at mid-cell, even in the absence of the above-mentioned regulators (Bailey et al. 2014). This is due to a direct physical linkage between the chromosomal Ter region (where the MatP protein binds) and the divisome (via ZapA/ZapB) (Espéli et al. 2012). Since the Ter region resides at mid-cell for a major part of the cell cycle, this Ter-linkage is a positive regulator of Z-ring placement. The redundancy in the mechanisms to place the Z-ring at mid-cell ensures its proper placement under a variety of growth conditions.

1.4 The bacterial chromosome

When bacteria and their even smaller nucleoids are studied with conventional fluorescence microscopy, only the chromosomal bulk is visible. Possible smaller structures are not detectable due to the resolution limit of optical diffraction. Therefore, the description of the nucleoid as an irregularly shaped, cloud-like nuclear body in 1937 did not change drastically until the first electron microscopes came into use. This allowed studying the bacterial nucleoid in much greater detail. Electron micrographs of an isolated *E. coli* nucleoid showed a dense scaffold with supercoiled loops extending from it (Kavenoff & Ryder 1976). This was the basis for the bottlebrush model shown in Figure 7.

Recent advances in the understanding of nucleoid organization are closely related to technological developments. Labeling of specific chromosomal loci using fluorescent fusion proteins and their specific binding sites, gave insight in the location of chromosomal regions during the cell cycle in real time (Wang, Possoz & Sherratt 2005; Espeli, Mercier & Boccard 2008; Cass et al. 2016). With next-generation sequencing, whole genomes could be analyzed for the occurrence of centromeric-like sites or other regulatory sequences (Livny, Yamaichi, & Waldor 2007; Mercier et al. 2008; Tonthat et al. 2011). High resolution microscopy methods like STORM allowed a detailed look at the chromosome and nucleoid-associated proteins in live cells (Spahn, Endesfelder, and Heilemann 2014). Furthermore, the genome-wide binding profiles of these proteins could be deduced using ChIP-Seq (Kahramanoglou et al. 2011; Prieto et al. 2012).

The nucleoid is a highly-organized structure that must be dynamic at the same time to allow chromosome replication, segregation and transcription to occur simultaneously (Wang et al. 2011; Youngren et al. 2014). The co-occurrence of these events makes it difficult to pinpoint the exact function of a single protein, since defects in chromosome organization often lead to problems with segregation. The forces and proteins that work on the nucleoid to form and maintain its shape are explained in the next sections.

1.4.1 Supercoiling and topological domains

The bacterial genome must be compacted a thousand-fold in order to fit within the confinement of the cell. Supercoiling contributes to such compaction. Topoisomerases can release the strain from negative supercoils by introducing DNA-breaks which allow the loose ends to unwind (Wang 2002; Koster et al. 2010). Gyrases can relax positive supercoils or introduce negative supercoils in relaxed DNA (Liu & Wang 1987; Massé & Drolet 1999; reviewed by Vos et al. 2011).

If supercoils were not constrained in any way, they could be transmitted along the entire chromosome. A break in the DNA would result in relaxation of the whole genome. The organization of the chromosome in smaller micro-domains prevents this from happening. In *E. coli*, 10 kb-sized loops were identified, that acted as isolated domains, independently of each other (Sinden & Pettijohn 1981; Postow et al. 2004). The boundaries of these looped microdomains are not fixed, but randomly distributed, highlighting the dynamic nature of the nucleoid. Stabilization of the observed domains is in the hand of a

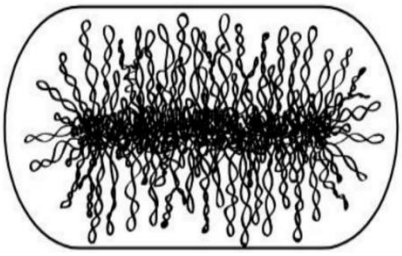

Figure 7| Bottlebrush model for chromosome organization in *E. coli*. Schematic representation of an *E. coli* cell with a chromosome that consists of supercoiled loops extending from a denser nucleoid core. Adapted from (Wang, Montero Llopis, and Rudner 2013).

variety of factors, such as histone-like proteins and structural maintenance of chromosome complexes (Rybenkov et al. 2014). Transcription and translation are also involved (Deng, Stein & Higgins 2005).

1.4.2 Chromosomal macrodomains

Larger chromosomal macrodomains (MDs) of roughly 1 MB in size were described by (Niki, Yamaichi, & Hiraga 2000) (Figure 7A). The Ori MD and the Ter MD are the genomic regions that span the chromosomal Ori and Ter regions, respectively. Loci within each domain cluster together at specific cellular locations in a cell cycle-dependent way. These domains, and an additional Left and Right MD were identified by observing an increased recombination frequency at phage lambda *att* sites, implying that these sites were spatially close (Valens et al. 2004). Except for the Ter MD, it is not known exactly what is responsible for the organization of these domains (Dame, Kalmykowa & Grainger 2011; Messerschmidt & Waldminghaus 2014).

It is thought that correct Ori MD placement and segregation direct and guide the proper segregation of the chromosomal portions that are replicated later. Depending on the growth conditions, the localization pattern of the MDs differ (Figure 8B, reviewed by Wang & Rudner 2014). In slow growing *E. coli* cells, the beginning of the cell cycle is characterized by the Ter and Ori MD being buried within the nucleoid at mid-cell while the chromosome arms are at the periphery. This way, the right and left arms of the chromosome are located in the right and left halves of the cell, respectively (Nielsen et al. 2006; Wang et al. 2006; Woldringh et al. 2015). After being replicated, the Ori MDs remain sequestered at mid-cell for a while, followed by abrupt localization to the ¼ and ¾ positions along the long axis of the cell (Figure 8B). It is not known whether a cellular landmark exists that guides the Ori MDs to the ¼ and ¾ positions. The Ter MD remains in the cell middle and segregates last (Hiraga 2000; Joshi et al. 2011).

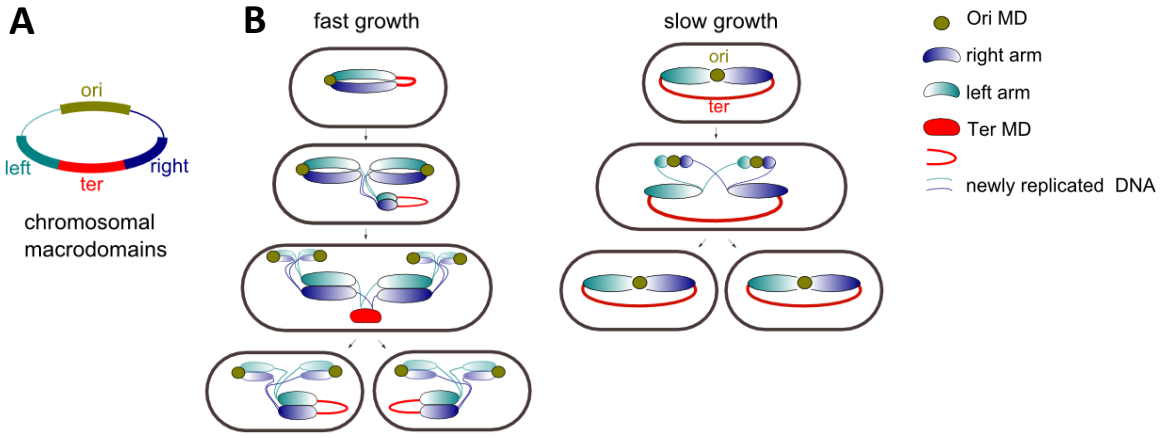

Figure 8| Cell cycle-dependent positions of chromosomal macrodomains. **A|** The *E. coli* genome (4.6 Mb) is organized in 4 macrodomains each of 0.8-1 MB in size and two less-well-structured regions. **B|** In fast growing cells that have to cope with multiple replication cycles going on simultaneously, the Ori and Ter MDs are positioned at the beginning of the cell cycle at opposite poles, in a longitudinal arrangement. After replication of more than half of the chromosome, the Ter MD moves to the cell middle. The Ter MD is shown either in a stretched conformation (red line) or compacted (red ellipse). In slow growing cells, in which only one round of replication occurs per cell cycle, the Ori and Ter MD are located at mid-cell at the beginning of the cell cycle, while the chromosomal left and right arms each occupy a different cell half. Image based on (Wang, Montero Llopis, and Rudner 2013).

Fast growing cells have a different arrangement of the domains. At the beginning of the cell cycle, the Ori MD is located close to one cell pole, whereas the Ter MD is close to the other pole. Before replication, the Ori MD migrates to the cell middle, and newly replicated Oris are extruded towards the cell poles. The not-yet-replicating Ter MD translocates to the cell middle and segregates at last after being replicated (Wang and Rudner 2014; Youngren et al. 2014). The next section provides more details about organization and segregation of the Ori and Ter MD. Ter MD will be described first since the players important for its organization are known.

1.4.3 Ter MD organization and segregation

With a bioinformatic screen, a 13 bp long motif *(matS*) was found to be present 23 times, exclusively in the Ter MD (Mercier et al. 2008). Those *matS* sites recruit the protein MatP, which compacts the nucleoid locally by bridging distant sites. MatP also interacts with the divisome component ZapB, which is associated with the divisome via ZapA. This interaction keeps the Ter MD in close proximity to the future division site, already prior to replication of the Ter MD. This physical coupling between the Ter MD and the division machinery has been called Ter-linkage (Thiel et al. 2012; Männik & Bailey 2015). Absence of MatP makes the Ter MD less structured, more dynamic and causes an early onset of segregation (Mercier et al. 2008).

Another interaction between the divisome and the Ter MD occurs via FtsK (Corre & Louarn 2005; Deghorain et al. 2011). This septum-associated DNA translocase binds to specific DNA sequence motifs (FtsK Orienting Polar Sequences) that are oriented towards the binding site for XerCD (called *dif* site),

a site-specific recombinase that removes the links between sister chromatids thereby resolving chromosome dimers (Liu, Draper & Donachie 1998). Only in a minority of cell division events, chromosomes are still entangled at this stage of cell division (Blakely et al. 1991).

1.4.4 Ori MD organization and segregation

Even though the localization of the Ori MD during the cell cycle has been studied under many different growing conditions, the mechanism(s) at play is/are still unclear. Factors that organize and guide the movement of this chromosomal MD in *E. coli* are highly speculative and will be described here below.

Many bacteria possess a spindle-like apparatus that is responsible for directing the duplicated Ori MDs towards opposite cell poles. These partitioning (Par) systems were originally discovered for their role in partitioning of low copy number plasmids and comprise a centromeric site and two proteins; ParA and ParB (Bignell & Thomas 2001). ParB binds specifically to this centromeric-like site and spreads from there to adjacent regions (Schumacher & Funnell 2005; Funnell 2016). ParA, a Walker-type ATPase, is usually anchored to the cell pole via adapter proteins and fuels the polar movement of the nucleoprotein complex via interactions with ParB (Hayes & Barillà 2006). The most likely mechanism at play is a Brownian Ratchet-like mechanism (Szardenings et al. 2011; Vecchiarelli et al. 2012; Le Gall et al. 2016).

A chromosomally encoded Par system was experimentally confirmed in many bacteria including *Bacillus subtilis* (Lee et al. 2003; Lee & Grossman 2006), *Vibrio cholerae* (Fogel & Waldor 2006; Saint-Dic et al. 2006), *Caulobacter crescentus* (Ptacin et al. 2010) *and Myxococcus xanthus* (Iniesta 2014). In the latter two, a knock out of this Par system renders the cells not viable. This is however not only due to defects in chromosome segregation, but also due to additional functions like regulation of transcription (Baek, Rajagopala & Chattoraj, 2014). A bioinformatic screen over many bacterial genomes was performed to identify chromosomal Par systems by searching for genomic *parS* sites. 70% of all bacterial species sequenced so far (both gram positive and negative) carried such a site in, or near, the Ori MD (Livny, Yamaichi & Waldor 2007).

In *E. coli* and other enterobacteria, a centromeric site was not found in that screen (Jonathan Livny et al. 2007). A non-related site *migS* was found in an experimental screen. *MigS* seemed to be involved in the bi-polar positioning of duplicated Ori MDs to the ¼ and ¾ quarter position of the cell (Yamaichi & Niki 2004; Fekete & Chattoraj 2005). However, the effects were rather small and could not be confirmed by others (Wang & Sherratt 2010).

It is likely that *E. coli* evolved an alternative strategy for organizing and guiding the Ori MD during segregation, to compensate for the loss of a *parABS* system.

SeqA was originally discovered for its task in preventing over-initiation of replication in fast growing cells (Lu et al. 1994). It co-localizes with the Ori MD for a major part of the cell cycle. After the Ori MD moves to the quarter cell positions, SeqA mainly trails replication forks (Helgesen et al. 2015). SeqA clusters in the ORI MD were found to interact with each other during exponential growth, confirming a role in organizing this domain during replication (Cagliero et al. 2013).

The Structural Maintenance of Chromosome (SMC) unit MukB also co-localizes with the Ori MD (Danilova et al. 2007) (see also 1.4.2). This interaction is mediated by MukE, which is brought to MukB by MukF (She et al. 2013). In a slow growing *mukB* null mutant, the chromosome adapts the longitudinal Ori-Ter MD conformation which is normally only observed in fast growing cells (as depicted in Figure 8) with defects in chromosome segregation as a consequence (Danilova et al. 2007). It is hypothesized that when the Ori is not compacted or organized sufficiently, it cannot localize at midcell simultaneously with the Ter MD due to space limitations (Wang & Rudner 2014).

Interestingly, SeqA and MukBEF co-evolved in enterobacteria such as *E. coli*, together with SlmA, MatP/*matS* and other factors with known and unknown functions (Brézellec et al. 2006). It has been proposed that these factors could (partially) compensate the lack of a *parABS* system in *E. coli* (Dame, Kalmykowa & Grainger 2011; Valens, Thiel & Broccard 2016). The interrelationship of these proteins and the exact mechanism at which they could facilitate chromosome organization and possibly segregation is not clear.

1.5 Global organizers of the chromosome and their impact on segregation

Segregation of the chromosomal bulk requires the nucleoid to be properly folded and organized. Absence of protein factors that are involved in compacting the nucleoid very often lead to defects in chromosome segregation (Rybenkov et al. 2014; Helgesen et al. 2016).

1.5.1 Nucleoid-associated proteins

E. coli and other bacteria lack histones, eukaryotic proteins that organize the DNA in the characteristic “beads on a string” structure (Kornberg 1974). However, nucleoid-associated proteins (NAPs) with histone-like functions have been identified in bacteria, too (reviewed in (Mazor et al. 2008; Dillon & Dorman 2010). The subset of histone-like proteins that is present in exponentially growing cells encompasses H-NS, Fis, HU and IHF (Figure 9).

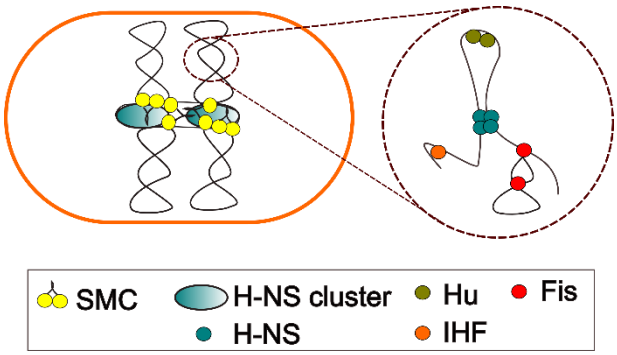

Figure 9| DNA organization by nucleoid-associated proteins. The nucleoid scaffold is formed by MukBEF and possibly large H-NS clusters. Smaller structures are stabilised by the indicated NAPs. Fis stabilises branched DNA, HU and IHF introduce sharp bends in the DNA and H-NS bridges distant DNA sites which result in the stabilisation of loops and supercoils.

Where HU, IHF and Fis are uniformly distributed along the nucleoid, H-NS forms two distinct clusters per chromosome (Wang et al. 2011). Since the H-NS binding sites are scattered around the chromosome, bringing together of these sites is thought to impact the global folding of the chromosome. Modulation of the H-NS levels impacts the shape of the nucleoid. Overexpression leads to an overly condensed nucleoid and even cell death (Kar, Edgar & Adhya 2005), while its absence results in loosely arranged nucleoids and problems with chromosome segregation (Helgesen et al. 2016).

Apart from their function in organizing and stabilizing the chromosome, many NAPs protein also act as global regulators of gene expression via several mechanisms (Opel et al. 2004; Kahramanoglou et al. 2011).

1.5.2 Structural maintenance of chromosome: MukBEF

Structural Maintenance of Chromosome (SMC) protein complexes are responsible for the higher-order chromosome organization in a wide range of organisms (Hirano 2006). While half a dozen is known in prokaryotes, enterobacteria such as *E. coli* have only MukBEF (Cobbe & Heck 2000). The core unit MukB forms the characteristic V-shaped dimers that bind to DNA in clamp-like way (Cui, Petrushenko & Rybenkov 2008). DNA-binding by MukB is highly cooperative, which results in spreading of the protein to adjacent chromosomal segments compacting the DNA by looping (Rybenkov et al. 2014). Despite being present at low concentrations in the cell (about 400 complexes), absence of MukB highly reduces nucleoid condensation (Petrushenko, Lai & Rybenkov 2006). The MukE and MukF subunits are not involved in direct DNA-binding but influence/stabilize interactions between MukB and the DNA (She et al. 2007; Petrushenko et al. 2010). Growth is completely abolished at 37°C in a MukB null mutant. At permissive temperatures, chromosomes appear less condensed and a-nucleate cells of normal size are formed due to defects in chromosome segregation (She et al. 2007; Nicolas et al. 2014). Inhibition of the *topA* gene, whose protein product leads to a larger amount of supercoiling, compensates mostly for this phenotype (Sawitzke & Austin 2000). Accordingly to its function, overexpression of MukB leads to an overly condensed nucleoid (Wang et al. 2006).

1.6 Mechanisms responsible for bulk chromosome segregation

Since the *E. coli* cell cycle is not always sequential like those of eukaryotic cells, many different processes are acting on the nucleoid simultaneously. While replication proceeds, the replicated part of the nucleoid already segregates. In the meantime, transcription and translation continue and are also influencing the chromosomal layout (Cabrera et al. 2009; Bakshi, et al 2014; Cagliero, Zhou & Jin 2014). It has been shown, however, that the above mentioned processes are not involved in chromosome segregation (Wang & Sherratt, 2010; Woldringh et al. 2015)

Physical phenomena such as conformational entropy of the nucleoid and macromolecular crowding also contribute to the folding of the bacterial chromosome (Odijk 1998; Jun & Mulder 2006). Chromosome segregation was described as the spontaneous de-mixing of two circular polymers confined by a box or cylinder (Jun & Mulder 2006; Jun & Wright 2010). According to this model, maximization of the conformational entropy is considered to be the major driving force for segregation of the chromosomal bulk. Proteins involved in chromosome organisation and compaction are thought to be there only to facilitate proper chromosomal organisation to fully exploit the entropic forces that lead to the de-mixing of the polymers. The model of Jun and colleagues even explains the repositioning of the Ter MD from the cell periphery to the cell center. The principles of such a biophysical framework for chromosome segregation are applicable to fast and slow growth. However, it is shown that these entropic forces alone are not sufficient to fully ensure proper chromosome segregation (Kuwada et al. 2013; Lampo et al. 2015; Mannik et al. 2016).

Another model for chromosome segregation is solely based on the mechanical properties of the nucleoid. To fit within the cell, the chromosome is compacted by protein factors and by radial confinement. This constant stress on the chromosome manifests itself as a mechanical pushing force (Kleckner et al. 2004; Bates & Kleckner 2005; Joshi et al. 2011; Fisher et al. 2013). Replicated chromosomal regions co-localise until their cohesion is lost in an abrupt manner. This happens when the mechanical tension becomes too great. Bulk chromosomal segregation is the effect of the two daughter chromosomes that mechanically push each other away and tend to localise themselves side by side to minimize radial confinement stress. Interestingly, it was observed that 5-10% of the chromosomal bulk moves in longitudinal waves back and forth within 5 seconds (Fisher et al. 2013). These movements occurred independently from replication and are proposed to arise from a dynamic not-yet known ATP-driven biochemical process, allowing more internal mobility for the nucleoid to rearrange.

1.7 The Min system and chromosome segregation

It has been discovered in our lab the Min system has an additional function beyond the selection of the division site. MinD was found to weakly interact with DNA, both *in vitro* and *in vivo* (Di Ventura et al. 2013). It was proposed this could be relevant for chromosome segregation in *E. coli*. (Di Ventura et al. 2013). A gradient of MinD-DNA-binding sites towards the poles would prevent back diffusion of the duplicated chromosome towards the cell middle, thereby biasing the movement towards the pole. This Brownian Ratchet/like mechanism would provide an additional mechanism to faithfully segregate daughter chromosomes (Figure 10). This hypothesis was supported by mathematical modeling, which revealed that not only oscillating, but also static polar gradients of DNA tethering sites at the membrane would augment segregation (Di Ventura et al. 2013).

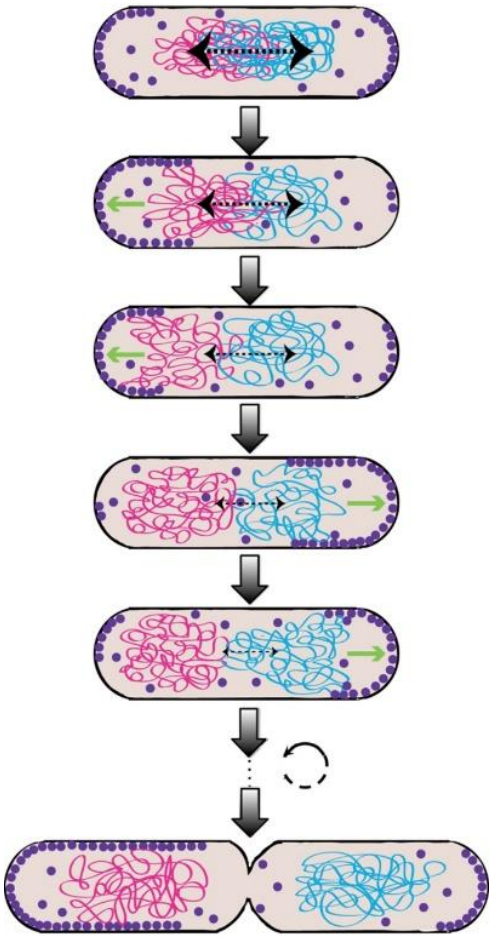

Figure 10| Proposed model of chromosome segregation by the Min system. After duplication of chromosomal DNA, sister chromatids (pink and cyan) are repelled by entropic forces (black arrows). These get weaker as the distance between the chromosomes increases. Additional forces acting on the nucleoid provided by the Min system are indicated with green arrows. Image taken from (Di Ventura et al. 2013).

The exact binding surface employed for DNA-binding, is not completely clear. An extensive (rational) mutagenesis has been described to identify mutants of MinD that lost the DNA-binding properties, but are still able to oscillate and bind to MinC (Di Ventura et al. 2013). Unfortunately, this approach led to the identification of many mutations that did not influence DNA-binding. Only two mutants showed reduced DNA-binding affinities, but this was coupled to either a loss of membrane binding ($MinD^{\Delta 10}$) or a defect in the interaction with MinC and the membrane ($MinD^{R219D}$, Di Ventura et al. 2013).

For the protein Soj from *Bacillus Subtilis*, the equivalent residue (R218) was directly involved in chromosome binding, in addition to several other surface exposed positively charged residues (Hester & Lutkenhaus 2007). Soj is structurally very similar to MinD, except for the lack of a membrane targeting sequence. Soj also forms dimers in an ATP dependent fasion and these dimers bind non-specifically to DNA (Leonard, Butler & Lowe 2005). However, the residue R219 in MinD would be shielded by the membrane when MinD dimers are lipid associated.

Where the Min system uses the membrane as the substrate to move on, some ParA/ParB protein couples can move in an oscillatory fashion onto the nucleoid, using a similar mechanism (Vecchiarelli et al. 2012). Among those are ParA/ParB from the *E. coli* low copy number plasmid pB171 (Ebersbach & Gerdes 2004) and Soj/Spo0J from *B. subtilis* (Marston & Errington 1999; Quisel, Lin & Grossman 1999). In the absence of Spo0J, Soj is statically associated with the nucleoid. Stimulation of its ATPase activity by Spo0J leads to dynamic movements (Leonard et al. 2005). For MinD, it is known that the intrinsic ATPase activity is stimulated by MinE in the presence of a lipid bilayer (Zhou et al. 2005; Park et al. 2012). The influence of DNA on the ATPase activity of MinD has not been studied.

In the past, it had been observed already that *E. coli* strains without a functional Min system show defects in chromosome segregation (Akerlund, Bernander, & Nordström, 1992 ; Akerlund et al., 1992). Due to the well-studied function of the Min system in division site selection, these studies received little attention and chromosome segregation defect were considered a consequence of polar divisions and mis-placement of the septum and received little attention.

1.8 Aim of the thesis

The role of the Min system in chromosome segregation has been described generally, but some of the molecular details are missing. So far, only the DNA-binding properties of MinD have been characterised. It is not known yet how MinD is able to form membrane associated dimers, bind to DNA and is still able to interact with its partners. In chapter 3.1, I investigate the binding surface of MinD to DNA. To this purpose, I mutated surface-exposed, positively charged residues into negative ones, purified the corresponding mutant proteins and tested their ability to bind to the DNA using *in vitro* assays, and microscopy to analyze chromosome segregation inside *E. coli* cells.

Additionally, MinD-DNA-binding seems to occur without apparent sequence specificity. Yet it is possible that the protein has a weak affinity for any DNA-sequence, but a higher affinity for a specific sequence or a genomic region. In chapter 3.2, I explore the possibility that MinD might preferentially bind to certain MDs *in vivo*. To this end, I established a protocol to perform ChIP-Seq overexpressing His-tagged MinD in wild type as well as Min^- *E. coli* cells. Additionally, using microarrays, I test whether the Min system might affect transcription globally in chapter 3.3.

The involvement of MinE and MinC must also be studied to fill in the molecular details. Do these proteins interact with DNA by themselves, or are there synergistic or cooperative effects at play? An interesting point is the recently observed formation of MinC-MinD co-polymers *in vitro*, which were speculated to bind stronger to FtsZ due to the higher binding avidity. Are such effects relevant for DNA-binding as well? I examine the role of all Min proteins in DNA-binding in chapter 3.4. To this aim, MinE and MinC were purified additionally and their interaction with DNA was studied in the presence

and absence of MinD with EMSA. Furthermore, I reconstituted the Min system on the surface of lipid vesicles to study the ability to pull down plasmid DNA to the lipid associated pellet. Furthermore, the effect of FtsZ was also studied in this context. Additionally, a subset of MinC mutants, that were predicted to have a reduced DNA-binding affinity, were characterized with EMSA and co-sedimentation assays as well.

2 Materials and Methods

2.1 Cloning, strains and growing conditions

2.1.1 Cloning

All plasmids used in this work are based on the vector backbones listed in Table 1 and are constructed using standard cloning techniques described in Materials and Methods 2.1.2 and 2.1.3. In general, PCR amplifications were set up with Phusion® High-Fidelity DNA Polymerase (NEB BioLabs) and primers purchased at Sigma Aldrich. PCR products and plasmid backbones were digested with restriction enzymes (New England Biolabs) followed by ligation with T4-DNA ligase (Thermo Fischer Scientific). For the introduction of point mutations, the Agilent QuickChange II XL site-directed mutagenesis kit was used with the manufacturer´s recommendations. Oligonucleotide sequences used for PCR amplification or oligo cloning are shown in Table 5.

Plasmid name	**Description**
pET-28a (Novagen)	N-terminal His-T7-tag and/or C-terminal His-tag; T7 promoter; IPTG inducible; pBR322 origin of replication; kanamycin resistant (Novagen).
pTrc99a	Hybrid trp/lac promoter; IPTG inducible; pBR322 origin of replication; ampicillin resistant (Amann, Ochs, and Abel 1988).
pBAD33	PBAD promoter (*araBp)*; arabinose inducible; p15A origin of replication; chloramphenicol resistant (Guzman et al. 1995).

Table 1| Plasmid backbones used in this thesis.

2.1.2 pET-28a expression constructs used for protein purification

All purified proteins mentioned in this work are expressed from the pET28a-plasmid. For the construction of the library containing MinD mutants, pET-28a-*minD* (Di Ventura et al., 2014) was used as template. Point mutations were introduced in a PCR reaction using the complementary primer pairs shown in Table 5. For mutants in which the affected residues are not adjacent to each other, the mutagenesis procedure was performed in subsequent rounds. All reactions were set up using the Agilent QuickChange II XL site-directed mutagenesis kit following the manufacturer´s recommendations. pET-28a-$minD^{\Delta 10}$ was is described by (Di Ventura et al., 2014). This plasmid was taken as input-DNA for the mutagenesis reaction to produce pET-28a-$minD^{D40A\text{-}\Delta 10}$.

MinC was amplified from *E. coli* MG1655 genomic DNA with primers LK21 and LK26. The *Bam*H1 and *Not*I restriction sites were used to insert MinC in the pET-28a plasmid in frame with the His-T7 tag. The same strategy was used for amplification of the N-terminal domain ($MinC^{1\text{-}115}$) with primers LK21/LK22 and the C terminal domain ($MinC^{116\text{-}213}$) with primers LK25/LK26. FtsZ was also amplified

from the *E. coli* MG1655 genome using primers LK31 and LK32. The PCR product was inserted in the pET28-a plasmid with the *Bam*HI and *Hin*dIII sites. pET28-*minE* was provided by Barbara Di Ventura. The protocol described in 2.1.4 was used for the transformation of plasmid DNA into *E. coli* TOP10 competent cells.

2.1.3 Constructs used for functional studies

To study oscillations of MinD and MinE-YFP, the bicistronic construct pTrc99a-*minD/minE-yfp* (Di Ventura and Sourjik 2011) was used. Point mutations in MinD were introduced with the same mutagenesis primers as used for the for the pET-28 constructs (listed in Table 5). For the analysis of chromosome segregation, I used a plasmid-borne Min system. The *minB* operon (including the transcription start site of MinC and two transcriptional terminator sites upstream of MinE) was amplified from the *E. coli* MG1655 genome with primers LK33 and LK34. The operon was inserted in the pBAD33 plasmid using the *Sac*I and *Hind*III restriction sites yielding pBAD33-*minB.* The same PCR product and restriction sites were used with to construct pTrc99a-*minB.*

The ChIP-Seq experiments required a tagged version of MinD for the immunoprecipitation procedure. Therefore*, minD* was PCR amplified from the genome with a forward primer which contained a His-tag followed by a short spacer that also contained a *Not*I restriction site; LK35. LK37 was used as reverse primer. The product was inserted in the pTrc99a plasmid with *Nco*I *and Pst*I which resulted in pTrc99a-^{His}*minD*. pTrc99a-^{FLAG}*minD* was constructed in a similar way using forward primer LK33. For obtaining MinD with a His-tag and a longer linker, pET28-*minD* was taken as a starting point. *MinD* was amplified with primer LK38, which anneals slightly upstream of the pET28a multiple cloning site to include the His-T7 tag which is present in the plasmid backbone. LK37 was used as a reverse primer. The PCR product was digested with *Nco*I and *Pst*I and ligated into pTrc99a which was digested with the same sites, to produce pTrc99a-$^{His\text{-}T7}$*minD*. SeqA was obtained in a PCR reaction with E. coli genomic DNA and primers LK39 and LK40. The *Bam*HI and *Pst*I restriction sites were used to exchange MinD for SeqA which resulted in plasmid pTrc99a-$^{His\text{-}T7}$*seqA.*

For measuring the promoter activity of the *motA* and *tar* promoter, reporter constructs were prepared. First, *yfp* was amplified from pTrc99a-*minD/minE-yfp* with primers LK41/LK42. The PCR product was digested with *Sac*I and *Hin*dIII and inserted in the pBAD33 plasmid. The *motA* promoter was amplified in a PCR reaction with genomic *E. coli* DNA and primers LK43 and LK44. The PCR product was digested with *Cla*I and *Sac*I and ligated into the pBAD33 backbone using the same sites. Usage of *Cla*I/*Sac*I eliminates the *araB* promoter and the region encoding the regulatory protein AraC from the pBAD33 plasmid. The *tar* promoter region was obtained by annealing the complementary

oligonucleotides (LK45/LK46) comprising the promoter region and overhanging ends compatible to the restriction sites *Cla*I and *Sac*I.

The LacZ coding sequence was PCR amplified from genomic *E. coli* DNA with primers LK47/LK48 and inserted in the pBAD33 plasmid with *Xba*I and *Hin*dIII by Manuel Goepferich. The *araB* promoter, and *araC* were removed from the plasmid backbone by digestion with *Cla*I and *Xba*I. Then, the *tar* or *motA* promoter were ligated at the same site using *Cla*I and *Xba*I. *MotA* was amplified from the *E. coli* genome with LK49 and LK50 while the *tar* promoter was obtained by annealing of LK51/LK52.

2.1.4 Transformation of competent cells

Chemically competent *E. coli* cells were thawed on ice followed by addition of at least 0.5 ng of plasmid DNA, or 50 ng for transformations with multiple constructs simultaneously. For ligation cloning, 3 µl of the ligation mixture was added. The same volume was used for the *Dpn*I digested mutagenesis PCR products. After 20 minutes of incubation on ice, the cells underwent a heat shock for 45s at 42°C and were placed back on ice for 5 minutes. Then, 1 ml of antibiotic-free LB was added to the cells followed by incubation at °37. For ampicillin, this step lasted 0-15 minutes, for kanamycin 30 minutes and for chloramphenicol 1 hour. Afterwards, the cells were spun down in a table top centrifuge (1 min, 13.000 G), resuspended in 200 µl LB and plated out on a LB-Agar plate with the appropriate antibiotics.

2.1.5 Strains

Strain name	**Genotype**	**Reference**
TB28	MG1555 *LacIZYA*	(Bernhardt and De Boer 2005)
TB43	MG1555 *LacIZYA* <> frt *minCDE* <> frt	``
TB115	MG1555 *LacIZYA* <> frt *minCDE* <> frt *slmA*	``
MG1655	MG1655 (K12 – wild type)	(Blattner 1997)
MG1655*ΔminB*	MG1655 *ΔminB::KanR::*	(Di Ventura and Sourjik 2011)
One Shot ® TOP10	F-, *mcrA* Δ(*mrr-hsd*RMS-*mcr*BC) , Φ80 *lac*ZΔM15 Δ *lac*X74 *rec*A1 *ara*D139 Δ(*araleu*)7697 *gal*U *gal*K *rps*L (StrR) *end*A1 *nup*G	Invitrogen
Rosetta™ DE3	F^- *ompT* $hsdS_B(r_B^- m_B^-)$ *gal dcm* (DE3) pRARE (Cam^R)	Novagen

Table 2|*E. coli* strains used in this study. <> denotes DNA replacement and frt indicates a scar that remains after deletion of the aph cassette by the FLP recombinase as described by (Bernhardt and De Boer 2005). Strain TB28, TB43 and TB115 were a kind gift of the lab of Tom Bernhardt.

2.2 Buffers and solutions

Name	**Components**
LB medium	10 g L^{-1} tryptone 5 g L^{-1} yeast extract 10 g L^{-1} NaCl
M9 medium	M9 minimal salts (1X) 1 mM MgCl 200 µM $CaCl_2$ 0.4 % glucose (0.2 % Casamino acids)
Antibiotic stock solutions	Ampicillin 1000x (100 mg ml^{-1}) in water Kanamycin 1000x (50 mg ml^{-1}) in water Chloramphenicol 3000x (34 mg ml^{-1}) in ethanol
Protein purification	
Lysis buffer	50 mM NaPi pH 7.5 300 mM NaCl 10 mM imidazole mM EDTA, protease inhibitor (complete EDTA-free, Roche 200 µM $MgCl_2$ 200 µM ADP
Wash buffer	50 mM NaP_i pH 7.5 300 mM NaCl 20 mM imidazole 10 % glycerol 0.1 mM EDTA
Elution buffer	50 mM NaP_i pH 7.5 300 mM NaCl 250 mM imidazole 10 % glycerol 0.1 mM EDTA
Storage buffer	50 mM HEPES pH 7.3 150 mM KCl 10 % glycerol 0.1 mM EDTA
Malachite green assay	
Solution A	5.37 % ammonium molybdate in 6N HCL

Solution B	2.32 % polyvinyl alcohol (1.16 g added to 50 ml boiling water).
Solution C	Malachite green in water (0.8 g L^{-1})
Solution D	Water
Malachite green working solution	A:B:C:D in a ratio of 1:1:2:2
ChIP-Seq	
Lysis buffer	1X Promega FastBreak™ lysis buffer 0.5 M NaCl 200 µg ml^{-1} lysozyme 5 mM Pefabloc®
Wash buffer	0.2 X Promega FastBreak™ lysis buffer 100 mM HEPES pH 7.5 5 mM imidazole 0.5 M NaCl 8M urea
Recovery buffer	100 mM Tris pH 8 % SDS 1 mM EDTA 600 µg ml^{-1} proteinase-K
Other	
Liposome buffer	20 mM HEPES pH 7.5 150 mM NaC 5 mM β-mercaptoethanol
Coomassie staining solution	0.1% Coomassie Brilliant Blue G-250 50% methanol 10% glacial acetic acid
TAE	45 mM Tris-Acetate 1 mM EDTA
TBE	45 mM Tris-Borate 1 mM EDTA
TB buffer pH 8.0	45 mM Tris-Borate
TBS(-T)	50 mM Tris-Cl, pH 7.6 150 mM NaCl (0.1 % Tween-20)

Table 3| Composition of buffers and solutions used in this work.

2.3 Protein purification

Protein purifications were performed as described by (Di Ventura et al. 2013) with minor modifications. Rosetta cells carrying the desired plasmid were grown to an OD600 of 0.5-0.9 and induced with 1 mM IPTG for 3 hours at 37°C. Cells were collected by centrifugation (4.000 r.p.m.) at 4°C for 20 minutes and stored at -20°C. Pellets were thawed on ice and resuspended in lysis buffer. The buffer compositions are listed in Table 3. Then, cells were lysed by sonication and the crude lysate was clarified by centrifugation (20.000 RPM) for 20 min at 4°C. Proteins were purified using the Profinia™ Protein Purification System (Bio-Rad), with a BIO-RAD® Bio-Scale™ Mini Profinity™ IMAC Cartridge (1mL) and the BIO-RAD® Bio-Scale™ Mini Bio-Gel® P-6 Desalting Cartridge (10 mL). The column was washed with imidazole buffer and the protein was eluted with elution buffer, followed by exchange of the elution buffer for storage buffer. The purified proteins were stored in small aliquots at -80°C. Protein concentrations were estimated based on the absorbance at 280 nm with a NanoDrop spectrophotometer (Thermo Scientific). The Qubit® Protein Assay was used additionally, following the manufacturer`s recommendations. The Qubit values were taken as a guidance whenever there was a small discrepancy between the estimated concentrations. Proteins were cleared from any aggregates by centrifugation (21.000 g) for 30 min at 4°C prior to use.

2.4 Malachite green assay

The purified proteins ^{His}MinD and ^{His}MinE were washed on a spin column with storage buffer to remove background amounts of free phosphate. The final reaction contained 5 µM MinD and 5 µM MinE in 50 mM Hepes pH 7.2, 75 mM KCl, 5% glycerol, 50 µM EDTA and 5 mM $MgCl_2$. If indicated, 10 nM of DNA was added to the sample. Different kinds of DNA were used: A 150 bp PCR product of the *E. coli* P1 promoter, pUC19 plasmid DNA (2.7 kb) or genomic DNA from *E.coli* MG1655 sheared to 200 bp by sonication. All DNA was purified with QIAquick spin columns and eluted in water. After incubation for 10 minutes at 37°C, 1 mM ATP was added to start the reaction. At this point, half of the sample was taken apart and quenched with 50 mM EDTA to stop the reaction (T_0). The remainder of the sample was left for 40 minutes at 37°C and subsequently quenched with EDTA.

In order to prepare the Malachite Green reagent, the following stock solutions were prepared: **(A)** 5.37 % ammonium molybdate in 6N HCL. **(B)** 2.32 % polyvinyl alcohol (1.16 g added to 50 ml boiling water). **(C)** Malachite green in water (0.8 g $L^{-1)}$. **(D**) Water. The working solution contained A:B:C:D in a ratio of 1:1:2:2 and was left on a rotator for 1 hour before use. For detection of free phosphate, 10 µl of sample was mixed with 190 µl of working solution. After 10 minutes of incubation at RT, 10 µl of 34% citric acid was added for signal stabilization. The absorbance was measured at 633 nm in a Tecan plate reader. A standard curve was prepared by making a serial dilution of phosphate buffer of known concentration.

2.5 Co-sedimentation assays

2.5.1 Vesicle preparation

E. coli total lipids (powder) were purchased from Avanti Polar Lipids. The lipids were dissolved in liposome buffer (20 mM HEPES pH 7.5, 150 mM NaCl and 5 mM β-mercaptoethanol) to a final concentration of 20 mg ml^{-1} and were allowed to stand for 30 minutes at 37°C. For better hydration, the sample was frozen in liquid nitrogen and heated up to 37°C in a heat block a total of 5 times. Lipid vesicles were obtained using the Avanti Mini Extruser with a 200-nm filter. The sample was passed through the filter 20 times, aliquoted and stored in the -80°C freezer.

2.5.2 Co-sedimentation of MinD and liposomes

The procedure was exactly followed as described before (Di Ventura et al. 2013). Vesicles (320 µg/mL, obtained from *E. coli* total lipid extract were incubated for 10 min with wild type or mutant MinD (6 µM) and 1 mM of either ADP or ATP in 50 µL reaction volume of ATPase buffer (25 mM Tris-HCl, pH 7.5, 50 mM KCl, 5 mM $MgCl_2$, 5% glycerol). The reactions were pelleted by centrifugation at 21.000 g for 15-30 min, the pellets were resuspended in 50 µL ATPase buffer, and supernatant and pellet samples were analyzed by SDS-PAGE, followed by Coomassie staining to detect MinD.

2.5.3 Co-sedimentation of MinC-MinD and plasmid DNA

Purified MinC and MinD (varying concentrations) were incubated with 800 µg ml^{-1} liposomes (prepared from *E. coli* total lipid extract), 32 ng $µl^{-1}$ plasmid DNA (mEos3.2, a kind gift from Sabine Aschenbrenner) and 1 mM of nucleotide in storage buffer supplemented with 5 mM $MgCl_2$. After 15 minutes of incubation at room temperature, the reaction mixture was spun down in a table top centrifuge at 21.000 g for 20 minutes. The supernatant was removed and mixed in a 1:1 ratio with 2x Laemli buffer. The pellet was dissolved in 1x Laemi buffer as such that the volume was similar to the supernatant fraction. After heating the samples for 5 minutes at 95°C, the protein content of the of pellet and supernatant fractions was analyzed with SDS-page followed by Coomassie staining. A 1% Agarose gel with Gel Red™ Nucleic Acid Stain was used to analyze the DNA content. The intensity of the DNA and protein bands was quantified with ImageJ.

2.5.4 Ultracentrifugation of MinC-MinD co-polymers

8 µM MinD and/or MinC were incubated in storage buffer with 1 mM ATP and 5 mM $MgCl_2$. After 10 minutes of incubation at room temperature, polymers where collected by ultracentrifugation in a Beckman Coulter Optima™ TLX centrifuge with rotor TLA 110 and tubes 357448. The samples were spun down at 4°C for 30 min and 50.000 RPM. Protein stock solutions were centrifuged with the same settings prior to experiments for the removal of possible aggregates. The supernatant was collected

and mixed with 25 µl 2x Leamli buffer. The pellets were resuspended in 50 µl 1X Laemli. After 5 min incubation at 95°C, samples were loaded on a 10 % Bis-Tris gel in MOPS running buffer.

2.5.5 Oscilations of MinD and MinE-YFP

A bicistronic construct of MinD and MinE-YFP under the control of the IPTG inducible Trc promoter (pTrc99a-*minD/minE-yfp*) was transformed into the *E. coli* MG1655 *ΔminB* strain and plated out. Colonies were picked and overnight cultures were grown in LB at 37 °C while shaking at 220 RPM. The next day, the cultures were diluted 100x times, grown for 2 hours followed by 1.5 h IPTG induction. Cells were imaged on soft agarose patches (0.5% agarose in PBS) with a ZEISS Axio Observer microscope using a 63x objective. Snapshots were taken every 15 seconds during a total time of 2 minutes. ImageJ was used for the construction of kymographs of the MinE-YFP signal.

2.5.6 Filamentation induced by overexpression of MinD

To study the interaction between MinC and MinD, I expressed plasmid-borne MinD and mutants (pET-28a constructs) in the *E. coli* Rosetta strain, which contains an endogenous Min system. In the presence of MinC, overexpression of MinD will result in a division block leading to cell filamentation. Overnight cultures were diluted 100 times in LB medium and grown for 1 hour, followed by a 2-hour induction with 100 µM IPTG to induce protein expression. Cultures were grown at 37 °C while shaking at 220 RPM. Cells were embedded in soft agarose patches (0.5 % agarose in PBS) and DIC (Differential Interference Contrast) images were acquired on a Zeiss Axio Observer with a 63x objective. The cell length for more than 150 cells was measured manually in ImageJ. One of the datasets was analyzed by Leonard Ernst.

2.5.7 Analysis of chromosome segregation

Overnight cultures were grown in M9-medium supplemented with 0.2% Cas amino acids, 0.4% glucose and the appropriate antibiotics. The next day, cultures were diluted 100 times in the same medium and incubated for 2.5 -3 hours (37°C, 220 RPM). Then, cells were crosslinked with formaldehyde (4%) for 20 minutes at room temperature on a rotating wheel. The cells were spun down for 1 minute at 13.000 RPM and were washed 2 times with TBS. The nucleoids were stained for 15 minutes with DAPI by mixing the samples 1: 1 with a 5 µg/ml DAPI solution (dissolved in water). Prior to imaging, the cells were embedded in soft agar patches. A DIC image and an image of the DAPI fluorescence were acquired with a ZEISS Axio Observer with a 63x objective. Cells were segmented in ImageJ based on the DIC image using a manual threshold, or by manually drawing a (segmented) line. The intensity profiles of the DAPI stained nucleoids along the lines were derived, and maxima and minima were found using the ImageJ plugin `*find peaks*`.

2.6 SDS-page and Western Blot

Samples were mixed with Laemli buffer (supplemented with β-mercaptoethanol) denatured for 5 minutes at 95°C and subsequently loaded on a polyacrylamide gel (NuPAGE® 10% Bis-Tris Gel). If the proteins of interest were smaller than 15 kD, the running buffer was MES, otherwise MOPS (Invitrogen). The gel was run for 35, respectively 50 min at 200V. The Novex® Sharp Pre-stained protein marker was used as a reference (3.5 – 260 kD range). If needed, the gel was stained with Coomasie staining solution for 10 minutes for protein detection.

For the Western Blot procedure, the Coomassie staining was omitted. A PVDF membrane (0.2 µm) was prewetted with methanol, rinsed with water and kept in TB buffer. Proteins from the SDS-page gel were transferred to the PVDF membrane in TB buffer overnight at 300 mA. The next day, the membrane was blocked with 5% milk in TBS for 45 minutes followed by a 1 hour incubation αPenta·His (QIAGEN, 1:1000 diluted in TBS-T) or ANTI-FLAG® M2 (Sigma Aldrich). The membrane was rinsed 3 times with TBS-T. Then an HRP-coupled secondary antibody (mouse IgG-HRP, Abcam) was added for 30 minutes (1:5000 times dilution in TBS-T). After rinsing the membrane 2 times with TBS-T and a final time with TBS, SuperSignal West Pico Chemiluminscent Substrate (Thermo Scientific) was added for 5 minutes. The chemiluminescent signal was recorded using a ChemoCam Imager (Intas).

2.7 ChIP-Seq

2.7.1 Sample preparation

Overnight cultures of *E. coli* MG1655-K12 (*ΔminB*) carrying His-tagged proteins expressed from the pTrc99a plasmid, were grown in M9 medium supplemented with 0.4% glucose. The next day, cultures were diluted to an OD_{600} of 0.02 and incubated at 37°C, 220 RPM. When the OD_{600} reached 0.4, 40 ml of culture was taken and subjected to crosslinking with 1% formaldehyde (methanol-free) for 20 minutes at room temperature on a roller bank. After quenching with 2.5 M glycine for 5 minutes, cells were spun down for 20 minutes at 4100 RPM, 4°C and washed with TBS two times. Pellets were collected and frozen for further use.

For the affinity precipitation, cells were lysed in Promega FastBreak™ lysis buffer supplemented with 0.5 M NaCl, 200 µg/ml Lysozyme and 5 mM Pefabloc® at RT for 15 minutes. Then, cells were sonicated in a Bioruptor® for 30 cycles, 30s on, 30s off with high intensity. Cell debris was removed by centrifugation for 5 min at 14.000 RPM. 10 µl was taken apart to process later as input-DNA. 400 µl of sample was taken and diluted 4 times in incubation buffer, final concentrations of buffer 100 mM HEPES pH 7.5, 5 mM imidazole, 0.5 M NaCl, ±0.05% Triton-X100, ±0.05% ethoxylated alkyl amine and 8M urea. Samples were incubated with 100 µl MagneHis™ beads from Promega for 5 hours at RT on a rotating wheel. The beads were washed in the same buffer supplemented with 10 mM Imidazole for

3 times followed by elution in 100 mM Hepes with 500 mM Imidazole. RNAse-A was added followed by incubation at 37°C for 1h. Samples were diluted 2 times in recovery buffer containing 100 mM Tris pH 8, 1% SDS and 1 mM EDTA with 600 µg ml^{-1} proteinase- K (Promega) and incubated for 2h at 42°C and for 4h at 65°C.

The DNA was purified with the QIAGEN nucleotide removal kit and final DNA concentration was measured with Qubit™ dsDNA High Sensitivity kit. At this point, the samples were submitted to the CellNetworks core facility (David Ibberson). The sequencing library was constructed with the NEBnext® Ultra™ DNA library Prep Kit for Illumina®. A size selection step with AMPure beads (Beckman) was performed. The library was amplified with NEBnext® Multiplex Oligos for Illumina® using 13-15 PCR cycles. The quality of the library was checked with the Agilent Bioanalyzer. The sequencing was done on the Illumina HighSeq®2500 sequencing system, 50 bp single reads, with V3 chemistry.

2.7.2 Genome alignment and peak calling

The Genbank file containing the complete genome of Escherichia coli str. K-12 substr. MG1655 was downloaded from NCBI (ecoli_U00096.2.gb). The file was converted to a Fasta reference sequence, using bowtie-1.0.0 and SAMtools -0.1.18. Reads were aligned with bowtie (-p 8, - m1) and sorted with SAMtools -1.2 (done by Naveed Ishaque).

The subsequent steps described below were done by Sebastian Steinhauser, he also provided me with the text;. First, PCR duplicates and ambiguous aligned reads were removed. However, since all samples were sequenced over saturation we had to perform an additional alignment down sampling step. For this random sampling was performed using the analogues SAMtools function, resulting in alignments containing 1%, 5%, 10%, 15%, 25% and 30% of the original library size [PMID: 19505943]. We performed all subsequent analysis steps on all of the alignments. Peak calling revealed a saturation of peak number at 25%, which corresponds to the point where most artificial peaks should be lost. Read enriched regions were determined against input using MACS2 with following parameters: '-g 4639675 –call-summits' [PMID: 18798982]. Consensus peak sets were constructed by keeping only peaks which are shared between two samples.

2.7.3 Signal track generation

Signal tracks were computed as signal extraction scaling (SES) normalized enrichment over input using 'bamCompare' from the deepTools framework with the additional parameters: '—scaleFactorsMethod SES –ratio log2 –bs 25' [PMID: 24799436]. All resulting signal and peak tracks were visualised using IGV.

2.7.4 Comparative ChIP-Seq analysis

We compared all ChIP-Seq samples via genome-wide correlation using 'bamCorrelate' from the deepTools framework. This computed the coverage in 250bp bins and correlated them via Pearson correlation, followed by performing hierarchical clustering. Heatmaps visualising the enrichment of Mock, MinD and SeqA were plotted within +/- 500bp around peak summits using deepTools. Further, we generated a binary motif track for the SeqA associated GATC motif and visualized it in a similar manner.

2.7.5 Motif analysis

De-novo motif discovery was performed using MEME-ChIP [PMID: 19458158] and Homer [PMID: 20513432] on consensus peak sets. Homer was used with a scrambled input sequence background and additional length constrains to find only motifs between 6-24bps. MEME-ChIP was used with default settings. Discovered motifs were compared with the SwissRegulon *E.coli* motif database

2.8 Electrophoretic mobility shift assays (EMSAs)

Samples with purified proteins were incubated in 33 mM Hepes, 100 mM KCl, 6.6% glycerol, 66 µM EDTA, 5 mM $MgCl_2$ 1 mM ATP and 50 nM double stranded DNA (labeled with 6-Hexachlore-Fluorecsein Phosphoramidite, HEX). Those concentrations refer to the final concentrations. After 10 minutes of incubation at room temperature, samples were loaded on a 6% non-denaturing polyacrylamide gel. The gel was run for 20 minutes at 150 V in 0.5 x TBE buffer supplemented with 5 mM $MgSO_4$. Afterwards, the HEX signal was visualized with a Typhoon gel laser scanner equipped with a green laser. The DNA probes were annealed beforehand by mixing two complementary oligos in NEB buffer 2 and heating up the mixture to 98°C. After 2 minutes, the heat block was switched off while the sample was left in there, in order to cool the sample gradually down. DNA probes longer than 120 bp were amplified with PCR (by Navaneethan Palanisamy) using a forward primer with a HEX label, followed by gel purification of the fragment using the Qiagen PCR clean up kit.

2.9 Transcriptome analysis

2.9.1 Sample preparation

For isolation of total RNA, 0.5 ml of culture was taken (OD 0.4-0.5) and 1 ml of RNAprotect Bacteria Reagent (QIAGEN) was added. I extracted the RNA with the QIAGEN RNeasy Mini Kit according to the manufacturers recommendations. An on- column DNAse digestion was performed to remove traces of genomic DNA (Turbo™ DNase (Ambion). At this point, I handed my samples over to the DKFZ Genomics and Proteomics Core Facility. There, the integrity of the RNA was checked with the Agilent 2100 Bioanalyzer. Labeling of the samples was done with Fairplay III Micro Array Labeling Kit, using

random hexamers for the generation of the cDNA. Samples were hybridized to the Agilent *E. coli* Gene Expression Microarray, 8x 15K.

2.9.2 Micorarray scanning and data analysis

Microarray scanning was done as well by the DKFZ Genomics and Proteomics Core Facility, according to the manufacturer`s protocols with an iScan array scanner. As test for significance the student's t-test is used on the expression values of the two groups of interest. In the case of significance of expression against background we tested for greater than all negative beads for this sample and in the case of comparing separate groups we tested for inequality of the means of the groups. In both cases Benjamini-Hochberg correction (Benjamini and Hochberg 1995) was applied to the complete set of p-values of all ProbeIDs on the chip. The average expression value is calculated as mean of the measured expressions together with the standard deviation. (The text in Materials and Methods 2.9.2 is provided by the Core Facility).

2.9.3 KEGG pathway analysis

Tobias Bauer performed the KEGG pathway analysis and wrote the following text. R statistical software (R Core Team 2014) (v3.1.0) was used for differential expression analysis. The data was QC-checked, and then log2-transformed and quantile normalized. Significance Analysis of Microarrays (SAM (R Core Team 2014) , R-package "siggenes" v1.40.0 (Tusher, Tibshirani & Chu 2001) was performed and the top 100 ranked genes selected for pathway enrichment analysis using the KEGG database. Significance values for the pathway enrichments were calculated by exact Fisher-tests.

2.10 Expression analysis of reporter genes

2.10.1 Flow cytometry

E. coli K12 MG1655 wild type and *ΔminB* strains were transformed with a reporter construct which contains *yfp* driven by the *motA* or *tar* promoter. Cells were grown in a similar fashion as those used for the microarray analysis. Then, the culture was diluted 20 times in PBS and transferred to a 96-wells plate. The YFP levels were measured using a FC500 MPL Flow Cytometer (Beckman Coulter) and the appropriate YFP filter set. A gate was used to make sure the selected cells from both the wild type and *ΔminB* were of a similar size. The YFP-intensity histograms of this population were analyzed with CyFlogic.

2.10.2 B-Galactosidase activity assay

Reporter constructs that contained the *lacZ* gene under the control of the Tar or MotA promoter were transformed in the *E. coli K12* MG1655 (*ΔlacIZY)* strains TB28 and TB43(*ΔminB*). The strains were chosen due to lack of a functional *lac* operon, thereby minimizing background LacZ activity (kind gift of Thomas Bernhardt and Derek Lau). The β-Galactosidase activity was assessed with the following

protocol: Betagalactosidase_Assay_(A_better_Miller) (http://openwetware.org/wiki), which is based on the publication from (Zhang and Bremer 1995).

2.11 Pull-down with beads coated with ATP-analogues

The interaction of the His-tagged Min proteins and ATP-analogues was assessed with a selection of ATP-coated beads: **1)** Aminophenyl-ATP-Agarose, **2)** 8-[(6-Amino)hexyl]-amino-ATP-Agarose, **3)** N^6-(6-Amino)hexyl-ATP-Agarose, **4)** 2´/3´ EDA-ATP-Agarose, purchased at Jena Biosciences. An empty agarose bead was taken as negative control. 8 µM of MinD or MinC, and 30 µM were incubated with the beads according to the recommended experimental conditions. After incubation, 100 mM of ATP was used to elute the proteins from the beads. The supernatant was collected, mixed with Laemli buffer and heated for 5 minutes at 98°C. The beads underwent the same treatment to verify if any protein was stuck to the beads. The protein contents were analyzed by SDS-page.

2.12 Biacore

The surface plasmon resonance experiments (SPR) were performed on a Biacore X100 system at room temperature and a flow rate of 30 µl min^{-1}. A 30 bp dsDNA probe (biotinylated-$Trc_{promoter}$) was immobilized on the surface of Biacore Sensor Chip SA (to a level of 400) using the manufacturer's recommendations. A serial dilution of the ^{His}MinE was prepared by dilution in storage buffer with 5% glycerol, supplemented with 0.005% Tween-20. After recording the background for 100 seconds, the protein was injected for 200 seconds. Then, the same buffer was flown in to study the dissociation for more than 300 s followed by a 30s surface regeneration step with regeneration buffer; 50 mM NaOH, 500 mM NaCl. All sensorgrams were corrected for unspecific binding, by subtracting the signal that was measured in a flow-cell that lacked immobilized DNA.

2.13 Microscale Thermophoresis

Binding of ^{His}MinD or ^{His}MinE to 30 bp dsDNA (Alexa Fluor®488-labeled) was studied with Microscale Thermophoresis (reviewed in Jerabek-Willemsen et al. 2014) using a Monolith N.T.115 BLUE/RED Instrument (Nanotemper Technologies). A serial dilution of the proteins was prepared in storage buffer (with 5% glycerol instead of 10%) followed by the addition of 75 nM of Alexa Fluor ™ 488-labeled DNA as well as 0.05 mg/ml BSA, 0.005% Tween-20, 1 mM ATP and 5 mM $MgCl_2$ (concentrations are final concentrations). Monolith™ NT.115 Standard Treated Capillaries were used, filled with sample originating from a 10 µl reaction. After performing a capillary scan, the thermophoresis of the labeled DNA probe was measured with the following settings: LED power (90 %), MST laser power (40%), fluorescence before (5 s) and fluorescence after (30 s). Binding is expressed as F_{norm} (F_{hot}/F_{cold}). F_{cold} is the homogeneously distributed fluorescent signal in the capillary before applying the temperature gradient. F_{hot} is the fluorescence distribution in the area which is heated by the IR laser.

3 Results

3.1 DNA-binding by wild type and mutant MinD proteins

3.1.1 Rational mutagenesis of MinD to characterize the DNA-binding surface

The surface of MinD that participates in DNA-binding is not known, despite the extensive mutagenesis study of MinD performed by (Di Ventura et al. 2013). Mutations that affected the DNA-binding, involved residues facing the membrane and are therefore unavailable for binding when MinD is lipid-bound. Proteins that bind non-specifically to DNA usually do so via surface-exposed positively charged residues, not necessarily via a specific protein fold. In order to screen for the presence of such residues, we constructed a small library of mutants that have N-terminal positive residues exchanged with negative ones. The selected residues could provide plausible DNA-binding sites since they are solvent accessible and not buried in the MinD-dimer or MinD-membrane interface (Figure 11).

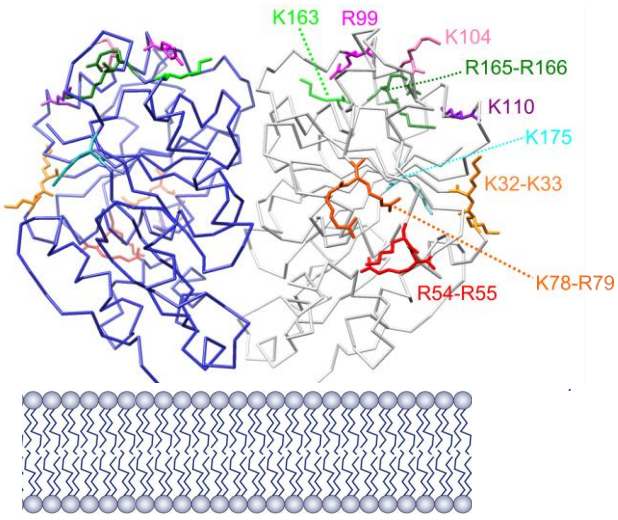

Figure 11| MinD N-terminal residues tested for DNA-binding. Crystal structure of a MinD dimer (PDB: 3Q9L). The individual MinD monomers are shown in blue and grey. Mutant versions of MinD were constructed by changing the indicated colored residues into glutamic acid acid (E). When double mutations were made, the residues are indicated separated by "-", e.g. R165-R166. The orientation of the MinD dimer was taken from (Wu et al. 2011). I constructed this figure with Chimera.

Wild type MinD and its mutants were cloned in the pET-28a vector (by Yuho Kuda) and transformed in the *E. coli* Rosetta expression strain followed by purification of the proteins (Materials and Methods, 2.3). MinD$^{K32E-K33E}$ was the only mutant that did not yield a stable/soluble product. All the other proteins could be purified.

3.1.2 Characterization of MinD mutants with reduced DNA-binding activity

The DNA-binding properties of the mutants shown in Figure 11 were studied with Electrophoretic Mobility Shift Assays (EMSAs). The mutants that displayed a reduction in DNA-binding are shown in Figure 12 A-C**.** I believe that the decrease in binding affinity is not simply due to the fact that I exchanged positive residues for negative ones, since mutating other positive residues such as K104, K163, R165/R166 and K175 for glutamic acid did not have an effect (data not shown). Morever, these mutations did not necessarily lead to loss of binding to negatively charged phospholipid vescicles (Figure 2D), thus suppiting my idea that the effect I see on DNA-binding is not only a matter of introducing negative chargers. For instance, MinD^{R99E} and MinD^{K110E} could bind to lipid vesicles in a comparable manner to MinD^{WT} (Figure 2D), all the while showing a reduction in DNA binding.

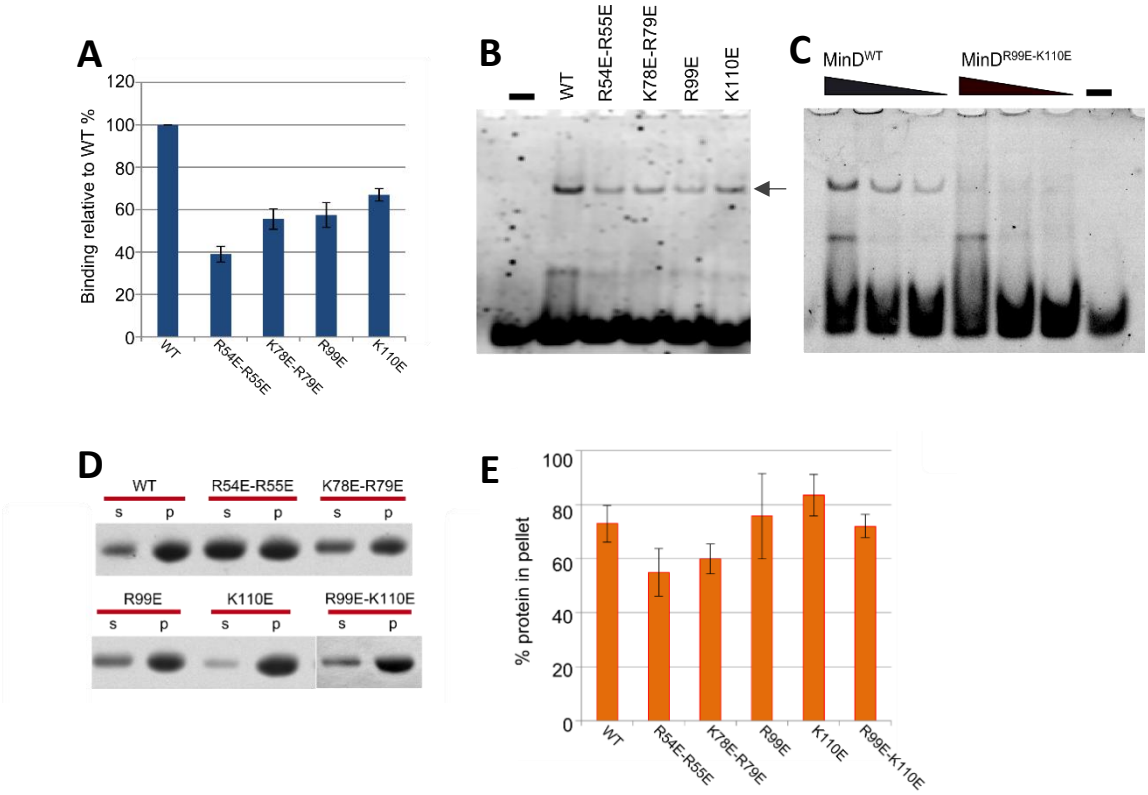

Figure 12 | **Interaction of MinD mutants with DNA and the lipid bilayer. A|** DNA-binding of MinD and the indicated mutants was studied with Electrophoretic Mobility Shift Assays (EMSAs). 5 µM of protein was incubated with 1 mM ATP and 50 nM fluorescently labeled 30 bp double-stranded DNA (P1-promoter), followed by separation on a 6% native acrylamide gel. The nucleoprotein band (arrow in panel B) was quantified and normalized to the signal for MinD^{WT}. The bars represent the mean ± S.E.M from 3 experiments. **B|** Typical result of an EMSA described in A. **C|** EMSA with MinD^{WT} and MinD$^{R99E-K110E}$ at 6 µM, 3 µM and 1.5 µM (from left to right). **D|** Interaction between MinD (mutants) and *E. coli* lipid vesicles. 6 µM of protein was incubated with 320 µg ml^{-1} lipid vesicles from *E. coli* total lipid extract. After 10 minutes of incubation at RT in the presence of 1 mM ATP, samples were spun down at 20.000 g. The protein content of the supernatant and pellet was analyzed with SDS-page followed by staining with Coomassie Brilliant Blue. **E|** Quantification of the results shown in panel D. The intensity of the protein bands in the supernatant and pellet were measured in ImageJ. Bars represent the mean of 2 experiments with S.E.M.

Those two MinD mutants were also able to oscilate from pole to pole with MinE-YFP and recruited MinC to the membrane leading to a division block and cell filamentation (Figure 13). For this reason the double mutant MinD$^{R99E-K110E}$ was constructed. It seemed to behave like wild type MinD (Figure 13), except for a reduction in DNA-binding (Figure 12) making it a suitable candidate for studying the effect of having reduced DNA-binding *in vivo.* The two other double mutants, MinD$^{R54E-R55E}$ and MinD$^{K78E-K79E}$, despite having the lowest affinity for DNA, showed also a diminished interaction with the lipid bilayer (Figure 12) and protein partners MinE and MinC (Figure 13), thus being inappropriate for further *in vivo* analyses.

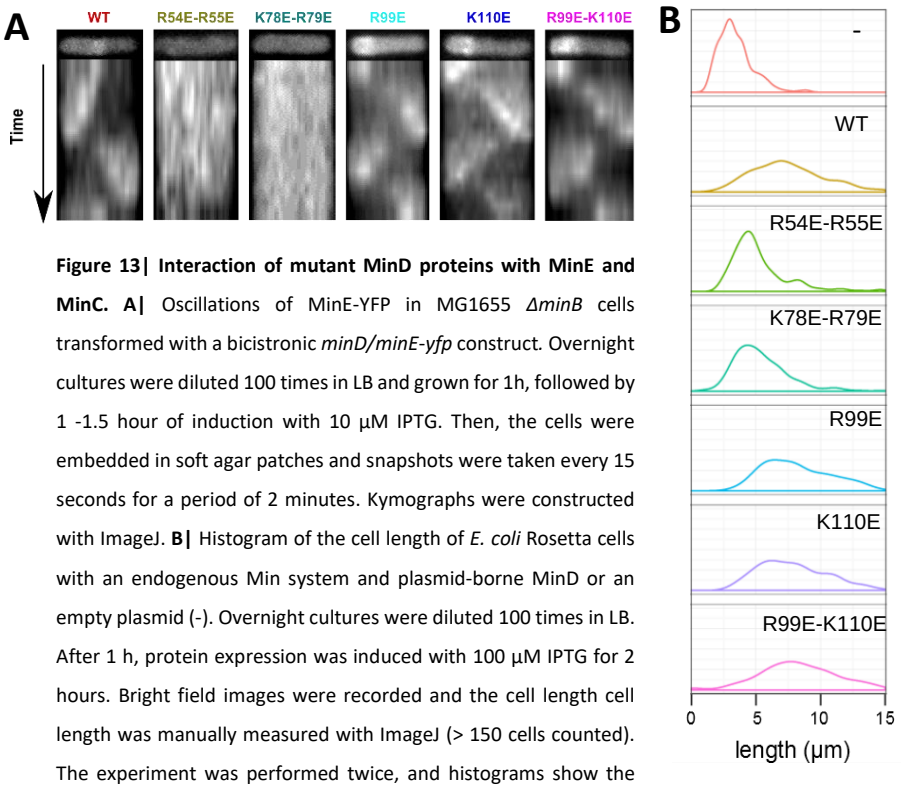

Figure 13| Interaction of mutant MinD proteins with MinE and MinC. A| Oscillations of MinE-YFP in MG1655 *ΔminB* cells transformed with a bicistronic *minD/minE-yfp* construct. Overnight cultures were diluted 100 times in LB and grown for 1h, followed by 1 -1.5 hour of induction with 10 µM IPTG. Then, the cells were embedded in soft agar patches and snapshots were taken every 15 seconds for a period of 2 minutes. Kymographs were constructed with ImageJ. **B|** Histogram of the cell length of *E. coli* Rosetta cells with an endogenous Min system and plasmid-borne MinD or an empty plasmid (-). Overnight cultures were diluted 100 times in LB. After 1 h, protein expression was induced with 100 µM IPTG for 2 hours. Bright field images were recorded and the cell length cell length was manually measured with ImageJ (> 150 cells counted). The experiment was performed twice, and histograms show the pooled data of the independent experiments.

3.1.3 In vivo analysis of the MinD^{R99EK110E} double mutant

To explore the effect on chromosome segregation *in vivo,* I wanted to study a mutant that binds less to the DNA while still being able to oscillate and properly place FtsZ-ring at midcell. MinD$^{R99E-K110E}$ seems to be a suitable candidate for this purpose. First, I constructed a plasmid that contains the *minB* operon starting from the transcription start site (+1 position) under the control of the arabinose promoter (pBAD33-*minB*). The R99E and K110E mutations in MinD were subsequently introduced using a mutagenesis PCR reaction. The expression levels were such that the mini-cell phenotype of the *ΔminB* strain (TB43; kindly provided by Derek Lau and Thomas Bernhardt) was complemented, which can be seen from the lack of minicells and the homogenous cell size distribution upon expressing *minCDE* (Figure 14A). For the mutant, the size distribution was a bit more heterogenous, and the cells were longer on average (Figure 14A).

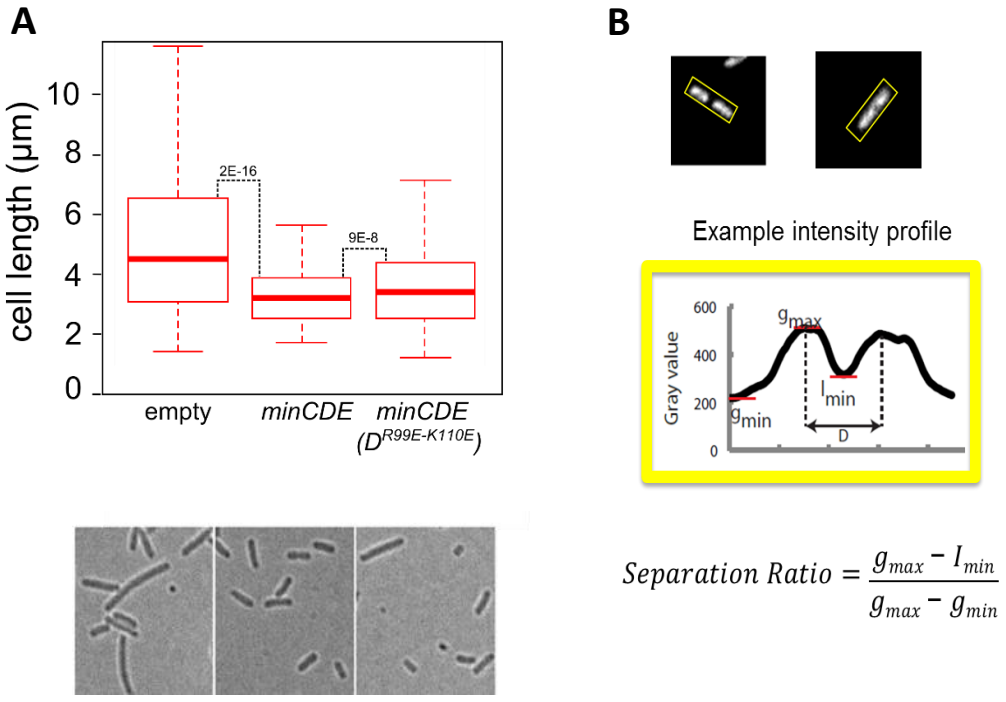

Figure 14| Complementation of the *ΔminB* minicell phenotype by plasmid-borne *minCDE*. A| The WT *minB* operon or the operon containing MinD$^{R99E-K110E}$ were expressed from the pBAD33 plasmid in MG1655 *ΔminB* cells (TB43). Empty refers to the negative control which only contains an empty plasmid. For each condition, the cell length of more than 450 cells was measured with ImageJ and the results were visualized in a box-plot. P-values were obtained from the Student`s *t*-test and are indicated between the boxes. Representative microscopy images are shown below the graph. **B|** Quantification of bulk chromosome segregation using the intensity profile of DAPI-stained nucleoids. Only cells with a bilobed nucleoid (2 peaks in the intensity profile) were analyzed. Both the distance between the peaks and the segregation ratio; ratio between the maximum peak intensity (I_{max}) and the minimum intensity between the peaks (I_{min}) were measured.

In order to study the segregation of the chromosome, I analyzed the DAPI-stained nucleoids according to the procedure described in (Di Ventura et al., 2014) (Figure 14C). The presence of the Min system with WT MinD clearly results in better separation (R) of the chromosomes as reported before (Akerlund et al. 1992; Åkerlund, Gullbrand & Nordström 2002; Di Ventura et al. 2013) (Figure 15). This effect was more pronounced in larger cells. I also observed that the distance between the two segregated nucleoids tends to be larger for cells that contain *minCDE,* but this effect was not significant. The effect of MinD$^{R99E-K110E}$ on chromosome segregation is mixed. Small cells with a size between 3 and 4 µm resemble the wild type situation, while larger ones with a size of 4 to 5 µm show larger defects (Figure 15).

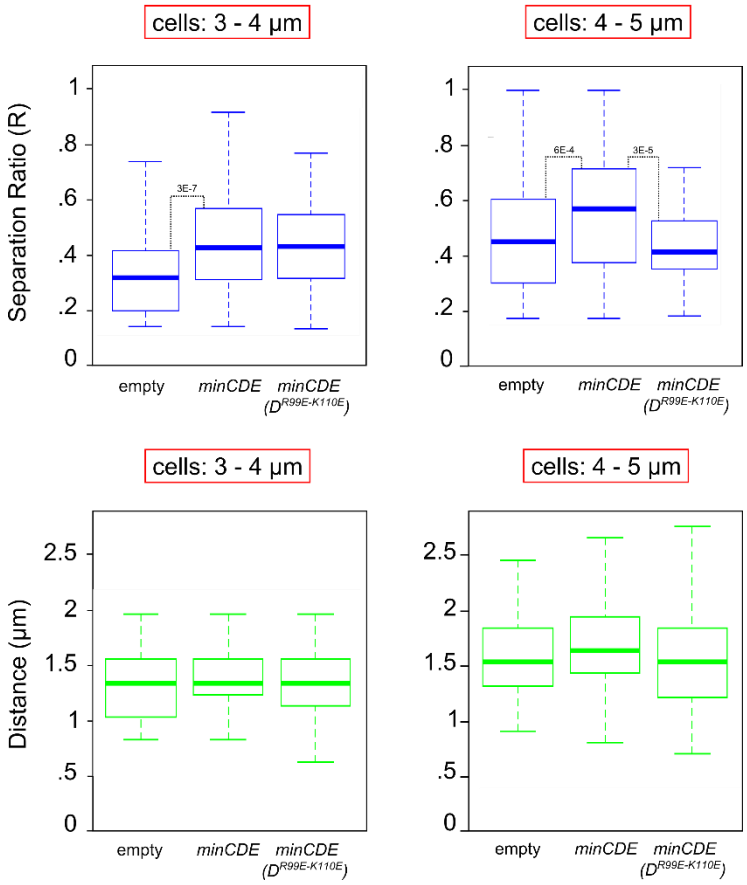

Figure 15| Comparison of chromosome segregation in cells with WT or mutant MinD. Nucleoids from cells harboring the indicated constructs were analyzed to extract the chromosome segregation ratio (R) and the distance (D) between the duplicated chromosomes. Only cells with a bilobed nucleoid were suitable for extracting the values for R and D. For cells with a size between 3 and 4 µm, 62, 138 and 159 intensity profiles could be analyzed for respectively *empty*, *minCDE* and *minCD$^{R99E-K110E}$E*. For larger cells (4 and 5 µm) those numbers were; 59, 62 and 159. As a test for significance, a Student`s *t*-test was performed. *P*-values > 0.05 are not shown.

If MinD$^{R99E-K110E}$ would interact properly with MinC and MinE at these expression levels, the small elongation of the cells could be explained solely by the presence of unsegregated chromosomes at mid-cell. SlmA blocks placement of the Z-ring on top of these unsegregated chromosomes (SlmA, Bernhardt & De Boer 2005) while the Min system blocks polar cell divisions leading to cell filamentation. To verify this, we repeated the experiment in a strain that is devoid of SlmA (TB115; *ΔminB/ΔslmA*). Absence of SlmA by itself does not affect the cell phenotype (Bernhardt & De Boer, 2005) due to the redundancy of septum placement control. The double knockout *ΔminB/ΔslmA* has a lethal phenotype in rich medium. When both negative regulatory systems are absent, FtsZ ring formation is not restricted to the cell middle. This leads to the formation of many rings that do not always reach the critical amount of components to form a mature ring (Bernhardt & De Boer 2005). Growing the cells in a less-rich medium is thought to result in higher FtsZ levels and overcomes the lethality. The medium I used: M9 supplemented with 0.4% glucose and 0.2 % CAS-amino acids is such a medium (Bernhardt & De Boer 2005).

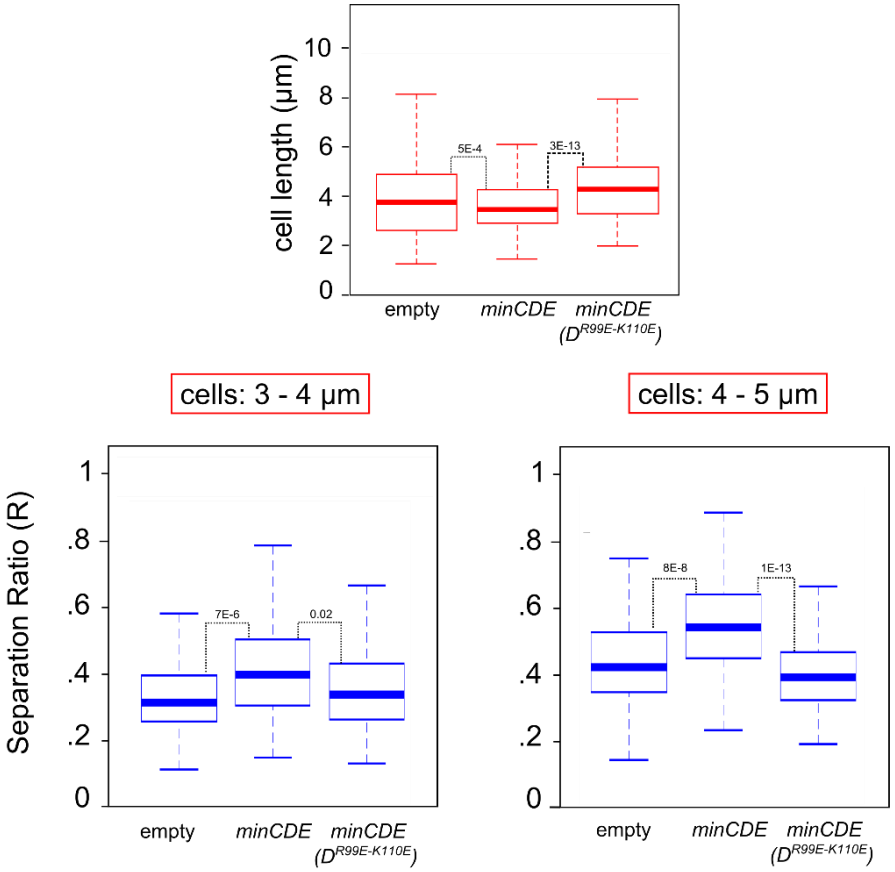

Figure 16| Effect of the Min system on chromosome segregation in a strain without SlmA (MG1655 *ΔminB/ΔslmA*). The *minB* operon was expressed from the pBAD33 plasmid in strain TB115. The total cell length was measured for 233, 258 and 527 cells for respectively *empty*, *minCDE* and *minCD$^{R99E-K110E}$E*. Among those cells, 43, 83 and 187 had a length between 3 and 4 µm and a bilobed nucleoid. For cells ranging from 4 and 5 µm, those numbers were 66, 47 and 148. A Student`s *t*-test was performed and only *p*-values < 0.05 are indicated in the image.

The minicell phenotype of a *ΔminB/ΔslmA* strain (TB115) could be complemented with the same plasmid-borne Min system as described before and as expected (Figure 16). The positive effect on chromosome segregation could be reproduced as well (Figure 16). For the mutant, the cells were actually longer than the wild type, but also longer than a strain without a Min system. This most likely indicate that under these conditions, even small changes in the Min oscillation pattern and thus localization pattern of MinC/MinD$^{R99E\text{-}K110E}$ could affect and most likely block septum formation everywhere resulting in a division block, which is more pronounced in the absence of SlmA.

The expression levels that are required to mimic the endogenous situation and complement a minicell phenotype are lower than the levels required for observing MinD/MinE-YFP oscillations. The higher expression levels that we used in the initial screens to study the interaction between MinD$^{R99E\text{-}K110E}$ could have masked potential defects in the interaction with MinE or MinC.

3.1.4 MinD ATPase activity

Some of the members of the Walker type ATPases family to which MinD belongs also function in chromosome segregation or plasmid partitioning. Their ATPase activity is stimulated by their cognate protein partner in the presence of DNA, which can result in dynamic movements onto the nucleoid and in pulling of the nucleoprotein complex towards the pole (Marston & Errington, 1999; Ebersbach & Gerdes 2004; Vecchiarelli, Mizuuchi & Funnell 2012). We wanted to investigate if the ATPase activity of MinD is influenced by DNA in presence and absence of lipids. To this aim, I first incubated MinD and MinE with ATP. In the absence of liposomes, the rate of ATP hydrolysis under these conditions resembled the basal hydrolysis rate produced by MinD alone (not shown).

Then, different kinds of DNA (purified plasmid, sheared genomic *E. coli* DNA and a 150 bp synthetic double stranded DNA) were added to the reaction. The presence of DNA did not change the ATP hydrolysis activity of MinD (Figure 17A). Addition of liposomes to MinD and MinE trigged a ± 7-fold increase in ATP hydrolysis by MinD, as previously documented (Hu & Lutkenhaus 2001; Suefuji, Valluzzi & RayChaudhuri 2002). When the different kinds of DNA were added to the samples that contained liposomes only a small decrease in ATP consumption was observed (Figure 17B). It could be speculated that DNA slows down ATP hydrolysis and thus enhances the lifetime of the MinD-DNA interaction.

3.2 Genome-wide binding by MinD

Given the proposed function of MinD in chromosome segregation and the lack of apparent sequence specificity seen so far in our *in vitro* studies, we wanted to investigate the genome-wide binding profile of MinD using ChIP-Seq. Since there are no commercial antibodies available for MinD, a proper tag was needed for the immunoprecipitation. First, I fused N-terminally to MinD either the FLAG- or the His-tag using a short spacer (GSS linker). Unfortunately, it turned out that the cognate antibodies did not pull down these tagged proteins efficiently especially after crosslinking of the samples (see Figure 18 for ^{FLAG}MinD; ^{His}MinD not shown).

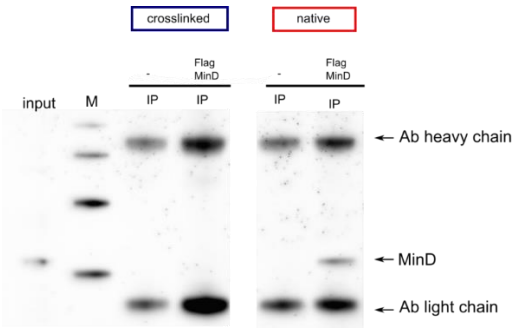

Figure 18|Immunoprecipitation (IP) of ^{FLAG}MinD from *E. coli* cell lysates (native or crosslinked). *E. coli* MG1655 cells with an empty plasmid (-) or ^{FLAG}MinD were grown until exponential phase. The samples were split in two, one part of the sample was left untreated (native) while the other half was crosslinked with formaldehyde. Cells were lysed by sonication and a small aliquot of the crosslinked ^{Flag}MinD sample was taken to serve as input control (input). Magnetic beads coated with the ANTI-FLAG® M2 antibody (Sigma Aldrich) were used for the IP. The IP fractions were analyzed with Western Blot using the same primary antibody as used for the IP, followed by incubation with α-mouse-HRP and ECL for detection.

Therefore, I continued with a His-tag that was connected to the protein by a longer linker that also includes a T7-tag. This is the exact same tag that is used when proteins are expressed from the commonly used pET28 plasmid. The advantage of the His-tag is that it allows pulling down the nucleoprotein complexes without antibodies using Nickel-coated (Ni-NTA) beads instead. This procedure is compatible with denaturing conditions (Ishikawa et al. 2007) in contrast to the procedure requiring antibodies, which would unfold and lose activity in denaturing conditions. Denaturation could unmask a potentially hidden tag, which is an advantage. Figure 19 shows the workflow that I employed for the ChIP-Seq study.

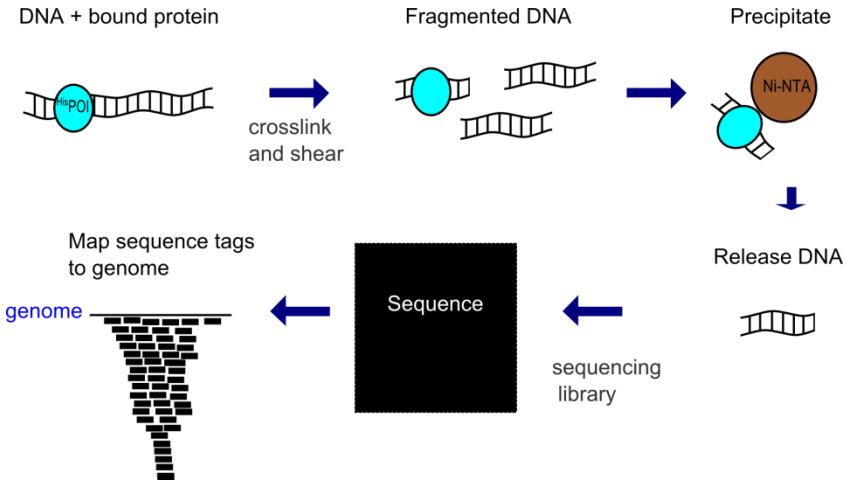

Figure 19| Cartoon of the ChIP-Seq procedure. *E. coli* cells carrying the His-tagged protein of interest (^{His}POI) are grown until mid-exponential phase followed by crosslinking with formaldehyde. The cells are lysed by sonication which also shears the DNA. Crosslinked ^{His}POI-DNA fragments are captured with Ni-NTA beads. After crosslink removal, the DNA is purified and a sequencing library is prepared (by the Cell Networks Core Facility) by adding Klenow fragments that function as barcodes. After sequencing, the sequenced reads are mapped to genome and peak calling algorithms were used to identify the binding regions.

3.2.1 Genome-wide DNA-binding by MinD, pilot experiment

As a starting point, I prepared samples for ChIP-Seq experiments that contain ^{His}MinD overexpressed in the wild type MG1655 strain and in MG1655 with a Min system knockout (*ΔminB*). The library preparation and the sequencing were done by the CellNetworks Deep Sequencing Core Facility while the subsequent data analysis was done by a variety of collaborators from the *eilslabs*. MinD-DNA-binding peaks were distributed randomly across the genome without macro domain preference (Figure 20). These results were found with two different methods for peak calling: Model-based Analysis of ChIP-Seq (MACS) (done by Naveed Ishaque), which is suitable for finding narrow peaks like single protein-DNA-binding events, as well as SICER (done by Roman Kurilov). The latter algorithm is more commonly used for finding binding peaks with a wider distribution.

As a positive control for the procedure and to exclude that the His tag might lead to un-physiological binding of the tagged protein to the DNA, I included the protein SeqA in my experiments. SeqA binds with high affinity to hemi-methylated GATC motifs (Han et al. 2004) that arise behind the replication fork, before the newly synthesized strand is methylated by Dam methylase (Kang et al. 1999). The genome-wide binding by SeqA has been already characterized with ChIP-chip (Sánchez-Romero et al. 2010; Waldminghaus et al. 2012), thus it is known that highly transcribed regions and the Ter MD are less often occupied by SeqA. In the Ori MD, where GATC motifs occur more frequently, SeqA binds even in the absence of methylation, albeit with lower affinity. The known motif of SeqA and the characteristic genomic distribution make SeqA a good control. Under our experimental conditions, we

could find the depletion of binding events in the Ter MD, but a motif search only yielded a partial binding motif (ATC). The motif search was executed by Suda Parimala Ravindran and Carl Herrmann.

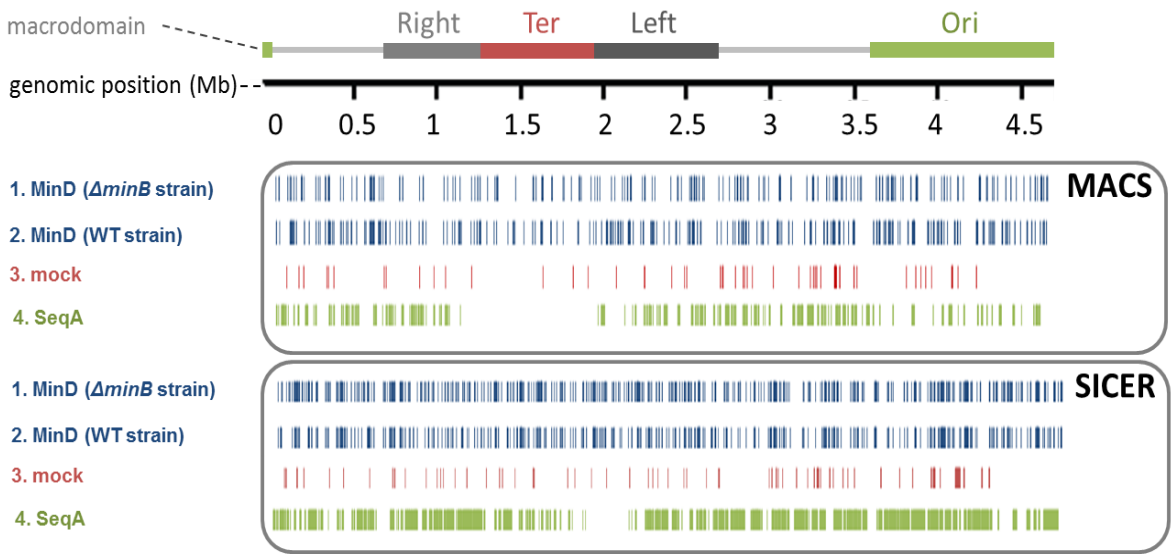

Figure 20| Distribution of MinD and SeqA binding peaks across the genome. Sequenced reads were aligned to the *E. coli* reference genome and peaks were called using MACS (by Naveed Ishaque) or SICER (by Roman Kurilov). MinD binding peaks are randomly distributed, while the SeqA binding profile indicates depletion of binding around the Ter MD.

3.2.2 ChIP-Seq at nearly endogenous expression levels

The results so far originated from samples with high levels of MinD and SeqA, which represent an un-physiological state. To get a better approximation of the endogenous situation, I prepared samples in which the His-tagged proteins were expressed at low levels (basal expression from Trc promoter in the absence of the IPTG inducer). ChIP-Seq experiments were performed on two different days with at least two biological replicates each time. Sebastian Steinhauser analyzed all the data originating from the samples with lower expression levels. For SeqA, sharp peaks could be observed, with binding signals being highly enriched above the background. A comparison between low and high levels of SeqA clearly shows that peaks are a lot broader and less defined at high protein levels (Figure 21). This is likely due to spreading of the protein towards lower affinity binding sites, which become occupied when the protein is expressed at high levels.

Expressing MinD at low levels did not change the results obtained with higher levels, i.e. distinct binding peaks could not be detected (Figure 21). Genome-wide correlation analysis of the signals actually showed that MinD samples mainly cluster together with the negative control (Supplementary Information, Figure 44). These data suggest that binding of MinD to the chromosome is rather non-sequence-specific. Furthermore, there was no difference between results obtained in the wild type strain, where ^{His}MinD could interact with the endogenous Min system and oscillate, and those obtained in the *ΔminB* strain, where ^{His}MinD would be simply statically membrane-bound (not shown).

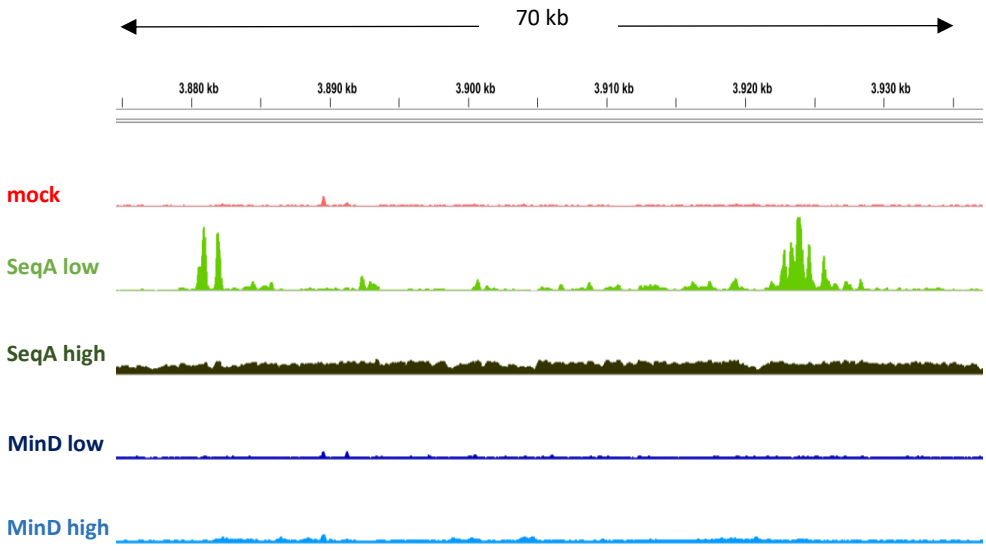

Figure 21| Representative genomic region with ChIP-Seq binding profiles of the indicated proteins in *E. coli* MG1655. Proteins tagged with the His-tag were expressed from the pTrc99a plasmid. The basal expression levels are referred to as low; higher expression was obtained by a 2-hour induction period with 1 mM IPTG.

3.2.3 Motif analysis

To further characterize the DNA-binding behavior of the proteins, the obtained peaks were scanned for the presence of sequences logos with different algorithms by Sebastian Steinhauser (Figure 22A). This approach yielded the highly significant GATC motif for SeqA, which is the known binding motif. No significant motifs were found specifically for MinD using a similar approach. The specificity of the SeqA binding, and the lack of specificity for MinD is also illustrated in the Supplementary Information, Figure 45.

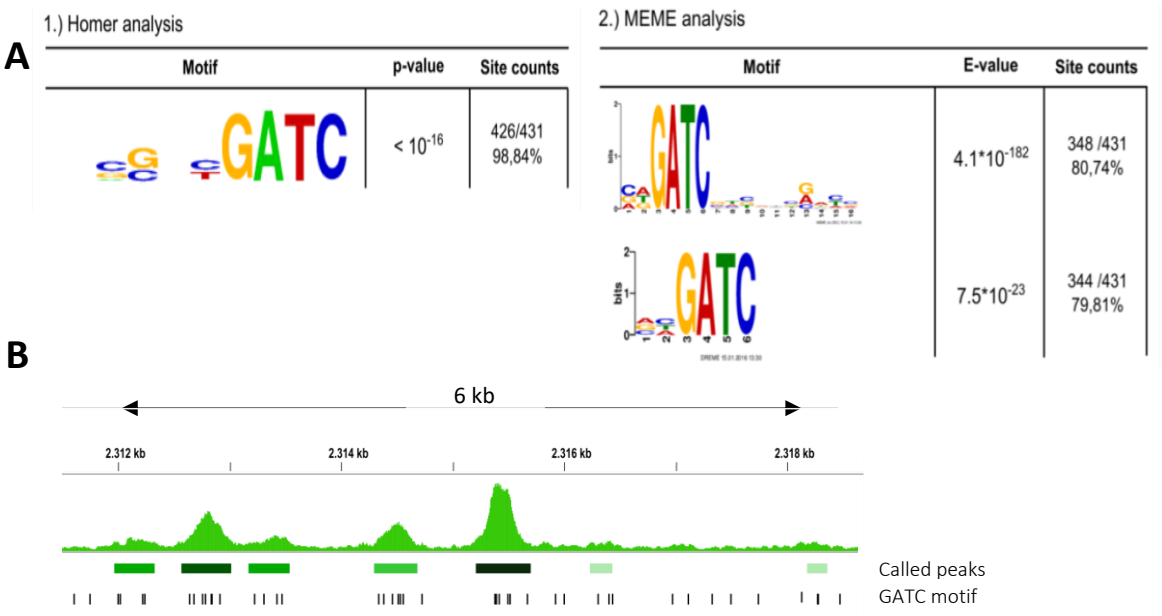

Figure 22| Validation of the peak calling algorithm and motif search using the positive control ^{His}SeqA. A| The known GATC motif of SeqA could be recovered with high significance using two different motif search algorithms, MEME and Homer. The image was provided by Sebastian Steinhauser. **B|** Representative SeqA binding peaks. The green horizontal lines mark the called peaks; the black vertical bars indicate the location of the GATC motif.

3.3 Transcriptome analysis in cells with and without the Min system

To complement our ChIP-Seq data, I wanted to investigate the influence of the Min system on the gene expression profile of *E. coli* using microarray analysis. Therefore, total RNA was extracted from the *E. coli* MG1655 wild type and *ΔminB* strains in order to analyze the effect of the Min system on the *E. coli* transcriptome (3 independent replicates each). Since the array provided space for 8 samples in total, I added to the experiment the *ΔminB* strain supplemented with plasmid-borne MinD (2 replicates).

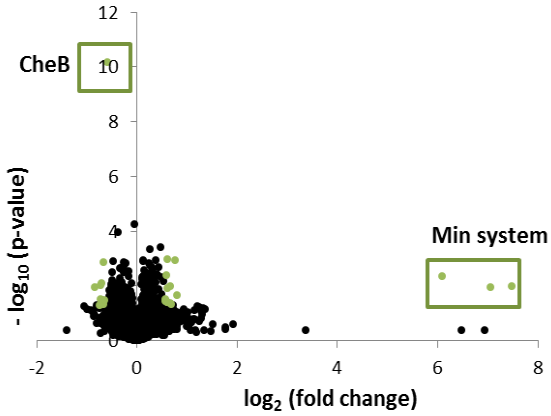

Figure 23| Comparison of the transcription profiles of MG1655 wild type and *ΔminB* strains. Significant (*p*-value < 0.05, Student's *t*-test) and differentially expressed genes (fold change > 1.5) are displayed in green. After adjusting the *p*-value for multiple testing (Bon Feroni) only MinCDE and the chemotaxis regulator CheB remained significant (green boxes).

When comparing the wild type and the *ΔminB* strains, only few genes were differentially expressed using the criteria of fold change > 1.5 and significance *p*-value < 0.05 (Student´s *t*-test, Figure 23). After adjusting the *p*-value for multiple testing (Bon Feroni), only MinCDE and the chemotaxis regulator CheB remained significant. Usage of different statistical tests gave similar results (SAM tools, ROTS, analysis done by Tobias Bauer). Unfortunately, for the samples corresponding to the *ΔminB* strain expressing plasmid-borne MinD (N=2), there was too much noise in the data, which did not allow us to draw any conclusion (one sample resembled the WT while the other was more similar to the *ΔminB* strain.

3.3.1 KEGG pathway analysis

In order to see wheter a cluster of genes involved in the same cellular process was affected, we used less stringent significance criteria and performed a gene ontology and pathway analysis (Tobias Bauer). The KEGG (Kyoto Encyclopedia of Genes and Genomes) database was used for exploring wheter our 100 most significantly affected gene were enriched in a particular pathway. It turned out that genes involved in flagellar assembly and bacterial chemotaxis were slightly upregulated in absence of the Min system (Figure 24). Furthermore, some genes involved in arginine and proline metabolism were either up- or down-regulated (Figure 24).

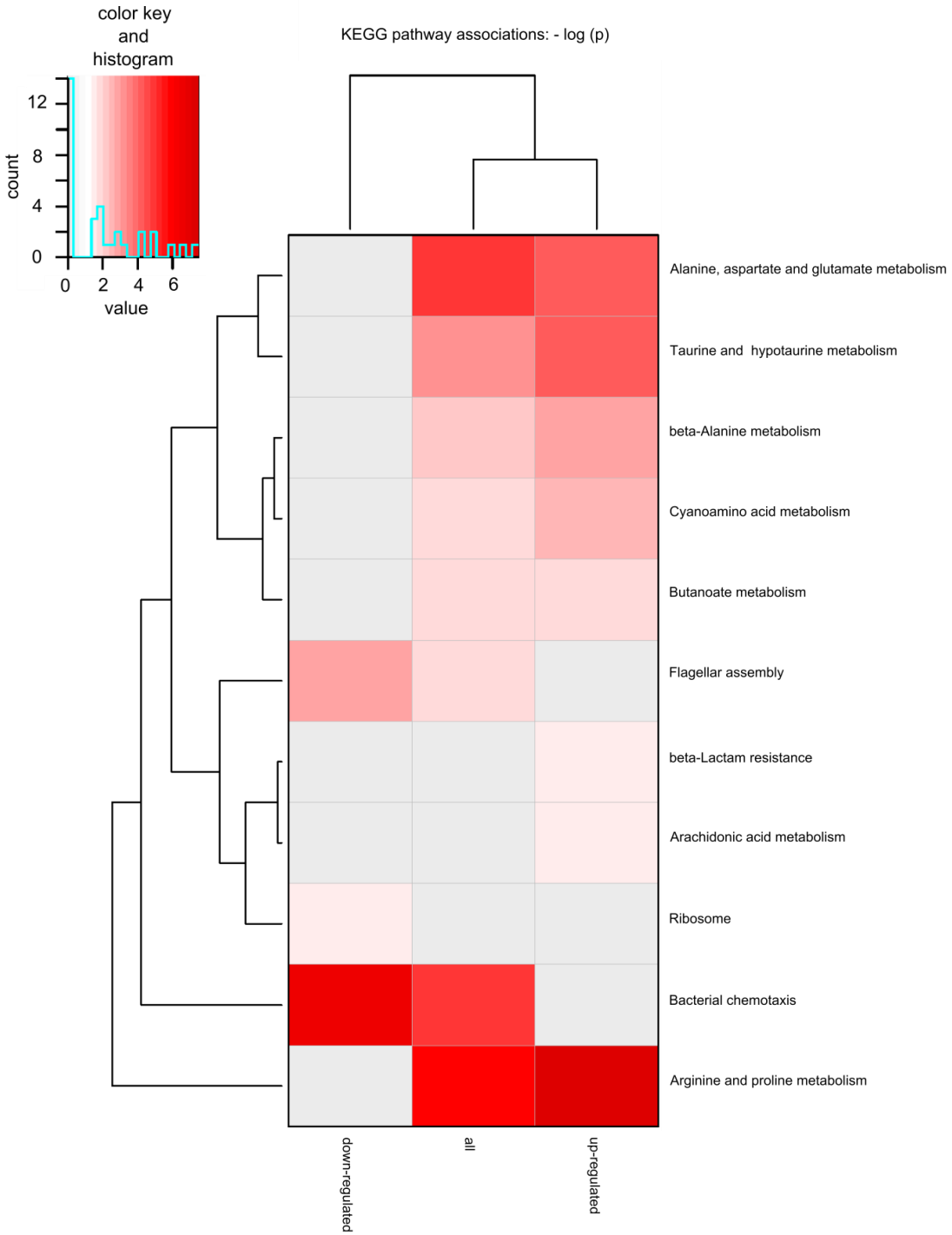

Figure 24| **KEGG pathway enrichments analysis using the top 100 most significant differentially expressed genes**. RNA Expression levels from the wild type *E. coli* MG1655 cells were compared with those from the *ΔminB* strain. The top 100 most significantly affected genes were used to perform the KEGG enrichment analysis. Downregulated refers to higher expression levels in the *ΔminB* strain compared to the wild type, while upregulated means the opposite (analysis and image provided by Tobias Bauer).

gene	Description	*p*-value	Fold change
cheB	fused chemotaxis regulator: protein-glutamate methylesterase in two-component regulatory system with CheA	6.4E-04	0.66
motB	protein that enables flagellar motor rotation	7.8E-04	0.70
cheR	chemotaxis regulator, protein-glutamate methyltransferase	2.1E-03	0.72
cheY	chemotaxis regulator transmitting signal to flagellar motor component	5.9E-03	0.72
motA	proton conductor component of flagella motor	7.2E-03	0.67
flgN	export chaperone for FlgK and FlgL	1.1E-02	0.70

Table 4| Selected genes involved in chemotaxis and flagellar assembly.

3.3.2 Experimental analysis of the motA and tar promoters

In order to verify whether the Min system is involved in the regulation of genes of the chemotaxis or flagellar assembly pathways, I decided to measure the promoter activity af the affected operons using a reporter gene (Figure 25A). Therefore, I constructed reporter plasmids where The *tar* and *motA* promoter regions were used to drive expression of the *yfp* gene. The constructs were transformed in the wild type and *ΔminB* strains and the expression of the fluorecent protein was measured with flow cytometry. A gate was used to select cells of similar size. For the *tar* promoter, the differences in expression levels between the two strains were in the same range as the fold change levels in mRNA as found in the microarray (Figure 25B,Table 4). Expression of YFP from the *motA* promoter was barely detectable.

In order to enhance the signal with an enzymatic amplification step, I exchanged the *yfp* gene with the β-Galactosidase gene (*lacZ* gene). A strain with a knockout of the Lac operon (*lacIZY*) was used in order to eliminate background expression levels (TB28: *ΔlacIZY* and TB43: *ΔlacIZY/ΔminB*). In this strain and with this specific reporter assay, the effect of the Min system on expression of chemotaxis genes was not observed (Figure 25C).

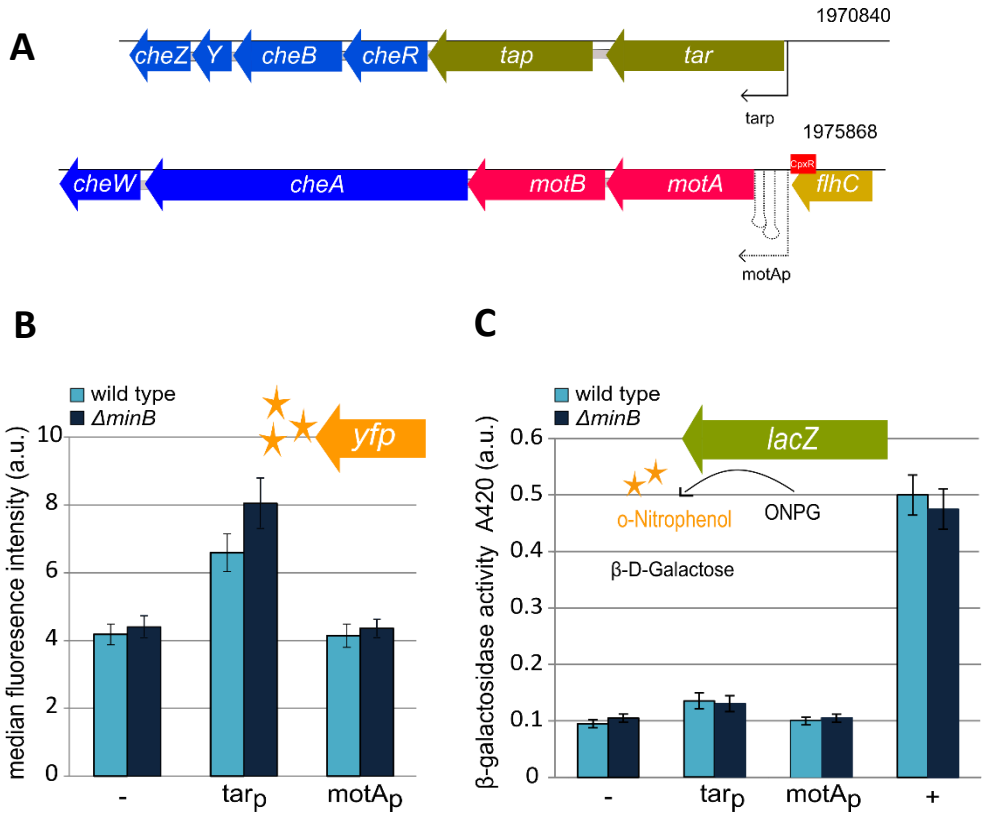

Figure 25| Activities of the *tar* and *motA* promoters in a wild type and *ΔminB E. coli* strain. A| Schematic representation of the operons that are controlled by the *tar* and *motA* promoters respectively. Image adapted from RegulonDB. **B|**A *yfp* reporter gene was placed under the control of the *motA* and *tar* promoters and expression levels were measured with flow cytometry. The negative control is an empty plasmid. Bars represent the median ± S.E.M. from 3 experiments. **C|** The *lacZ* reporter gene was placed under the control of the *motA* and *tar* promoters and the enzymatic LacZ activity was determined by measuring the absorption at 420 nm to follow the conversion of the substrate ortho-Nitrophenyl-β-galactoside (ONPG) to the yellow-colored O-Nitrophenol (and galactose) at 420 nm with a Tecan plate reader. The negative control represents an empty plasmid while the positive control is the *lacZ* gene expressed from the Trc promoter. Bars represent the mean ± S.E.M from 2 independent experiments.

No clear binding was found in the *motA* and *tar* promoter regions when using ChIP-Seq, indicating that gene regulation does not involve specific binding of Min proteins in the regulatory region. Further studies are needed to understand whether the observed modest increase in mRNA levels of the chemotaxis (*che*) genes could have a physiological effect. A functional comparison between the wild type and *ΔminB* strains regarding motility and chemotaxis would clarify our findings.

3.4 Biochemical analysis of the DNA-binding properties of the Min proteins

3.4.1 DNA-binding by ^{His}MinC-^{His}MinD complexes

As MinD in the cell interacts with MinC and MinE, I wanted to understand if these two proteins play a role in DNA-binding by MinD. To this aim, I cloned MinC and MinE in the pET28a vector and purified the proteins. Using Electrophoretic Mobility Shift Assays (EMSAs), I first tested if MinD could bind better to a short fluorescently labeled double-stranded (ds) DNA probe when in complex with MinC. In presence of ATP, I observed a remarkable increase in DNA-binding compared to the binding observed with the individual proteins (Figure 26A). The binding was ATP dependent, which is not surprising, since MinD is monomeric in the presence of ADP and not able to interact with MinC (Lackner, Raskin & de Boer 2003; Wu et al. 2011). I reasoned that a longer DNA-binding probe would provide more binding sites, thus allowing us better to study the binding behavior of the Min proteins despite their transient interaction with the DNA. Increasing the length of the DNA probe to 120 bp, did not enhance the apparent affinity (Figure 26B). I assume that I did not observe DNA-binding while MinC-MinD complexes do not form at lower protein concentrations (Hu, Saez & Lutkenhaus 2003).

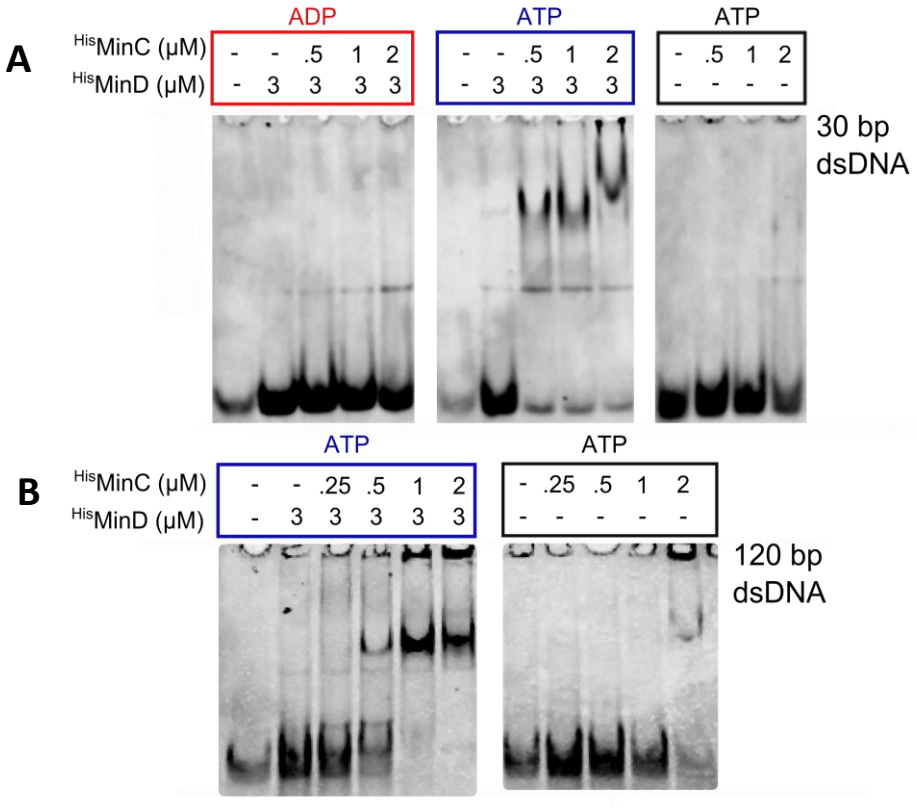

Figure 26| The MinC-MinD complex binds to DNA with a higher affinity than MinD or MinC alone. **A|**DNA-binding of MinC-MinD complexes was studied with EMSA. Purified proteins with His-tag were incubated at the indicated concentrations together with 50 nM of 30 bp dsDNA (HEX-labeled) in the presence of 1 mM nucleotide and 5 mM $MgCl_2$ in storage buffer, followed by separation on a 6% native polyacrylamide gel. The HEX-labelled DNA probe was visualized on a Typhoon™ Scanner equipped with a green laser. **B|** Binding of MinC-MinD complexes or MinC alone to 120 bp dsDNA. The conditions are like those in panel A except for the length of the DNA probe.

I realized that ^{His}MinC did not migrate far into the gel, likely due to the isoelectric point of the protein (pI: 7.8), which is only slightly below the pH of the running buffer (pH 8.2). This results in a low net negative charge on the protein and thus a poor migration rate during electrophoresis. The

nucleoprotein complexes are therefore stuck in the well, which became more apparent when the DNA probe was longer (Figure 26B).

3.4.2 Influence of the His-tag on MinC-MinD DNA-binding.

In order to reduce the pI of MinC, I decided to remove the His-tag from MinC using the thrombin cleavage site downstream of it. The T7-tag, located between the cleavage site and the protein, is still present (standard pET-28a expression vector).

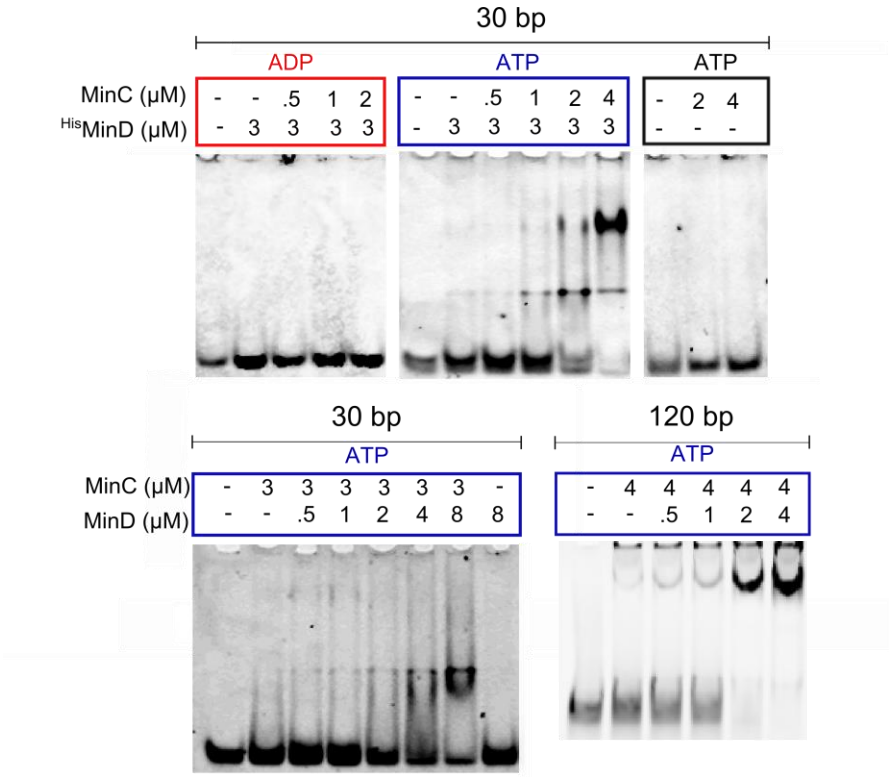

Figure 27| Influence of the His-tag on MinC-MinD binding to dsDNA. The DNA-binding properties of the purified Min proteins were studied with EMSA. Proteins were incubated in storage buffer with 50 nM of HEX-labeled dsDNA (30 or 120 bp) in the presence of 1 mM nucleotide and 5 mM $MgCl_2$, followed by separation on a 6% native bis-acrylamide gel. This figure shows representative results of at least 2 independent experiments.

Removal of the His-tag from MinC affected the way the nucleoprotein complexes ran into the gel when performing EMSAs with MinC and ^{His}MinD and appeared to reduce the overall binding (Figure 27). To investigate whether the His-tag influenced MinD too, I ran EMSAs with both proteins after removal of the His-tag. Indeed, when using MinC and MinD without His-tag, I saw the appearance of different bands (Figure 27). Moreover, the overall binding was further decreased compared to the situation in which the His-tag was present on MinD. The His-tag-free MinC-MinD complex binds well to a longer strand of DNA (Figure 27). This indicates that the His-tag influences the binding to the DNA of both MinC and MinD and their complex. For this reason, I opted to work later on only with proteins from which the His-tag is removed, unless otherwise mentioned.

3.4.3 Further characterization of DNA-binding by His-tag free MinC-MinD complexes

To understand the DNA-binding by the MinC-MinD complex, I kept one protein at a constant level while titrating the partner. In both cases, the binding curve followed a sigmoidal shape, indicating an apparent cooperative way of binding (Figure 28). The lack of DNA-binding at low protein concentrations likely reflects absence of MinC-MinD complexes, since the interaction between those proteins is weak at low concentrations (Hu et al. 2003). MinC seems to have a higher DNA-binding affinity by itself compared to MinD, but the estimated k_D is also overall weak (> 8 µM). Formation of MinC-MinD complexes lowers the k_D to an estimated 1 – 1.5 µM.

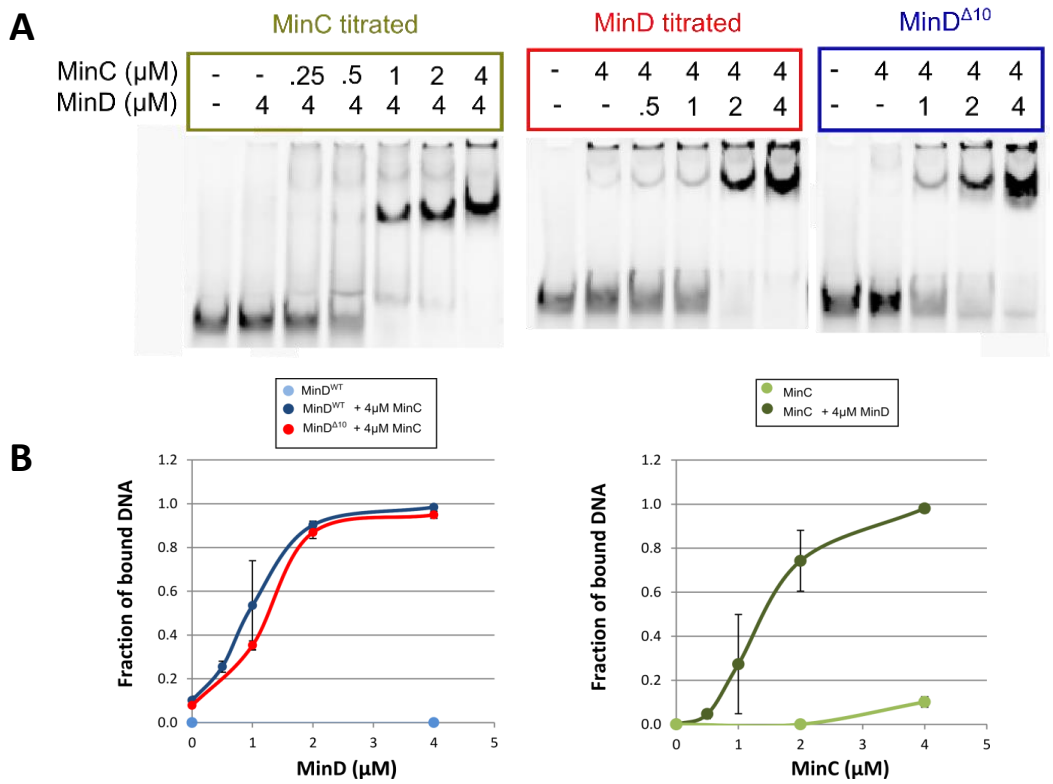

Figure 28| DNA-binding by MinD or MinD$^{\Delta 10}$ in complex with MinC. A| The DNA-binding of the purified Min proteins without His-tag was studied with EMSA. Proteins were incubated in storage buffer with 50 nM of HEX-labeled dsDNA (120 bp) in the presence of 1 mM ATP and 5 mM $MgCl_2$, followed by separation on a 6% native bis-acrylamide gel. This figure shows representative results of at least 2 independent experiments. The EMSA in which MinD^{WT} is titrated is similar to the one shown in Figure 27. **B|** Quantification of DNA-binding by MinC and MinD. The intensity of the HEX-labeled DNA bands from EMSA experiments (as the ones shown in Figure 28) was measured with ImageJ. The fraction of bound DNA was calculated as follows: bound / (bound + unbound). Each data point is the average of at least two individual experiments. Error bars represent S.E.M.

I also looked at the behavior of the mutant MinD$^{\Delta 10}$ which is structurally like the wild type protein, except that it lacks the membrane targeting sequence (last ten residues). Figure 28 shows that the complex of MinC-MinD$^{\Delta 10}$ behaves like the wild type complex. Thus, removal of the MTS does not influence the DNA-binding of the MinC-MinD complex. Since truncation of the MTS (MinD$^{\Delta 15}$) was not

capable of forming higher order structures together with MinC (Conti, Viola & Camberg 2015) it can be concluded that the polymers are not needed necessarily for DNA-binding *per se*. The concentrations of MinC and MinD used here are below the critical concentrations needed to form co-polymers, which further support this finding.

I then tested the effect of ATPγS on the MinC-MinD DNA-binding. It is known that this slowly hydrolysable ATP-analogue is still able to support MinD dimer formation, even though such dimers have a slightly reduced interaction with lipid vesicles (Hu, Gogol & Lutkenhaus 2002). In EMSAs, DNA-binding in presence of ATPγS was slightly worse in comparison to ATP (Figure 29).

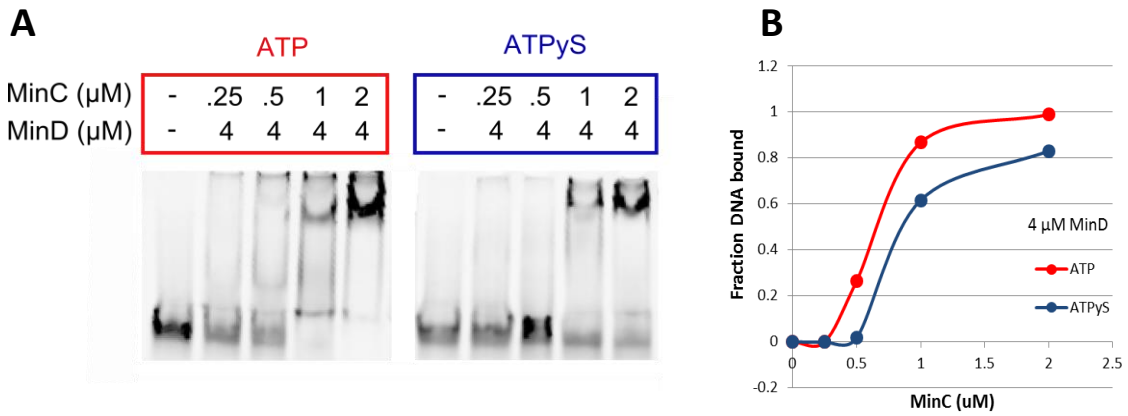

Figure 29|Comparison of ATP and ATPγS in supporting MinC-MinD DNA-binding. **A|**The binding of the purified MinD and MinC without His-tag was studied with EMSA. Proteins were incubated with 50 nM of HEX-labeled dsDNA (120 bp) in the presence of 5 mM $MgCl_2$, 1 mM ATP or 1 mM ATPγS followed by separation on a 6% native Bis-Acrylamide gel. **B|** The results from panel A were quantified with ImageJ.

3.4.4 Estimation of the minimal DNA length required for MinC-MinD DNA-binding

Next I wanted to determine the length of double stranded DNA which would result in optimal binding by MinC-MinD complexes. A fragment of 51 bp already led to detectable binding (Figure 30). The formation of high-molecular-weight (HMW) nucleoprotein complexes was more pronounced when MinC and MinD were both present at a concentration of 4 µM. A longer piece of dsDNA comprising 500 bp showed similar behavior, and was surprisingly still able to migrate into the gel despite its large size (Figure 30).

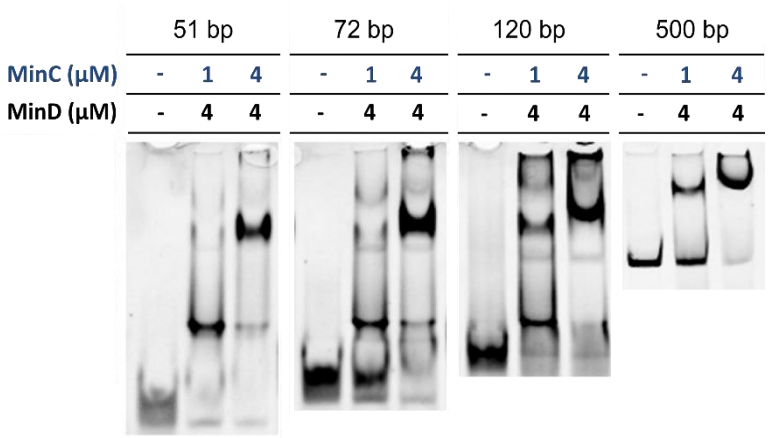

Figure 30|Representative EMSA that shows binding of MinC-MinD complexes to dsDNA of different lengths. Purified proteins were incubated with 50 nM HEX-labeled DNA probes of different lengths. The 51, 72 and 120 bp probes were generated by annealing of complementary oligos. The 500 bp product was synthesized by Navaneethan Palanisamy using a PCR reaction with a HEX-labeled forward primer. This experiment is done twice.

3.4.5 Role of MinE in DNA-binding.

The role of MinE in DNA-binding was investigated as well. I initially performed EMSAs with the His-tagged version of MinE. As for MinC, the tag influenced the way the protein migrated into the gel and caused nucleoprotein complexes to be stuck in the well (Figure 31A). After His-tag removal, the observed DNA-binding decreased drastically, but weak binding was still observed (indicated with the arrow in Figure 31A). Co-incubation with MinD did not lead to a significant increase in binding in contrast to what is observed for the complex of MinC and MinD (Figure 31B).

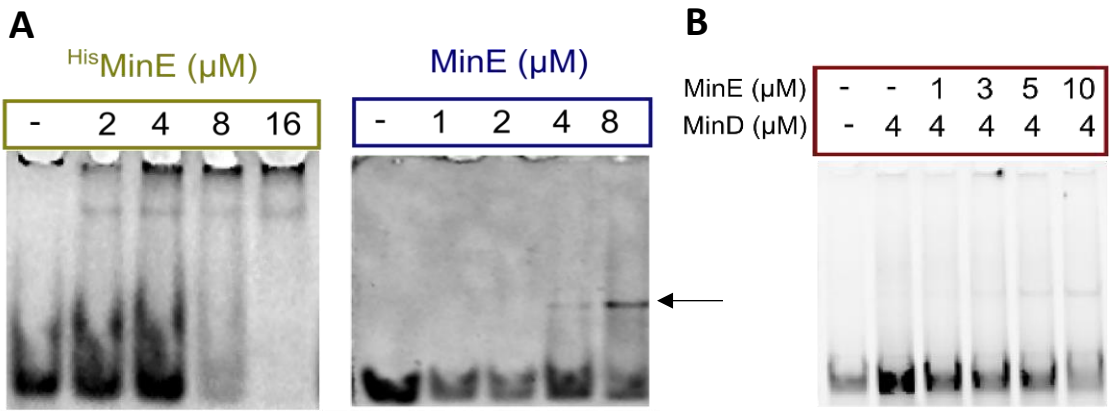

Figure 31|Characterisation of DNA-binding by ^{His}MinE and MinE with EMSA. A| An EMSA was performed with a 43 bp dsDNA (HEX-labeled) and purified proteins at the indicated concentrations. Proteins and DNA were incubated in storage buffer with 1 mM ATP and 5 mM $MgCl_2$ for 15 minutes followed by separation on a native gel. **B|** Binding of His-tag free MinD and MinE co-incubated at the indicated concentrations with HEX-labeled 120 bp dsDNA studied with EMSA.

To complement the EMSA experiments with a method that allows to study the DNA-protein interaction in solution, I continued with thermophoresis experiments. The interaction between MinE and DNA was very weak. Even at concentrations as high as 50 µM, no saturated binding was observed (Supplementary Information, 5.5., Figure 48).

3.4.6 Co-sedimentation of DNA by lipid-associated MinC-MinD complexes.

An important component needed for Min oscillations is the lipid bilayer. Addition of lipid vesicles from *E. coli* total cell extract to the EMSA reaction resulted in smears on the gel that were difficult to interpret (data not shown). For this reason, I thought of performing rather liposome co-sedimentation assays in which liposome-associated material is separated from the rest by sedimentation of the liposomes to the bottom of the test tube with centrifugation at 21.000 g. In the active ATP-bound state, MinD binds to lipid vesicles and these MinD-coated vesicles are found in the pellet (Lackner, Raskin & De Boer 2003). I added MinC and plasmid DNA to the reaction mixture to see if that resulted in co-sedimentation. I collected the supernatant and the pellet after centrifugation and analyzed the protein content on an SDS-page followed by Coomassie staining, while the presence of DNA was

analyzed on a separate agarose gel stained with Gel Red. In the dimeric ATP-bound state, almost all MinD was lipid-bound and therefore present in the pellet fraction that contains liposome-associated material (Figure 32). Most of the plasmid DNA was located in the supernatant indicating that MinD by itself has a low DNA-binding affinity, which is consistent with the EMSA results. In complex with MinC, most the plasmid DNA co-sedimented with the liposomes. MinC is also found in the pellet, consistent with the complex formation with MinD (Figure 32).

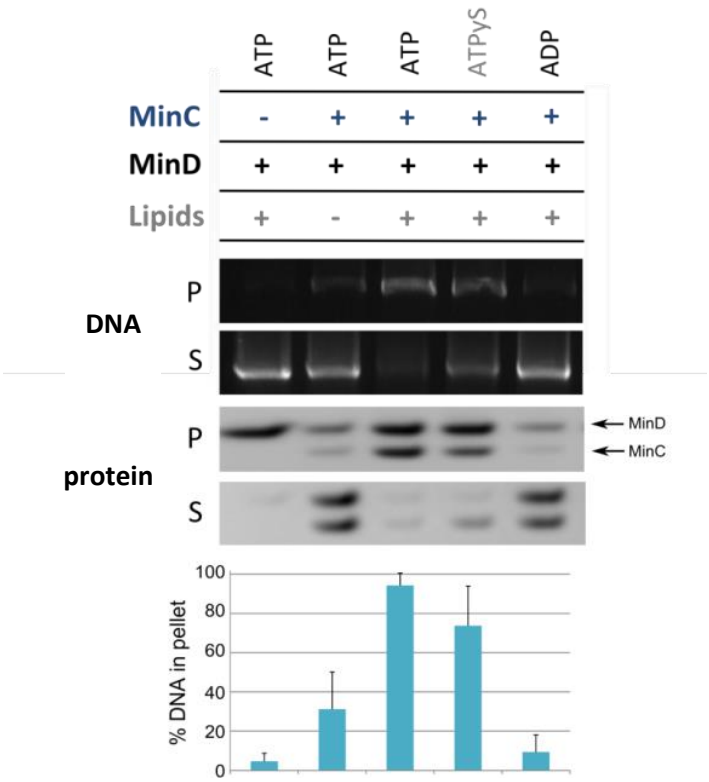

Figure 32| interaction between MinC-MinD-coated lipid vesicles and plasmid DNA. Purified MinC and MinD (both at 8 µM) were incubated with 800 µg ml^{-1} liposomes (prepared from *E. coli* total lipid extract), 32 ng $µl^{-1}$ plasmid DNA (800 ng in total) and 1 mM of the indicated nucleotide (ADP, ATP or ATPγS) in storage buffer supplemented with 5 mM $MgCl_2$. After centrifugation of the reaction mixture, the pellet and supernatant fractions were analyzed with SDS-page followed by Coomassie staining for protein visualization, or with an agarose gel (1%) followed by Gel Red staining for DNA visualization. Quantification of the pellet-associated DNA was done with the results from 3 independent experiments. Values shown represent the mean. Error bars represent S.E.M.

Usage of the ATP-analogue ATPγS decreased the amount of DNA in the pellet (Figure 32). Looking at the amount of MinC in the supernatant, I conclude that ATPγS affects the binding between MinC and MinD rather than the MinD-lipid interaction. This results in a reduction of DNA-binding. In the monomeric, ADP-bound state of MinD, hardly any MinC, and consequently any DNA, was found in the pellet. From these results, I postulate that the amount of MinC in the pellet is the main determinant of the amount of plasmid DNA found in the pellet.

3.4.7 MinE dissociates lipid-bound MinC-MinD-DNA complexes

Next I investigated the effect of MinE on DNA-binding by the MinC-MinD complex. The interactions between these proteins are well-characterized (see Introduction 1.2.2). MinE binds to MinD and anchors itself to the membrane with its cryptic MTS (Hsieh et al. 2010). There it stimulates the ATPase activity of MinD resulting in dissociation of the dimer and membrane release. Due to the higher binding affinity, MinE can displace MinC from the shared binding patch located in the MinD dimeric interface. When MinD-dimers are formed with ATPγS, the MinD-MinE complex on the membrane is more stable due to the reduced hydrolysis rate of ATPγS (Hu, Gogol & Lutkenhaus 2002; Lackner, Raskin & de Boer 2003). These findings could be easily reproduced (Figure 34.). The distribution of plasmid DNA, which was present in the same samples is shown in Figure 34.

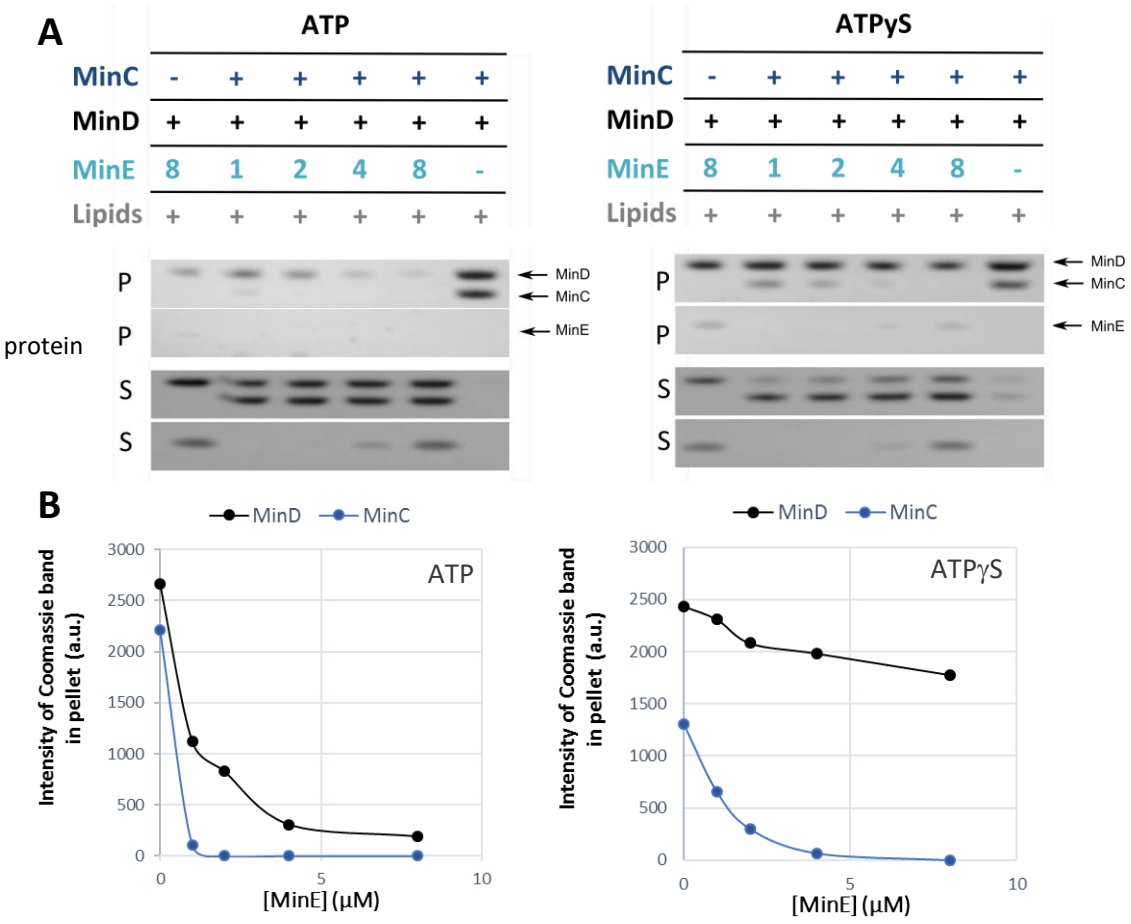

Figure 33|MinE dissociates the lipid-associated MinC-MinD complex. A| Co-sedimentation assay with *E. coli* lipid vesicles, plasmid DNA and purified MinC and MinD present at 8 µm. MinE is titrated at the indicated concentrations. Further experimental conditions are identical to those described in Figure 32. The DNA fraction that belongs to this experiment is shown in Figure 34. **B|** The amount of MinC and MinD in the lipid-associated pellet show (shown in panel A) is quantified with ImageJ and plotted against the concentration MinE.

MinE interferes with DNA-binding by the MinC-MinD complex in a concentration dependent way (Figure 34). This is very apparent in the presence of ATP, where 1 μM of MinE abolishes disrupts > 65 % of the the DNA-binding to 8 μM of the lipid-bound MinC-MinD complex. In presence of ATPγS, higher concentrations of MinE are needed to equal this effect. This indicates that MinE interferes with the formation of the nucleoprotein complex both by competition with MinC, as well as by triggering MinD membrane release.

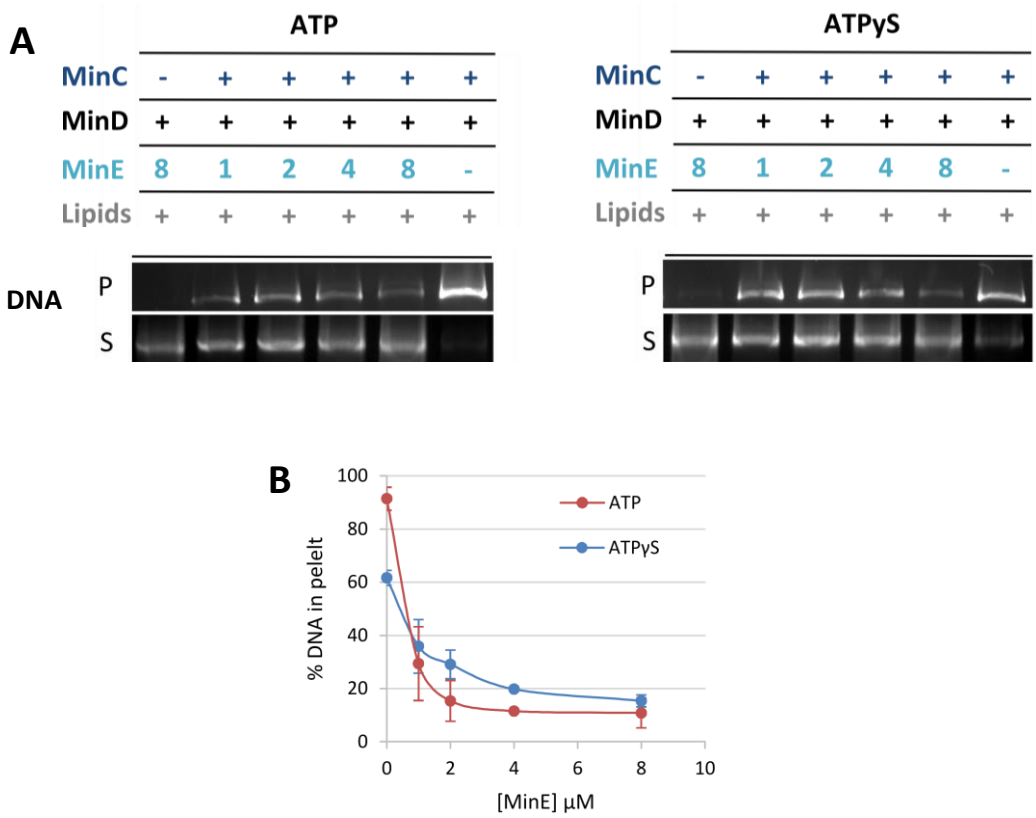

Figure 34| MinE dissociates the lipid-associated MinC-MinD nucleoprotein complexes in a concentration dependent manner. A| Co-sedimentation assay with *E. coli* lipid vesicles, plasmid DNA and purified MinC and MinD present at 8 μm. MinE is titrated at the indicated concentrations. **B|** Quantification of the relative amount of DNA in the lipid-associated pellet. Each data point in the graph is the average of 3 experiments (except for the data point at 4 μM MinE which was measured in this experiment only). Error bars are S.E.M.

3.4.8 Role of the N- and C-terminal domains of MinC in DNA-binding

To study DNA-binding by MinC in more detail, I purified the isolated N- and C-terminal domains of MinC. The N-terminal domain, which is a dimer in isolation, did not bind to DNA, even at concentrations as high as 20 µM (Figure 35). Since this domain is not reactive towards MinD, it was not tested with the liposomes co-sedimentation assay. The C-terminal domain of MinC, denoted $MinC^C$, contains a dimerization domain and the interaction surface for binding MinD (Hu & Lutkenhaus 2000). This isolated domain was expressed well in *E. coli*, but most of the protein was present in the non-soluble pellet after cell lysis resulting in a low yield. For this reason, a fusion with His-tagged

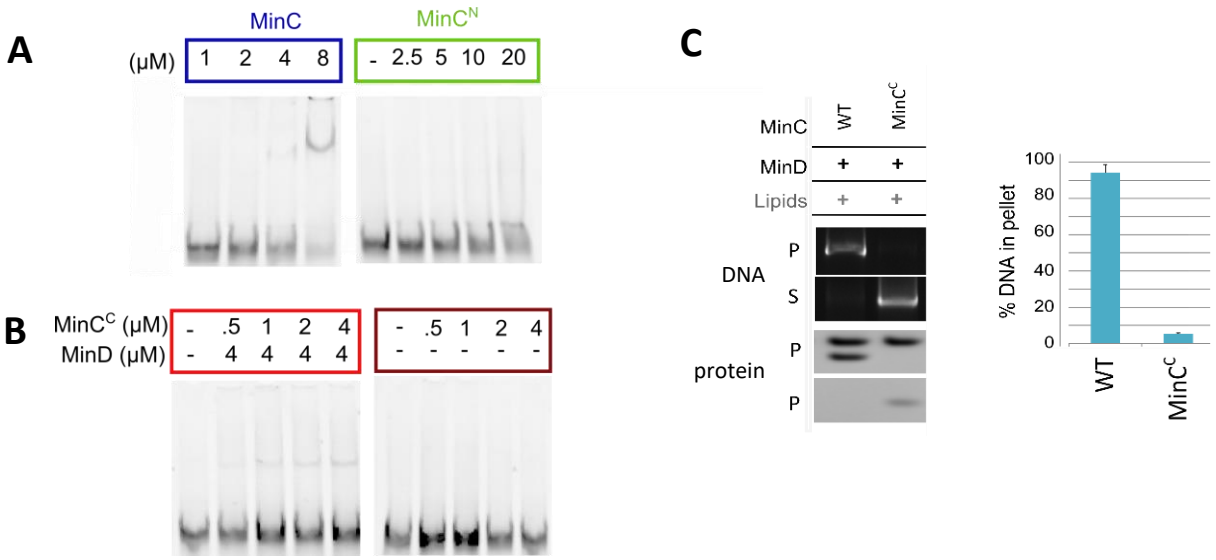

Figure 35| Role of the C- and N-terminal domains of MinC in DNA-binding. A| An EMSA was performed with full length MinC and the individual domains MinC and $MinC^N$. 120 bp HEX -labeled dsDNA was incubated with the indicated amount of protein in storage buffer supplemented with 5 mM $MgCl_2$ and 1 mM ATP. **B|** $MinC^C$ does not interact with DNA in the presence of MinD and liposomes. An EMSA was performed with MinD and $MinC^C$ using experimental conditions as described in A. **C|** Purified MinC or $MinC^C$ and MinD (both 8 µM) were incubated with 800 µg ml^{-1} liposomes (prepared from *E. coli* total lipid extract), 32 ng $µl^{-1}$ plasmid DNA (800 ng in total) and 1 mM ATP in storage buffer supplemented with 5 mM $MgCl_2$. After centrifugation, the pellet and supernatant fractions were analyzed with SDS-page followed by Coomassie staining for protein visualization, and a Gel-Red stained 1% Agarose gel to visualize the DNA content (left panel). Quantification of the DNA was done with the results from 2 independent experiments, bars represent mean ± S.E.M (right panel).

Maltose-Binding Protein (^{His}MBP) was made to increase the solubility and the yield (done by Navaneethan Palanisamy). Then, ^{His}MBP was removed from the protein using a Thrombin cleavage site. I found with EMSA that $MinC^C$ was not able to bind to DNA by itself (Figure 35B). Complex formation with MinD did not enhance the binding as effectively as observed for the full-length protein (Figure 28). The faint band that is visible in the EMSA indicates rather weak binding. Liposome co-sedimentation assays confirmed this finding, MinD could recruit $MinC^C$ to liposomes, but less than 10% of the plasmid DNA was pulled down. This indicates an important role for the N-terminal domain in DNA-binding. These data show that full length MinC is required for the interaction of the MinC-MinD complex with DNA.

3.4.9 Importance of residues in the N-terminal domain of MinC in DNA-binding by the MinC-MinD complex

For studying the DNA-binding surface of the MinC-MinD complex, a computational approach was chosen to screen for residues that are of importance for DNA-binding of this complex. A Brownian docking approach suggested the involvement of MinC residues G10 and K66 (Mehmet Özturk and Rebecca Wade, personal communication). G10 and K66 are located on opposite sites of the N-terminal domain in a positive patch (Figure 36).

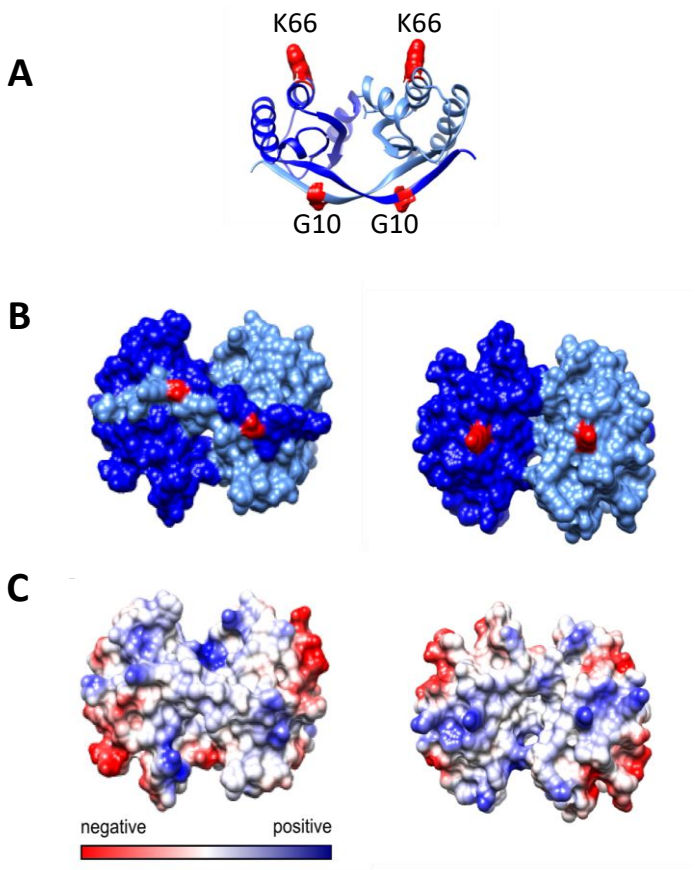

Figure 36| Residues of *E. coli* MinC^N predicted to be involved in DNA-binding. A| Ribbon structure of the MinC N-terminal domain (PDB:4l1c). The individual monomers are shown in light and dark blue with residues G10 and K66 colored red. **B|** The structure from A is rotated in such a way that G10 (left image) or K66 (right image) residues are facing forward. The surface view is shown with the same coloring as used in panel A. **C|** The electrostatic potential is calculated using the coulombic surface coloring tool from Chimera with default settings. Positive charges are shown in blue and negative ones shown in red.

To experimentally test the potential involvement of these residues in DNA-binding, We first mutated glycine at position 10 to aspartic acid (G10D) and lysine at position 66 to alanine (K66A) and then used the mutants in EMSA and co-sedimentation assays. Both mutants were less potent in comparison with the wild type protein. Interestingly, the difference in DNA-binding between wild type and $MinC^{K66A}$ was mostly apparent in the co-sedimentation assay, where about $MinC^{K66A}$ had a binding that was 70% of that of wild type MinC (Figure 37). With the EMSA (Figure 37A), the synergistic binding of MinC-MinD was not observed at all for this mutant in complex with MinD. In the co-sedimentation assay, $MinC^{G10D}$ showed 60% of the binding relative to the wild type protein. These results indicate that the two assays are not identical to each other and give complementary information about the binding. In the co-sedimentation assay, a larger piece of DNA is used (a plasmid) allowing the MinC-MinD co-polymers to form and achieve a binding strength that is not observed in solution without lipids and with shorter pieces of DNA.

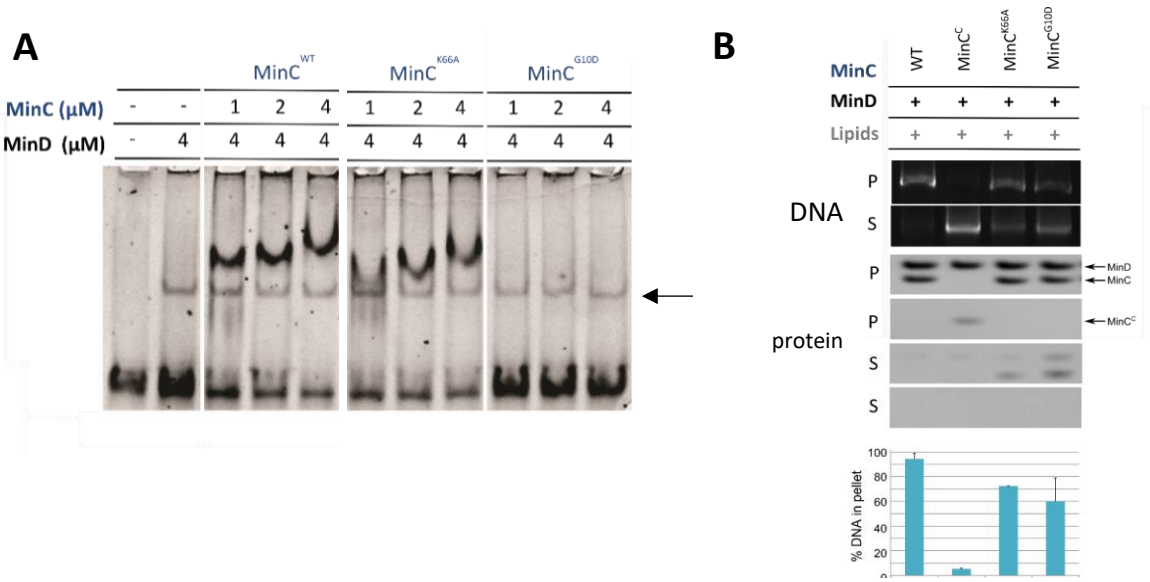

Figure 37| Characterization of DNA-binding by MinC mutants predicted to have a reduced DNA-binding affinity. A| 120 bp dsDNA probe was incubated with the indicated proteins for 15 minutes and the nucleoprotein complexes were then resolved on a native gel and visualized using a gel scanner equipped with a green laser. The arrow points at a non-specific band which is unreactive towards MinC and visible for this specific batch of MinD. **B|** Plasmid DNA was incubated with the indicated proteins and liposomes for 15 minutes at room temperature, then pellet and supernatant were separated with centrifugation at 21.000G. Upper panels: agarose gel stained with Gel Red for DNA visualization, and Coomassie stained bis-acrylamide gel for the detection of proteins. Bottom panel: Quantification of the DNA content in the pellet relative to the total amount. The values are mean ± S.E.M from two independent experiments. All proteins used in this experiment were purified by Naveethan Palanisamy.

3.4.10 Secondary structure of MinC^{G10D} studied with circular dichroism

In order to make sure that the reduction in DNA-binding by MinC^{G10D} is not due to changes in protein structure, we performed circular dichroism (CD) experiments at the protein expression and purification core facility at EMBL Heidelberg. Since structural elements like α-helices, β-sheets or unfolded regions all contribute in a different but characteristic way to the CD spectrum (Greenfield 2007), we decided to perform these experiments with just the N-terminal domain. This keeps the spectrum simpler and would allow changes to be detected more easily. The fact that the N-and C-terminal domains of MinC function independently and are properly folded upon truncation justifies this choice (Hu & Lutkenhaus 2000).

MinC^{N} and MinC$^{N\text{-}G10D}$ were purified by Navaneethan Palanisamy using the standard protocol (Materials and Methods 2.3). Size exclusion chromatography using a Superdex 75 column was performed by Jacob Scheurich at EMBL. MinC^{N} eluted as a dimer which is consistent with previous reports (Hu & Lutkenhaus 2000) and apparent from the structure (An et al. 2013, Figure 36). The dimeric structure is formed via so-called domain swapping, in which a β-sheet of one monomer is tightly packed to the β-sheet of the other monomer (An et al. 2013, Figure 36). The G10D mutation is located within this β-sheet, but did not affect dimerization, since MinC$^{N\text{-}G10D}$ was dimeric as well (not shown). The CD experiments and data analysis were done by Robert Opitz. A comparison of the CD spectra from the mutant and the wild type only shows minor structural perturbations (Figure 38). This indicates that the protein is overall properly folded, with probably small local changes due to the G10D mutation.

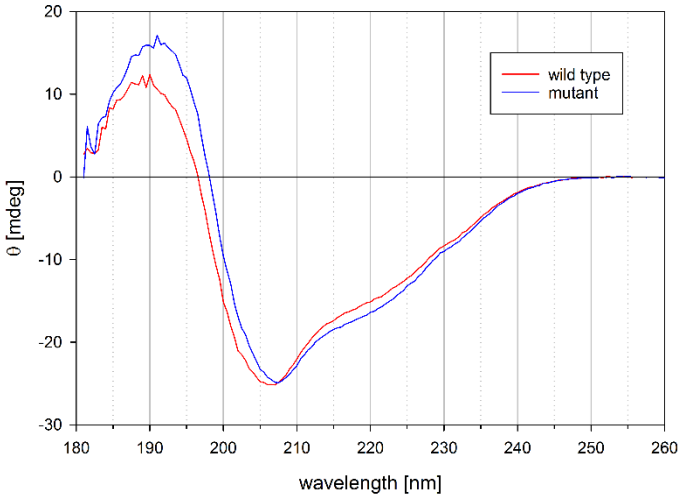

Figure 38 | Far UV CD spectra of MinC^{N} and the mutant MinC$^{N\text{-}G10D}$. Spectra were recorded on a Jasco–815 spectrometer using 10 µM MinC^{N} wild type or G10D in 10 mM NaPi pH 8.0 and 100 mM KF. The temperature was kept constant at 20°C. The spectra were normalized by protein concentrations and are expressed in molar ellipticity per mean residue [θ]. This image was provided by Robert Opitz.

3.4.11 DNA-binding by MinC^{WT}-MinC^{R133A} heterodimers

In order to test if the MinC-MinD co-polymers are required for DNA-binding, I employed a previously established strategy of mixing wild type and mutant MinC to allow formation of MinC heterodimers incapable of forming co-polymers with MinD (Park et al. 2015). To this aim, I mixed MinC^{WT} (2 µM) with an excess of MinC^{R133A} (4,8 and 16 µM; Figure 39). The heterodimers that are formed can only interact with MinD on the wild type side of the dimer (thus they do not form co-polymers) and are subsequently recruted to liposomes. The MinC^{R133A} homodimers remain in the supernatant since they are impaired in the interaction with MinD. Incubation of 8 µM or 16 µM MinC^{R133A} with 2 µM MinC^{WT} resulted in formation of heterodimers, which could be seen after quantification of the MinC protein band in the pellet (Figure 39C).

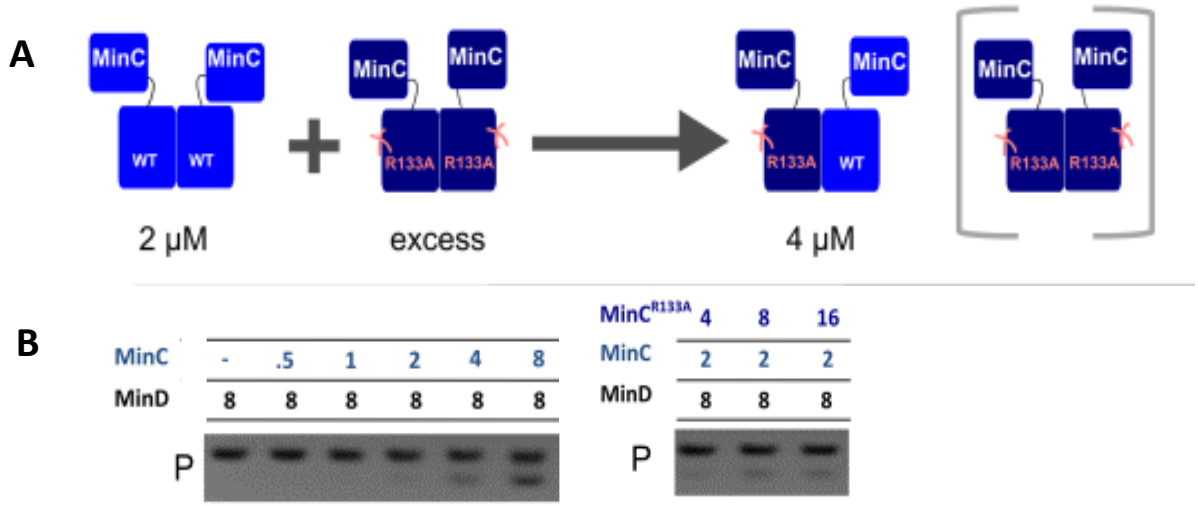

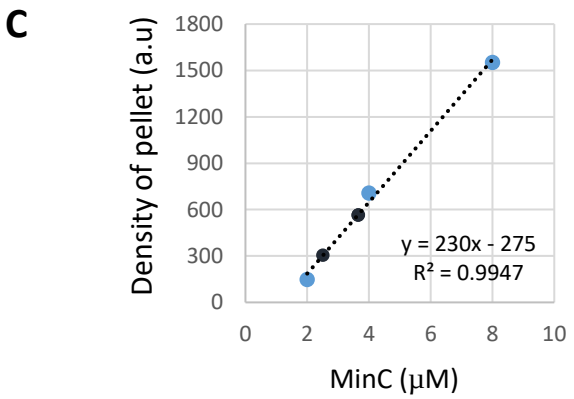

MinC	MinC^{R133A}	Estimated MinC-MinC^{R133A}
2 µM	4 µM	2.5 µM
2 µM	8 µM	3.6 µM
2 µM	16 µM	3.7 µM

Figure 39| Formation of MinC^{WT}-MinC^{R133A} heterodimers in complex with MinD. A| Schematic representation of heterodimers between wild type MinC and mutant MinC that are only capable of interacting with MinD on the wild type side of the dimer. **B|** Co-sedimentation assay. A fixed amount of MinD (8 µM), lipid vesicles (800 µg ml^{-1} prepared from *E. coli* total lipid extract) and plasmid DNA (32 ng µl^{-1} of plasmid DNA, 800 ng in total) were incubated with a varying amount of MinC or heterodimeric MinC^{WT}-MinC^{R133A} in the presence of 1 mM ATP and 5 mM $MgCl_2$. **C|** The amount of wild type MinC (shown in panel B, left) was plotted as a function of the MinC concentration (dotted line). The amount of pellet-associated heterodimeric MinC (dark blue dots) was calculated using this standard curve and is sumarised in the table below the graph.

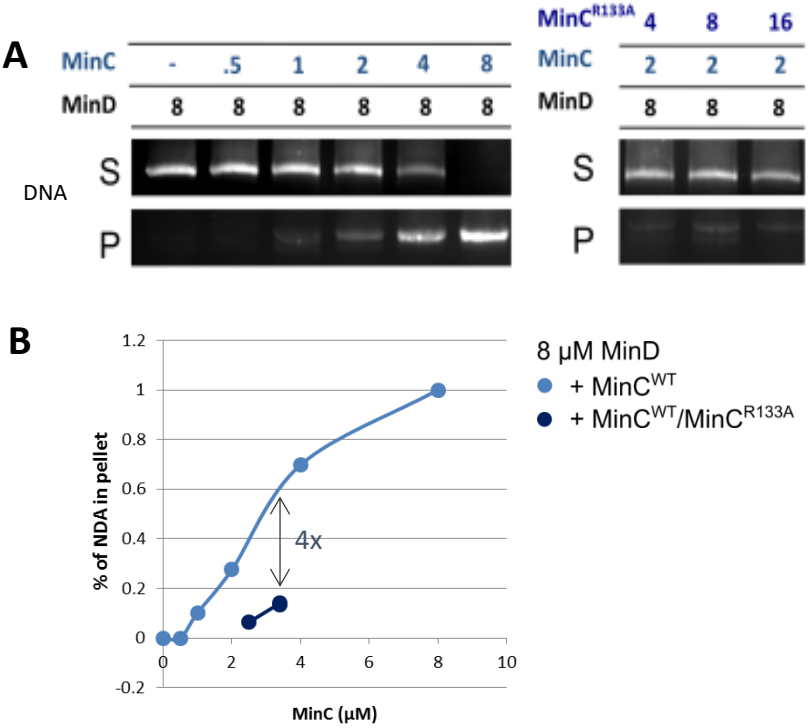

Figure 40| Reduced binding by MinC^{WT}-MinC^{R133A} heterodimers in complex with MinD. A| Co-sedimentation assay. A fixed amount of MinD (8 µM), lipid vesicles (800 µg ml^{-1} prepared from *E. coli* total lipid extract) and plasmid DNA (32 ng µl^{-1}, 800 ng in total) were incubated with a varying amount of MinC or heterodimeric MinC^{WT}-MinC^{R133A} in the presence of 1 mM ATP and 5 mM $MgCl_2$. **B|** Quantification of the pellet-associated DNA from the gels shown in panel A. The concentrations of the MinC^{WT}-MinC^{R133A} were obtained from Figure 39C.

The co-sedimentation assay shows that a complex of heterodimeric MinC^{WT}-MinC^{R133A} with MinD recruits 4 times less DNA to the liposomes than the MinC-MinD complex (Figure 40). This result, suggests that the co-polymers make the binding to plasmid DNA more efficient.

3.4.12 Formation of MinC-MinD co-polymers

In order to fully understand if MinC-MinD co-polymers play a role in DNA-binding, I wanted to verify if these structures form with our purified proteins and buffer conditions. To this aim, I co-incubated MinD and MinC and collected the possible co-polymers with ultracentrifugation at 130.000 g for 30 minutes. Titration of equimolar amounts of MinC and MinD shows that 50% of the protein is in the pellet when both proteins are present around 4-5 µM (Figure 41) . Truncation of the last 10 C-terminal amino acids of MinD (MinD$^{\Delta 10}$) highly reduced the formation of co-poylmers (Figure 41B). This is consistent with the results from (Conti et al. 2015) in which similar effects were seen for MinD$^{\Delta 15}$.

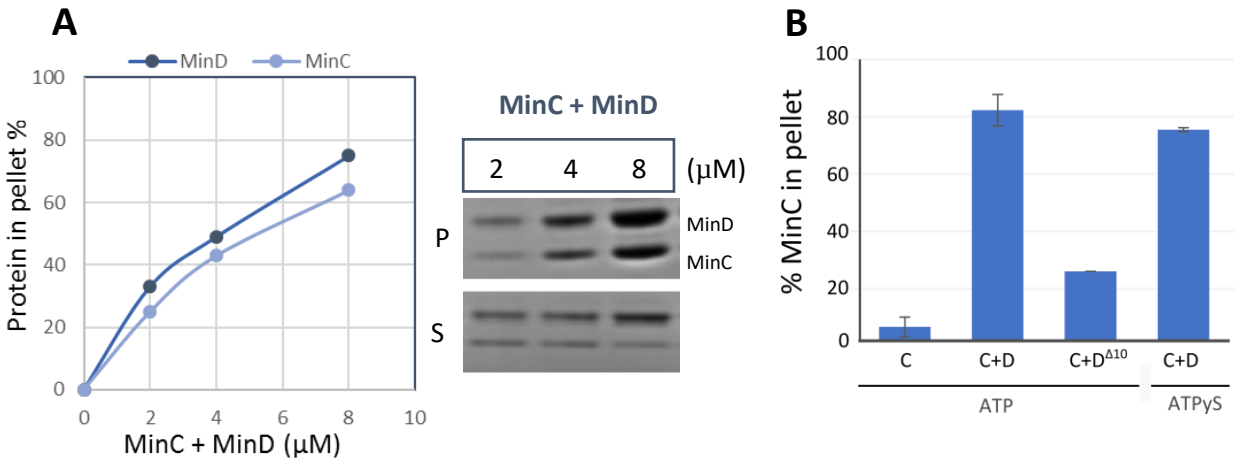

Figure 41| MinC-MinD co-polymer formation. Equimolar amounts of MinC and MinD or MinD$^{\Delta 10}$ were incubated at the indicated concentrations (in µM) in storage buffer supplemented with 1 mM ATP or ATPγS and 5 mM $MgCl_2$. After 10 minutes of incubation at room temperature, samples were centrifuged at 130 000 g for 30 minutes. The contents of the supernatant and the pellets were analyzed with SDS-page followed by Coomassie staining. **B|** The intensity of the Coomassie signal for MinC and MinD was measured for the supernatant and pellet fractions with imageJ. **C|** The plot shows the relative amount of the indicated protein in the pellet after ultracentrifugation. Bars represent mean values

The co-polymers did not form with ADP, nor when used MinD^{K11A}, which does not dimerise and thus does not interact with MinC (data not shown). The role of ATPγS in formation fo the co-polymers is not clear from the literature (Ghosal et al. 2014; Conti et al. 2015). I found that dimerisation of MinD with ATPγS did reduce, but not impair, the formation of co-polymers.

3.4.13 DNA binding by MinC-MinD complexes is inhibited by high levels of FtsZ

Since MinC is a well-characterized regulator of the FtsZ ring, I wanted to know if the presence of FtsZ would influence the DNA-binding properties of lipid-associated MinC-MinD complexes. I show that FtsZ can be tethered to liposomes in the presence of MinC and MinD. The amount of protein recruited to the liposomes did not seem to vary much between the two different nucleotides (Figure 42). I assume that that is due to the intrinsically high GTPase activity of FtsZ which leads to accumulation of GDP in the sample which contained initially only GTP.

Upon incubation with 10 µM FtsZ, the protein ratio MinC/FtsZ in the lipid-associated pellet was ± 2:1. This led to a small decrease in DNA-binding (Figure 42). Increasing the concentration of FtsZ to 30 µM resulted in an equal amount of MinC and FtsZ in the pellet. In this case, the amount of plasmid DNA in the pellet was highly reduced (Figure 42). Since FtsZ binds to both the C- and the N-terminal domains of MinC, it most likely prevents DNA-binding by blocking the binding sites on MinC (and possibly MinD).

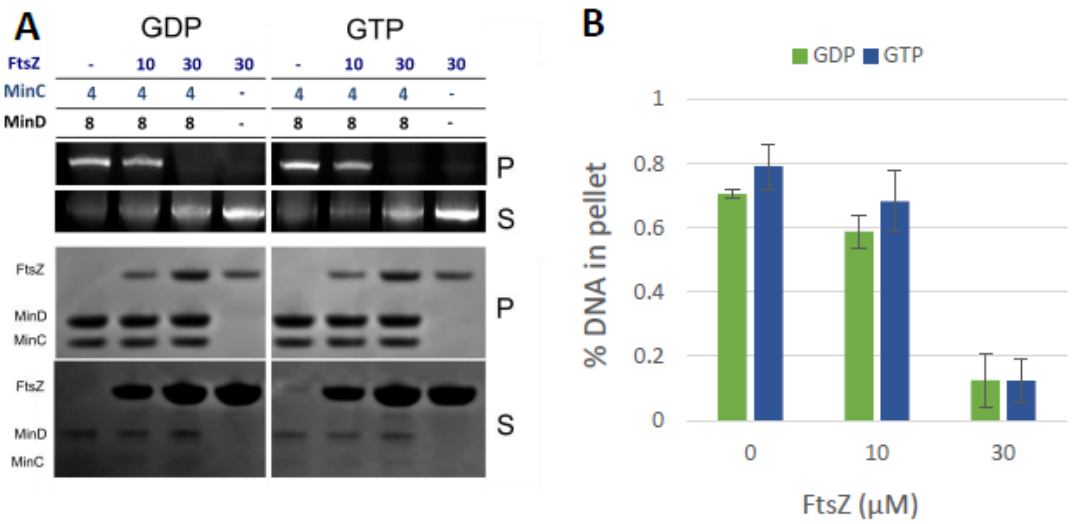

Figure 42| **Influence of FtsZ on DNA-binding by lipid-associated MinC-MinD complexes**. **A|** Lipid vesicles made from *E. coli* total lipid extracts were incubated with the indicated amounts of protein in storage buffer supplemented with 5 mM $MgCl_2$, 1 mM ATP and additionally 1 mM GTP or GDP. After 15 minutes of incubation, samples were spun down and protein and DNA content of the supernatant and pellet were analyzed with SDS page stained with Coomassie (for protein visualization) and an agarose gel (1%) stained with Gel Red (for DNA visualization). **B|** The DNA in the pellet and supernatant fractions was quantified with ImageJ and the % of DNA in the lipid-associated pellet is plotted. The bars are the mean from two experiments with S.E.M.

4 Discussion

In *E. coli*, a plethora of factors and mechanisms have been suggested to play a role in chromosome segregation, either directly or indirectly (summarized in Introduction 1.6.). It has been proposed in our lab that the Min system, more specifically MinD, is involved in chromosome segregation. MinD forms polar gradients of weak DNA-binding sites, which transiently capture the duplicated chromosomes, biasing their movement towards the poles (Introduction 1.7). This mechanism relies on the initial separation of the duplicated chromosomes achieved by conformational entropy (Jun & Mulder 2006; Jun & Wright 2010) and the prerequisite that the nucleoid is properly folded and organized (Introduction 1.5).

4.1 Enhanced DNA-binding by the MinC-MinD complex

I studied the DNA-binding properties of all three Min proteins *in vitro* with electrophoretic mobility shift assays (EMSAs). Of the Min proteins, MinC has the highest affinity for DNA, although this is, all in all, still rather low (k_D > 8 µM). Formation of the ATP-dependent MinC-MinD complex highly enhances binding and lowers the apparent k_D to ±1 µM (Figure 28). Presence of the lipid bilayer did not interfere with this binding, which is consistent with previous data on MinD alone (Di Ventura et al. 2013). Since MinD has a weak affinity for the DNA, when alone, it is not able to pull a large plasmid (5 kb) down to the pellet fraction where liposome-bound material is found (Figure 32). On the other hand, in the presence of MinC and ATP, the plasmid is found exclusively in the pellet fraction (Figure 32). This suggests that the surface which is involved in DNA-binding is distinct from the one that is interacting with, or facing, the lipid bilayer. Additionally, it argues that the membrane targeting helix of MinD does not play a direct role in DNA-binding since it is not accessible due to its insertion in the lipid bilayer (Szeto, Rowland, Habrukowich & King, 2003; Hu & Lutkenhaus 2003). This is also consistent with previous data (Di Ventura et al. 2013) and was confirmed here with EMSA assays performed with the truncated MinD ($MinD^{\Delta 10}$) that cannot bind to the membrane but bound to the DNA together with MinC as efficiently as the wild type protein (Figure 28).

Since the MinC-MinD complexes have practically the same bi-polar distribution of MinD in *E. coli* cells (Hu & Lutkenhaus 1999; Raskin & de Boer 1999) the overall proposed mechanism of chromosome segregation does not change (Figure 10). The only difference between the previously proposed model and the current one is that the real “unit” responsible for tethering on the membrane the DNA is the MinC-MinD complex and not MinD alone.

4.2 Importance of MinC-MinD co-polymers for DNA-binding

Recently it has been shown that MinC forms co-polymers with MinD *in vitro* (Conti et al. 2015; Ghosal et al. 2014). However, the physiological relevance of these structures has been soon after questioned,

since cells expressing a mutant MinC unable to form co-polymers with MinD ($MinC^{R133A}$) were seen to have normal size (Park et al. 2015). It is possible that the relevance of these polymeric structures on Z-ring placement would become apparent in cells devoid of other Z-ring regulators like SlmA or the Ter-linkage. Indeed, the role for SlmA became clear in fast growing cells with a knock-out of the Min system (Bernhardt and De Boer 2005).

Here I tested whether the MinC-MinD co-polymers might play a role in DNA-binding in *in vitro* assays. Interestingly, when mixing an excess of $MinC^{R133A}$ with wild type MinC, a four-fold reduction in DNA-binding is observed in liposome co-sedimentation assays (Figure 40). This would suggest that the co-polymers are important for Min-mediated chromosome segregation in living cells. However, it is not easy to explain why cells not having MinC-MinD co-polymers were observed to succeed in placing the septum at mid-cell (Park et al. 2015), considering that unsegregated chromosomes present at mid-cell are likely to halt the formation of the septum there. Further work is needed to clarify the role of the co-polymers in chromosome segregation, for instance by following this process in real time in cells with and without the MinC-MinD co-polymers.

4.3 Role of MinE

In early EMSA experiments in which purified His-tagged MinE was used, an unambiguous binding to the DNA was observed (Figure 31). However, when I started removing the His-tag from the proteins, this binding was highly reduced (Figure 31). This very weak binding is consistent with the thermophoresis results, where no saturated DNA-binding was observed at MinE concentrations up to 50 µM (Figure 48). Furthermore, I found that MinE dissociated MinC-MinD-DNA complexes from the liposomes in a concentration dependent manner (Figure 34). Since MinE displaces MinC from MinD (Lackner et al. 2003; Wu et al. 2011) it is reasonable that, in doing so, it also dissociates the nucleoprotein complex. Moreover, MinE stimulates the ATPase activity of MinD which results in the dissociation of the MinD dimer and subsequent release of MinD from the membrane (Hu and Lutkenhaus 2001; Lutkenhaus and Sundaramoorthy 2003). Thus MinE likely terminates the transient tethering of the DNA to the membrane by the MinC-MinD complex.

4.4 Measurements of binding kinetics and stoichiometry

In this work, the mechanism used to describe DNA-binding by the Min system is rather qualitative. The kinetic or stochiometric parameters could not be determined despite usage of several experimental techniques. Surface plasmon resonance experiments to analyze binding of MinE or MinD to surface-immobilized DNA showed mainly non-specific binding and artefacts due to protein self-interactions (specifically for MinE) (Supplementary Information, 5.3). With thermophoresis, I studied the binding of a labeled DNA probe with the different Min proteins. The formation of higher order

structures of MinC and MinD was not compatible with this method and distorted the binding curves (Supplementary Information 5.5.). For individual Min proteins, the interaction with the DNA was too weak and the k_D could not be fitted since saturated binding was not reached. The EMSAs assays seemed sensitive and consistently showed the synergistic DNA-binding by the MinC-MinD complex. However, sometimes the results were troubled by non-specific bands, or smeary bands that were difficult to quantify.

Currently, MinC-MinD-DNA complexes are being analyzed by electron microscopy by our collaborators Götz Hofhaus and Johan Zeelen. The initial experiments show that MinC-MinD assemble into the previously observed co-polymers (Ghosal et al. 2014), which, in presence of DNA, form sheets where individual filaments are kept together by the DNA that runs perpendicular to the sheet. The width of the observed sheets correlates with the length of the DNA probe used (personal communication). Follow up studies with electron tomography with a higher resolution might provide clarity on the binding surface and binding stochiometry.

4.5 Role of the His-tag

The initial EMSAs were done with purified proteins that harbored the His-tag. Only after I started performing EMSAs with proteins cleared of the tag, it became apparent that the His-tag caused a profound increase in the observed DNA-binding affinity (Figure 27). Looking in the literature, I realized that a variety of unwanted effects have been reported by others. For some proteins, the His-tag affected the ability to distinguish the cognate binding site from a random DNA sequence, most likely by enhancing non-specific DNA events (Plumbridge 2001). In the case of ZapA, the tag led to the formation of bundles with FtsZ differently arranged compared to those formed by the native protein (Mohammadi et al. 2009). Moreover, the tag impaired the protein function in such a way that the *ΔzapA* phenotype could not be complemented with ^{His}ZapA (Mohammadi et al. 2009). In the zinc finfer protein AreA from *Aspergillus nidulans*, the His-tag caused a conformational change of the DNA-binding pocket, which however did not affect the DNA-binding properties of the protein (Chant et al. 2005). Furthermore, on an antibody, the tag interfered with antigen binding depending on where it was placed (Goel et al. 2000). Even though the His-tag is commonly used and makes protein purification easy, in some circumstances it is recommended to remove it, or at least to test if the tag influences the behavior of the protein. It should be noted that the T7- tag is still present on all proteins used in this study. This tag has a neutral charge and does likely not interfere with DNA-binding; however, the only way to be sure about any potential influence of the tag is to experimentally test it.

4.6 Prediction of the DNA-binding surface

The isolated C-terminal domain of MinC is still able to interact with MinD, but this complex did not (or very weakly) interact with DNA, just like the isolated N-terminal domain of MinC (Figure 36). This indicates that the full-length protein is required for proper binding. The exact role MinC C-terminal domain within the complex is not completely clear. It could function as molecular glue to establish the interaction with MinD and position $MinC^N$ close by, or it could stabilize DNA-binding by providing low affinity binding sites.

With a computational approach, our collaborator Mehmet Oezktuerk predicted that residues G10 and K66 (located in $MinC^N$ on opposite sides) play a role in DNA-binding of the MinC-MinD complex. This was validated biochemically by using the mutants $MinC^{K66A}$ and $MinC^{G10D}$, of which the latter showed the largest reduction in DNA-binding (Figure 37). The fact that these residues are located on opposite sides of the protein, in combination with the conformational flexibility of $MinC^N$ due to the unstructured linker which connects it to $MinC^C$, makes it difficult to clarify the binding surface of the complex.

The G10D mutation is known to impair the interaction between MinC and FtsZ (Labie, Bouche, and Bouche 1990; Z Hu et al. 1999). The binding interface is composed of a negative patch of FtsZ (Figure 43) and a positive patch of MinC (Shen and Lutkenhaus 2010). Based on the charge, the same interface of MinC would be suitable for interactions with the negatively-charged DNA backbone.

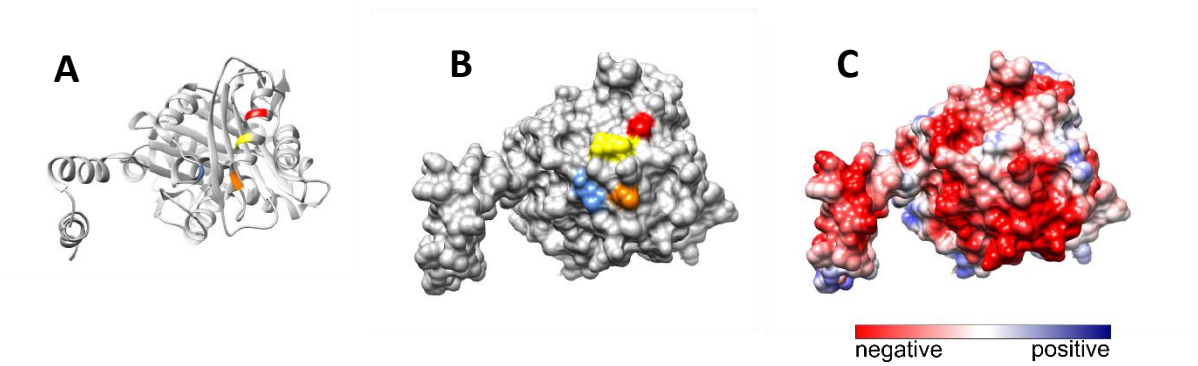

Figure 43| Location of MinC interaction sites on a FtsZ monomer. **A|**FtsZ residues that were found to be involved in MinC binding were mapped onto the FtsZ crystal structure of M. Jannaschii (PDB: IW5B), as was done in (Shen and Lutkenhaus 2010). Shown in red is A305, yellow: R301 and orange: T296 and blue: L231. Those residues correspond to the *E. coli* residues N280, E276, R271 and L205**. B|** Surface view of the structure shown in A. **C|** Electrostatic potential coloring according to the coulombic surface coloring tool from Chimera with default settings. Positive charges are shown in blue and negative ones shown in red.

With the co-sedimentation assay, I found that FtsZ completely blocked the DNA-binding of lipid-associated MinC-MinD when it was present at concentrations above 30 µM (Figure 42). Since FtsZ

binds simultaneously both to $MinC^{C}$ and $MinC^{N}$ (Shen and Lutkenhaus 2009, 2010). It is not clear if this DNA interaction is blocked by steric hindrance, or by specifically competing for the binding interface around residue G10.

The cellular concentration of FtsZ is relatively high with 5000 - 15.000 molecules per cell (5- 15 µM**,** Table 6). Approximately 30% of the protein is present in the Z-ring while the remainder is found cytoplasmic (Stricker et al. 2002). MinC is non-abundant and reaches levels around 0.5 µM (Supplementary data, Table 6). Upon recruitment by membrane-bound MinD, the local concentration of MinC increases to an estimated 10 µM. This is illustrated by the fact that absence of MinD requires a 25-50 times higher concentration of MinC in order to establish a cell division block (De Boer et al., 1992). Considering these protein concentrations inside the *E. coli* cells, and the different cellular location of the Z-ring and the polar Min proteins, the weak interaction between MinC and FtsZ is not likely to affect the DNA-binding properties of the Min system away from mid-cell.

4.7 Segregation of the chromosomal bulk by the Min system

ChIP-Seq experiments revealed that the genome-wide ^{His}MinD-DNA-binding does not occur in a sequence specific manner. The lack of specific binding peaks is commonly observed when the protein of interest binds to DNA without sequence specificity (Kahramanoglou et al. 2011; Prieto et al. 2012). Since ChIP-Seq experiments are based on the enrichment of specific genomic regions above a certain background, it is impossible to distinguish non-specific binding from absence of binding. However, given previous *in vivo* data attesting the binding of MinD to DNA (Di Ventura et al., 2013), I would conclude from the ChIP-Seq results that there are no preferred regions for binding under the conditions tested. This strongly suggests a role for the Min system in segregation of the chromosomal bulk, rather than of specific regions such as the Ori MD, contrary to the function of *parABS* systems (Livny, Yamaichi, and Waldor 2007; Ptacin et al. 2010). Importantly, there was no difference between the samples with oscillating or statically membrane-bound MinD, indicating that the absence of enrichment to specific loci was not due to having MinD not properly localized.

There is however the possibility that the Min system binds to specific chromosomal regions or motifs in a cell cycle-dependent way. Since the *E. coli* cells were not synchronized in this study, the results represent an average from a mixed population of cells in different cell cycle stages. This could dilute out cell cycle-specific effects. For SeqA, for example, cell synchronization and sampling at different time points elegantly showed that SeqA binding is centered on GATC motifs and moves from the Ori MD towards the Ter MD over time (Waldminghaus et al. 2012). Since I executed the ChIP-Seq experiments before I characterized the enhanced binding by the MinC-MinD complex, I performed them overexpressing ^{His}MinD only rather than, for instance, ^{His}MinC-MinD. Surely, one of the ChIP-Seq

datasets has been obtained with cells overexpressing MinD over the endogenous levels of all three Min proteins, indicating that, at least to some extent the MinC-MinD complexes could have formed. As a net difference between the samples from wild type versus *ΔminB* cells was not detected, I would conclude that most likely the absence of specific binding reflects the physiological reality.

Furthermore, I analyzed the transcriptome of *E. coli* wild type and *ΔminB* cells to see if the Min system would cause direct or indirect effects on the expression levels of certain genes. I found only minor differences in gene expression between the wild type strain and the *ΔminB* strains (Figure 23, Figure 24). Even if it would be interesting in the future to follow up closely those few (chemotaxis and flagellar) genes that resulted up-regulated in the absence of the Min system, the conclusion important to this work is that the Min proteins do not globally regulate transcription in *E. coli.*

4.8 Redundancy in the mechanisms that ensure chromosome segregation

Minor defects in chromosome segregation were already reported in early studies on cells with a mini-cell phenotype (Akerlund, Bernander, and Nordström 1992; Åkerlund, Gullbrand, and Nordström 2002). In a *ΔminB* strain, proteins that form the septum like the DNA pump FtsK are not always properly localized at mid-cell, which can affect chromosome segregation (Capiaux, Lesterlin, Pérals, Louarn, & Cornet, 2002; Stouf, Meile, & Cornet, 2013 ; Nolivos et al., 2016). However the DNA pumping activity of FtsK only becomes efficient in cells with a highly constricted septum (Männik. J. et al. 2017). Åkerlund and colleagues showed that overexpression of MinE on top of an endogenous Min system decreased the separation ratio between the duplicated chromosomes (Åkerlund, Gullbrand, and Nordström 2002). The authors only analyzed cells without a constricting septum to rule out that this effect is due to FtsK.

Another way to rule out indirect effects of having a displacement of the septum is to use mutants of the Min proteins that behave like the wild type proteins except for the ability to bind DNA. Unfortunately, almost every mutant which we found to have a large reduction of DNA-binding was to some extent impaired in its interactions with the other Min proteins or with FtsZ, thus making it impossible to truly identify a mutant where only DNA-binding is affected. For instance, both $MinC^{C}$ and $MinC^{G10D}$, which have very low DNA-binding activity in complex with MinD (Figure 35 and Figure 37) also show a reduction in their ability to bind to FtsZ (Labie, Bouche, and Bouche 1990; Z Hu et al. 1999), which disqualifies them for usage in such an experiment.

I studied chromosome segregation in cells with and without the Min system (Figure 15). As expected, cells with a knock-out of the Min system showed defects in chromosome segregation, but the cells looked surprisingly well overall. In our model, we propose that the Min system provide an additional mechanism that supplements entropic forces and potential further mechanisms (Introduction, 1.7). It

is hard to isolate the role of the Min system in this case, since conformational entropy is not something that can be experimentally removed from the cells. However, a prerequisite for the entropy based model is a nucleoid which properly compacted and organized in the distinct macrodomains (Jun & Mulder, 2006; Jun & Wright, 2010). By interfering with nucleoid organisation, the contribution of the Min system on chromosome segregation might become more pronounced. This can be tested in a strain devoid of the NAP H-NS, in which the chromosome is less condensed (Helgesen et al. 2016) just like in a strain devoid of the chromosomal organizer MukB (Hiraga et al. 1991; reviewed in Badrinarayanan et al. 2012). The latter is also characterized by misplaced Ori and Ter MDs (Danilova et al. 2007).

Recently, MinD from *B. subtilis* has been also proposed to have a dual function in division site selection and positioning of the Ori MD (Kloosterman et al. 2016). In this bacterium, the Min system forms static polar gradients (Marston et al. 1998). MinD does not interact directly with the membrane but associates with the topological factor MinJ, which connects MinCD to polarly-localised DivIVA (Marston et al. 2008). When attached to the pole via, MinJ, DivIVA and another protein called ComN, MinD can recruite Soj instead of MinC. As a consequence, the Ori MD is found closer to the cell pole (Kloosterman et al. 2016). Deletion of MinD did not cause significant defects in chromosome segregation, but rather decreased the distance of OriC to the pole (Kloosterman et al. 2016). For *E. coli*, I have clarified the role of MinC and MinE in DNA-binding, but there is still much to understand *in vivo.* The effect of the Min system on chromosome organisation and localisation of specific macrodomains within the cell, has not been touched upon yet.

5 Supplementary information

5.1 Primers

LK1 FW-*minD*$^{K32E-K33E}$	GGCCCAGAAGGGAGAGGAAACTGTCGTGATAG
Lk2 RV-*minD*$^{K32E-K33E}$	CTATCACGACAGTTTCCTCTCCCTTCTGGGCC
LK3 FW-*minD*$^{R54E-R55E}$	GACGAAATCGTAAACGACCTCTTCTTCACAACCCATAATCAGGTCGAG
LK4 RV-*minD*$^{R54E-R55E}$	CAGGCGTTAATTAAAGATGAGGAAACTGAAAATCTCTATATTCTGCCGGCATCG
LK5 FW-*minD*$^{K78E-R79E}$	CGATGCCGGCAGAATATAGAGATTTTCAGTTTCCTCATCTTTAATTAACGCCTG
LK6 RV-*minD*$^{K78E-R79E}$	GATAAAGATGCCCTCACCGAAGAAGGGGTCGCCAAAG
LK7 FW-*minD*^{R99E}	CTTTGGCGACCCCTTCTTCGGTGAGGGCATCTTTATC
Lk8 RV-*minD*^{R99E}	CGTGAAGGGGTCGCCGAAGTTCTTGATGATCTG
LK9 FW-*minD*^{K104}	CAGATCATCAAGAACTTCGGCGACCCCTTCACG
LK10 RV-*minD*^{K104}	CAGATCATCAAGAACTTCGGCGACCCCTTCACG
LK11 FW-*minD*^{K110E}	GTTCTTGATGATCTGGAAGCGATGGATTTTG
LK12 RV-*minD*^{K110E}	CAAAATCCATCGCTTCCAGATCATCAAGAAC
LK13 FW-*minD*^{K163E}	GGCATTCTGGCGTCGGAATCACGCCGCGCAG
LK14 RV-*minD*^{K163E}	CTGCGCGGCGTGATTCCGACGCCAGAATGCC
LK15 FW-*minD*$^{R165E-R166E}$	GGCCTGGCGTCGAAATCAGAAGAAGCAGAAAATGGCGAAGAG
LK16 RV-*minD*$^{R165E-R166E}$	CTCTTCGCCATTTTCTGCTTCTTCTGATTTCGACGCCAGGCC
LK17 FW-*minD*^{K175E}	GGCGAAGAGCCTATTGAAGAGCACCTGCTGTTAACG
LK18 FW-*minD*^{K175E}	CGTTAACAGCAGGTGCTCTTCAATAGGCTCTTCGCC
LK19 FW-*minD*^{D40A}	TGTCGTGATAGATTTTGCTATCGGCCTGCGTAATC
LK20 RV-*minD*^{D40A}	GATTACGCAGGCCGATAGCAAAATCTATCACGACA
LK21 FW-*Bam*HI-*minC*	CCAAGGATCCGGAAACACGCCAATCGAGCTTAAAG
LK22 RV-*minC*^{N}-stop-*Hin*dIII	TTGGAAGCTTTTATGGAGCCTGCGGTGTGGGAG
LK23 FW-*minC*^{G10D}	GCCAATCGAGCTTAAAGACAGTAGCTTCACTTTATC
LK24 RV-*minC*^{G10D}	GATAAAGTGAAGCTACTGTCTTTAAGCTCGATTGGC
LK25 FW-*Bam*HI-*minC*^{C}	CCAAGGATCCGCGCAAAATACAACGCCGGTACA
LK26 RV-*minC*-stop-*Not*I	GGTTGCGGCCGCTTAACGGTTGAACGGTCAAAGCGTTTTCG
LK27 FW-*minC*^{K66A}	CTGGTCAGCGATGCATGCGGCGGTTTCGGCAACC
LK28 RV-*minC*^{K66A}	GGTTGCCGAAACCGCCGCATGCATCGCTGACCAG
LK29 FW-*minC*^{R133A}	CGTTTAATAGATACCCCGGTGGCTTCCGGTCAGCGTATTTATG
LK30 RV-*minC*^{R133A}	GCATAAATACGCTGACCGGAAGCCACCGGGGTATCTATTAAACG

LK31 FW-*Bam*H1-*ftsZ*	CGTTGGATCCTTTGAACCAATGGAACTTACCAATGA
LK32 RV-*ftsZ*-stop-*Hin*dIII	GACCAAGCTTTTAATCAGCTTGCTTACGCAGGAATGCTG
LK33 FW-*Sac*I-TSS-*minC*	GGTTGAGCTCTCTTCGGAACATCATCGCGCGC
LK34 RV-*minB*-terminator-*Hin*dIII	TATCAAGCTTGTATCAGCAAGAATACTCGCCGC
LK35 FW-*Nco*I-6His-*Not*I-*minD*	CCAACCATGGCGCATCATCACCATCACCACAGCGGCCGCGCACGCATTATTGTTGTTACTTCGG
LK36 FW-*Nco*I-FLAG-*Not*I-*minD*	CCAACCATGGACTACAAGGACGACGATGACAAAAGCGGCCGCGCACGCATTATTGTTGTTACTTCGG
LK37 RV-*minD*-stop-*Pst*I	GGTTCTGCAGTTATCCTCCGAACAAGCGTTTGAGG
LK38 FW-pET-28a-before MCS	TAGGGGAATTGTGAGCGGATAACAATTCCCCTCT
LK39 FW-*Bam*HI-*seqA*	AATTGGATCCAAAACGATTGAAGTTGATGATGAACTCTACAGC
LK40 RV-*seqA*-stop-*Hin*dIII	AATTTCTGCAGTTAGATAGTTCCGCAAACCTTCTCAATCAATTC
LK41 FW-*Sac*I-*yfp*	TTTTGAGCTCATG GTG AGCAAGGGCGAGGAGCTG
LK42 RV-*yfp*-*Hin*dIII	GGGGAAGCTTTTACTTGTACAGCTCGTCCATGCCGAG
LK43 FW-*Cla*I-$motA_{promoter}$	GTACCTGCAGTTATTTTTGACACCAGACCAACTGGTAATGG
LK44 RV-$motA_{promoter}$-*Sac*I	AAAAGAGCTCATCCTTCCACTGTTGACCATGACAGG
LK45 FW-*Cla*I-*NdeI*-$Tar_{promoter}$-*Sac*I	CGATCATATGCAATTTCGCGGCGGGTGGCATCAGCAATAAAGTTTCCCCCCTCCTTGCCGATAACGAGATCAACTTGTTTTCAGGAAGGGAGCT
LK46 RV-*Sac*I-$tar_{promoter}$-*Nde*I-*Cla*I	CCCTTCCTGAAAACAAGTTGATCTCGTTATCGGCAAGGAGGGGGGAAACTTTATTGCTGATGCCACCCGCCGCGAAATTGCATATGAT
LK47 FW-*Xba*I-*lacZ*	TGCATCTAGAATGACCATGATTACGGATTCACTGGC
LK48 RV-*lacZ*-*Pst*I	GTACCTGCAGTTATTTTTGACACCAGACCAACTGGTAATGG
LK49 FW-*Cla*I-$motA_{promoter}$	GTACCTGCAGTTATTTTTGACACCAGACCAACTGGTAATGG
LK50 RV-$MotA_{promoter}$-*Xba*I	AAAATCTAGAATCCTTCCACTGTTGACCATGACAGG
LK51 FW-*Cla*I-*Nde*I-$Tar_{promoter}$-*Xba*I	CGATCATATGCAATTTCGCGGCGGGTGGCATCAGCAATAAAGTTTCCCCCCTCCTTGCCGATAACGAGATCAACTTGTTTTCAGGAAGGT
LK52 RV-*Cla*I-*Nde*I-$Tar_{promoter}$-*Xba*I	CTAGACCTTCCTGAAAACAAGTTGATCTCGTTATCGGCAAGGAGGGGGGAAACTTTATTGCTGATGCCACCCGCCGCGAAATTGCATATGAT
LK53 FW-[HEX]-P1-promoter (30bp)	[Hex]-GAATCAGCGCCATTTATCACAGAATAGACT
LK54 FW-[Alexa Fluor™488]- P1-promoter (30 bp)	[Alexa-488]-GAATCAGCGCCATTTATCACAGAATAGACT
LK55 RV-P1-promoter (30bp)	AGTCTATTCTGTGATAAATGGCGCTGATTC
LK56 FW-[HEX]-P1-promoter (52 bp)	GAATCAGCGCCATTTATCACAGAATAGACTTTTACTCTGAATAAATGGGAGG
LK57 RV-P1-promoter (52 bp)	CCTCCCATTTATTCAGAGTAAAAGTCTATTCTGTGATAAATGGCGCTGATTC

[HEX]FW-P1-promoter (72 bp)	GAATCAGCGCCATTTATCACAGAATAGACTTTTACTCTGAATAAATGGGAGGGTGACTTGC CTCAATATAAT
RV-P1-promoter (72 bp)	ATTATATTGAGGCAAGTCACCCTCCCATTTATTCAGAGTAAAAGTCTATTCTGTGATAAATG GCGCTGATTC
[HEX]FW-P1-promoter (120 bp)	GAATCAGCGCCATTTATCACAGAATAGACTTTTACTCTGAATAAATGGGAGGGTGACTTGC CTCAATATAATCCAGACTATAACATGCCTTATAGTCTTCGGAACATCATCGCGCGCTGG
RV-P1-promoter (120 bp)	CCAGCGCGCGATGATGTTCCGAAGACTATAAGGCATGTTATAGTCTGGATTATATTGAGGC AAGTCACCCTCCCATTTATTCAGAGTAAAAGTCTATTCTGTGATAAATGGCGCTGATTC

Table 5| Primers used in this work. All sequences are denoted from ‘5 to ‘3 end, restriction sites are underlined.

5.2 ChIP-Seq

5.2.1 Genome wide correlation of the ChIP-Seq signals

By plotting the genome wide correlation of the ChIP-Seq signals, the mock and MinD samples cluster together, based on the day in which the experiment and the library preparation were done. For SeqA, all ChIP-signals form one cluster, independent of the day.

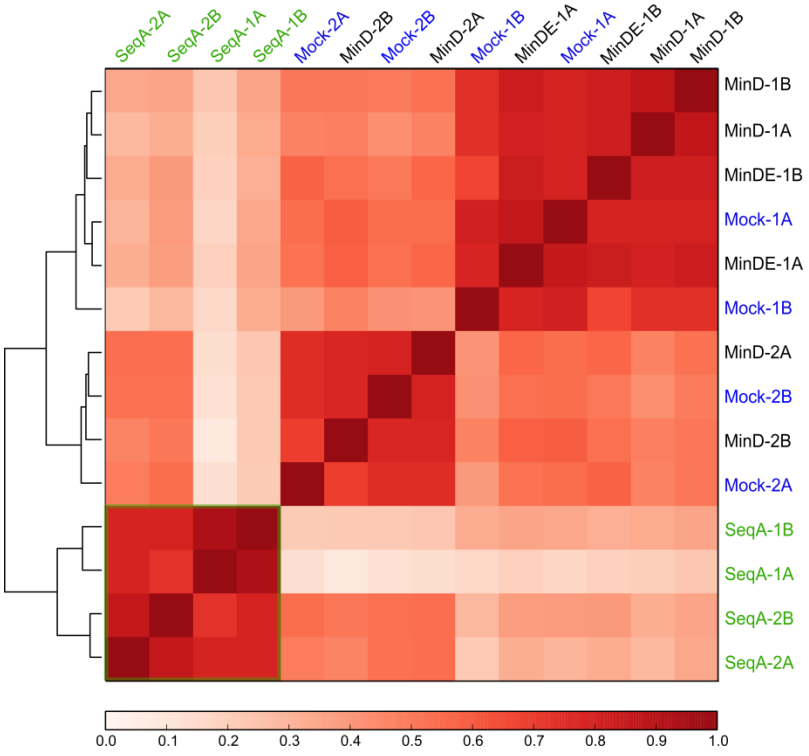

Figure 44| Genome wide correlation of the ChIP-seq signals for SeqA, MinD in a wild type *E. coli* MG1655 strain. MinD forms clusters together with the negative control (mock, empty plasmid) and other MinD (or MinDE) containing samples processed in the day (indicated with 1 or 2). For the positive control SeqA, all samples form 1 cluster (Image and analysis provided by Sebastian Steinhauser).

5.2.2 Heatmap of peak distribution

The DNA-binding specificity by SeqA is illustrated in Figure 45. There is a high binding signal around the peaks in the SeqA samples, while this area does not contain a signal in the negative control or MinD. Additionally, almost every peak contains the GATC motif.

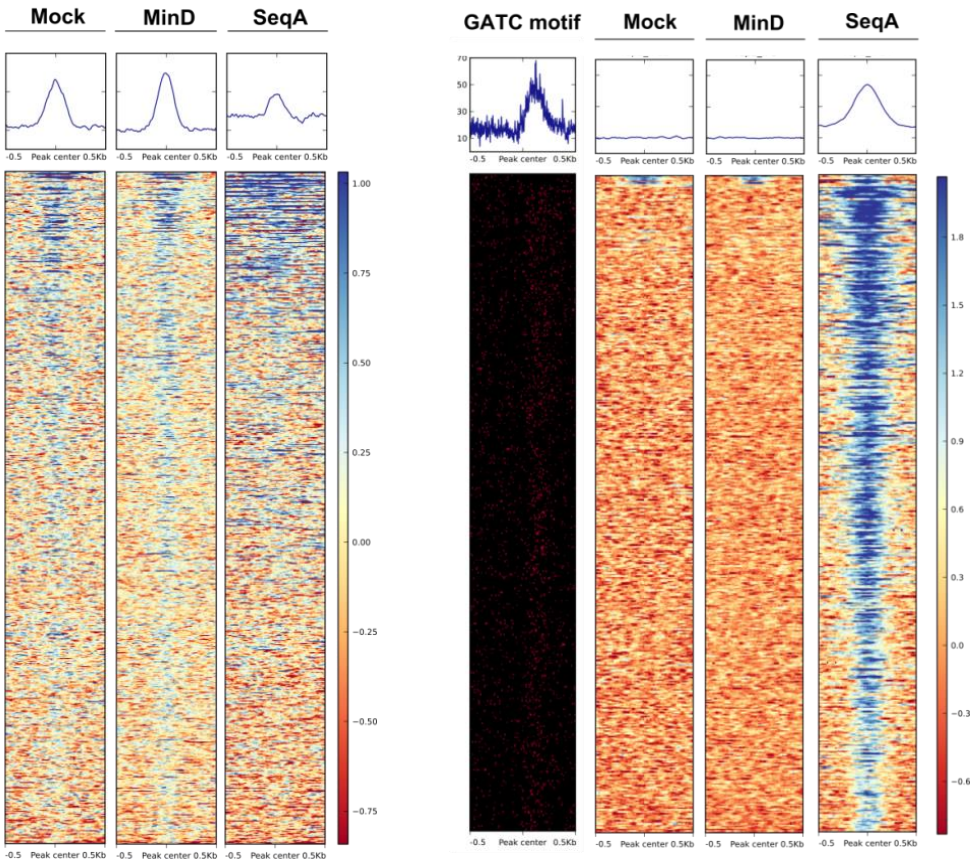

Figure 45| Heatmap showing the spatial signal distributions for SeqA, MinD and the mock, ± 500 bp around MinD peak centers. **B|** Same as A, for peak centers in the SeqA samples, the distribution of the GATC motif within the peaks is also shown (Image provided by Sebastian Steinhauser).

5.3 Surface Plasmon Resonance, preliminary experiments

Surface plasmon resonance experiments were carried out to characterize DNA-binding by ^{His}MinE and ^{His}MinD, and ideally extract some of the kinetic parameters of this interaction. For this purpose, a short biotinylated dsDNA probe (30 bp) was immobilized on the surface of a sensor chip coated with streptavidin (Biacore Sensorchip SA). Then, varying concentrations of ^{His}MinD or ^{His}MinE were flown over the surface to study the DNA-interaction.

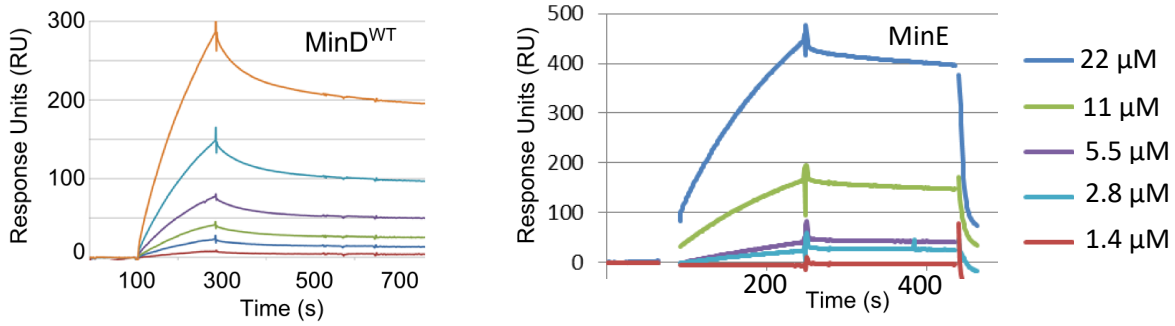

Figure 46| Binding of ^{His}MinD and MinE to immobilized DNA. 30 bp biotinylated dsDNA (Trc promoter) was immobilized on the surface of a sensor chip coated with Streptavidin (Biacore Sensorchip SA). Different concentrations of MinD were studied: 3.4 µM (orange), 1.7 µM (blue), 0.9 µM (purple), 0.45 µM (green), 0.25 µM (dark blue) and 0 µM (red). After 200 seconds of association, the running buffer was flown in for > 300 seconds to follow dissociation of DNA-bound protein. After each cycle, the surface was regenerated with a 50 mM NaOH, 500 mM NaCl.

For both proteins, saturation of binding was not reached within 150-200 seconds. Additionally, the shape of the curve could indicate mass transport limitations. Immobilizing less DNA or increasing the flow rate did however not change this (not shown). This kind of binding curves could also be the result of non-specific binding. Despite the usage of an empty flow cell to correct for non-specific binding to the sensor surface, distinct non-specific interactions can occur with the immobilized probe. The tendency for especially MinE to self-interact, could further lead to an increase in binding not related to a direct protein-DNA interaction. Incorporating higher amounts of BSA of Tween-20 did not affect the curves.

I then tried to immobilize ^{His}MinD via the interaction of the His-tag with a Ni-NTA sensor chip. The binding of ^{His}MinD to this chip was not reversible as the tagged protein could not be eluted with imidazole or EDTA, but only with regeneration buffer. This makes it likely that MinD formed aggregates on the surface, which makes this method unsuitable.

5.4 Nucleotide binding by MinE and MinC

In some of the early experiments, we observed that DNA-binding by ^{His}MinE showed a slight nucleotide dependency (not shown). This was not due to a drop in pH caused by the slightly acid nature of ATP in solution, since the stock solutions were pH adjusted. I therefore investigated if MinE and MinC could bind to ATP. To this aim, I used agarose beads coated with several ATP analogues in a pull-down experiment. Since MinD is known to bind to ATP, I used this protein as positive control for the procedure. MinD was pulled down by Aminophenyl-ATP-agarose and 2'/3' EDA-ATP-agarose beads, but not by the other types of beads (Figure 47). Interestingly, 100 mM ATP were not sufficient to fully elute MinD from the beads. MinE and MinC were not pulled down by any of the immobilized ATP versions (Figure 47).

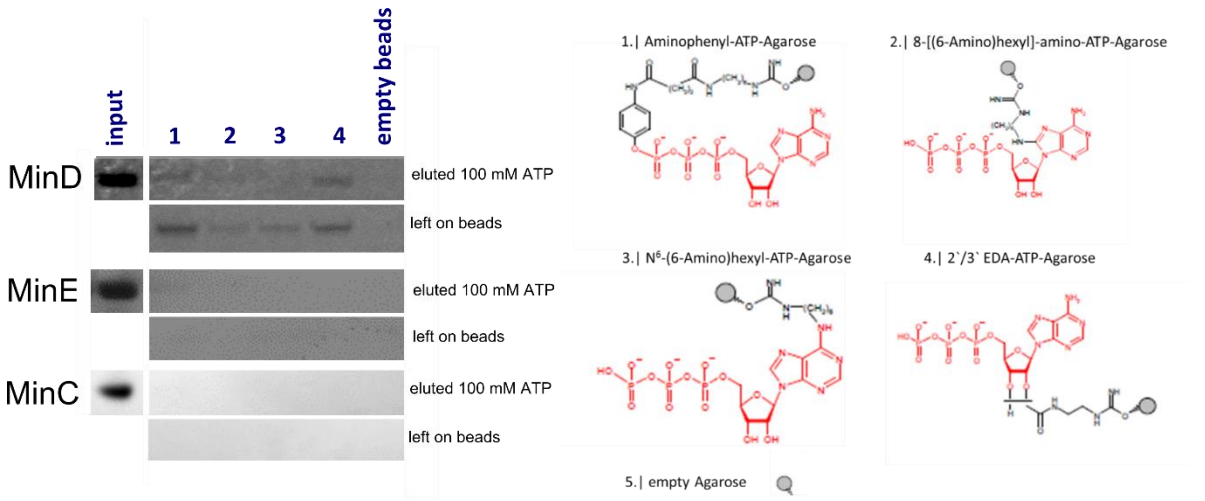

Figure 47| Pull-down assay with beads coated with ATP analogues to study the binding of the Min proteins to ATP. Beads were purchased at Jena Biosciences, and the recommended experimental recommendations from the manufacturer were followed. The concentrations of protein were 8 µM for MinC and MinD, and 30 µM for MinE.

5.5 Thermophoresis Measurements

In order to complement the EMSA experiments with another method to study protein-DNA interactions in solution, I performed thermophoresis measurements (reviewed by Jerabek-Willemsen et al. 2014).

In a typical thermophoresis experiment, an infrared laser creates a temperature gradient within a focused spot of the sample. A coupled fluorescence detector follows the movement of labeled- or unlabeled (autofluorescent) molecules within this spot. This directed movement of molecules within the temperature gradient depends on several factors like hydration shell, charge or size, which change upon complex formation (reviewed by Jerabek-Willemsen et al. 2014). Therefore, the signal of the free probe (0 % binding) and the signal upon saturated binding (100% bound) are essential for plotting the binding curves and extraction of the parameters like the k_D.

^{His}MinD and ^{His}MinE were incubated at the indicated concentrations with Alexa Fluor®488-labeled DNA (30 bp, P1-promoter). Increasing concentrations of protein led to an increase in signal, but no saturation was reached.

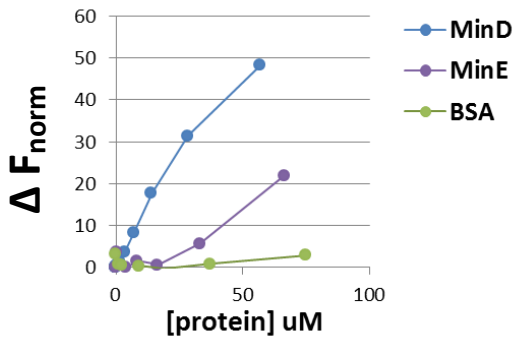

Figure 48| Binding to DNA by MinD and MinE measured by microscale thermophoresis. The DNA probe (30 bp) was fluorescently-labeled with Alexa-488, while proteins were left un-labeled. Proteins in this assay bear the His-tag. BSA was used as negative control. The normalized fluorescence F_{norm} is calculated by the Nanotemper software (F_{cold}/F_{hot}) where F_{cold} refers to the signal before heating up the sample, and F_{hot} after. Since saturated binding was not reached, I show here the difference in thermophoresis signal for the free (DNA) probe, and the decrease in thermophoresis upon binding to the proteins.

After I discovered the enhanced DNA-binding by the MinC-MinD complex, I wanted to use thermophoresis to see if could confirm the findings from the EMSA with this assay. However, the binding curves were quite distorted and I could not use them for quantification (data not shown). This was likely due to the formation of the MinC-MinD co-polymers. Surprisingly I observed the same phenomenon when I used MinD$^{\Delta 10}$ instead of wild type MinD (data not shown), even if MinD$^{\Delta 10}$ is not able to form these structures to the same extent as MinD (see Figure 41).

5.6 Estimated levels of cell division proteins in *E. coli* from the literature

Molecules per cell	**Comments**	**Method and source**
MinC: 300-800 MinD: 2.000-6.000 MinE: 2.000-4.000	MOPS minimal and MOPS complete medium	Extrapolation from ribosomal profiling. (Li et al. 2014).
MinE: 200 – 500	LB	Quantitative Western Blot (Zhao et al. 1995)
MinC: 400 ± 80	medium not mentioned 0.65 µM (cytoplasmic volume of 1 fL)	Quantitative Westernblot (Szeto et al. 2001)
FtsZ: 4.800 ± 1.300	4.2 µM Minimal medium	Quantitative Westernblot (Mohammadi et al. 2009)
FtsZ: 15.000	10 µM 400 µg/ml	Quantitative Westernblot Mops complete medium (Lu, Stricker, and Erickson 1998)

Table 6| Estimated protein levels of the Min system and FtsZ in *E. coli*.

6 List of abbreviations

ADP	adenosine diphosphate
ATP	adenosine triphosphate
C-period	chromosome replication period
ChIP-Seq	chromatin immunoprecipitation followed by deep sequencing
D-period	division period
DAPI	4'-6-diamidino-2-phenylindole DNA deoxyribonucleic acid
DTT	dithiothreitol
EDTA	ethylenediaminetetraacetic acid
Fts	filamentous temperature sensitive
GCC	genome conformation capture
GDP	guanosine diphosphate
GTP	guanosine triphosphate
His-tag	hexahistidine affinity tag
IPTG	isopropyl-β-thiogalactopyranoside
LB	Luria-Bertani medium
KEGG	Kyoto encyclopedia of genes and genomes
MD	macro domain
MTS	membrane targeting sequence
Ori	origin of replication
OD	optical density
PALM	Photoactivated Localization Microscopy
Par system	Partitioning system
SAM	Sequence Alignment /Map
STORM	Stochastic Optical Resolution Microscopy
Slm	synthetic lethal without min
Ter	replication terminus region
YFP	yellow fluorescent protein

7 Bibliography

Aarsman, M. E. G., et al. 2005. “Maturation of the Escherichia Coli Divisome Occurs in Two Steps.” *Molecular Microbiology* 55(6):1631–45.

Ahijado-Guzmán, R., et al. 2013. “Control by Potassium of the Size Distribution of Escherichia Coli FtsZ Polymers Is Independent of GTPase Activity.” *Journal of Biological Chemistry* 288(38):27358–65.

Åkerlund, T., R. Bernander and K. Nordström. 1992. Cell Division in Escherichia Coli minB Mutants. *Molecular Microbiology* 15(6):2073-2083

Åkerlund, T., B. Gullbrand, and K. Nordström. 2002. “Effects of the Min System on Nucleoid Segregation in Escherichia Coli.” *Microbiology* 148(10):3213–22.

Amann, E., B. Ochs and K. Abel. 1988. “Tightly Regulated Tac Promoter Vectors Useful for the Expression of Unfused and Fused Proteins in Escherichia Coli.” *Gene* 69(2):301–15.

An, J. Y. et al. 2013. “Crystal Structure of the N-Terminal Domain of MinC Dimerized via Domain Swapping.” *Journal of Synchrotron Radiation* 20(6):984–88.

Anderson, D. E., F. J. Gueiros-Filho and H. P. Erickson. 2004. “Assembly Dynamics of FtsZ Rings in Bacillus Subtilis and Escherichia Coli and Effects of FtsZ-Regulating Proteins.” *Journal of Bacteriology* 186(17):5775–81.

Arumugam, S., Z. Petrašek and P. Schwille. 2014. “MinCDE Exploits the Dynamic Nature of FtsZ Filaments for Its Spatial Regulation.” *Proceedings of the National Academy of Sciences of the United States of America* 111(13): 1192-200

Badrinarayanan, A., C. Lesterlin, C. Reyes-Lamothe and D. Sherrat. 2012. “The Escherichia Coli SMC Complex, MukBEF, Shapes Nucleoid Organization Independently of DNA Replication.” *Journal of Bacteriology* 194(17):4669–76.

Baek, J.H., S. V. Rajagopala and D. K. Chattoraj. 2014. “Chromosome Segregation Proteins of Vibrio Cholerae as Transcription Regulators.” *mBio* 5(3).

Bailey, M. W, P. Bisicchia, B. T. Warren, D. Sherratt and J. Männik. 2014. “Evidence for Divisome Localization Mechanisms Independent of the Min System and SlmA in Escherichia Coli.” *PLoS Genetics* 10(8).

Bakshi, S., H. Choi, J. Mondal and J. Weisshaar. C. 2014. “Time-Dependent Effects of Transcription- and Translation-Halting Drugs on the Spatial Distributions of the Escherichia Coli Chromosome and Ribosomes.” *Molecular microbiology* 94(4):871–87.

Bates, D., and N. Kleckner. 2005. “Chromosome and Replisome Dynamics in E. Coli: Loss of Sister Cohesion Triggers Global Chromosome Movement and Mediates Chromosome Segregation.” *Cell* 121(6):899–911.

Benjamini, Y., and Y. Hochberg. 1995. “Controlling the False Discovery Rate: A Practical and Powerful Approach to Multiple Testing.” *Journal of the Royal Statistical Society B* 57(1):289–300.

Bernhardt, T. G., and P. A. J De Boer. 2005. “SlmA, a Nucleoid-Associated, FtsZ Binding Protein Required for Blocking Septal Ring Assembly over Chromosomes in E. Coli.” *Molecular Cell* 18(5):555–64.

Bi, E., and J. Lutkenhaus. 1990. “Interaction between the Min Locus and ftsZ.” *Journal of Bacteriology* 172(10):5610–16.

Bi, E.,and J. Lutkenhaus, J. 1991. “FtsZ Ring Structure Associated with Division in Escherichia Coli.” *Nature* 354(6349):161–64.

Bignell, C., and C. M. Thomas, 2001. “The Bacterial ParA-ParB Partitioning Proteins.” *Journal of Biotechnology* 91(1):1–34.

Blakely, G., S. Colloms, G. May, M. Burke and D. Sherrat . 1991. “Escherichia Coli XerC Recombinase Is Required for Chromosomal Segregation at Cell Division.” *New Biologist* 3(8):789–98.

Blattner, F. R. 1997. “The Complete Genome Sequence of Escherichia Coli K-12.” *Science* 277(5331):1453–62.

De Boer, P. A. J., R. E. Crossley, and L. I. Rothfield. 1992. “Roles of MinC and MinD in the Site-Specific Septation Block Mediated by the MinCDE System of Escherichia Coli.” *Journal of Bacteriology* 174(1):63–70.

de Boer, P. A. J., R. E. Crossley, and L. I. Rothfield. 1989. “A Division Inhibitor and a Topological Specificity Factor Coded for by the Minicell Locus Determine Proper Placement of the Division Septum in E. Coli.” *Cell* 56(4):641–49.

Bramhill, D. and C. M. Thompson. 1994. “GTP-Dependent Polymerization of Escherichia Coli FtsZ Protein to Form Tubules.” *Proceedings of the National Academy of Sciences of the United States of America* 91(13):5813–17.

Brézellec, P., M. Hoebeke, M. S. Hiet, S. Pasek, and J. L. Ferat. 2006. “DomainSieve: A Protein Domain-Based Screen That Led to the Identification of Dam-Associated Genes with Potential Link to DNA Maintenance.” *Bioinformatics* 22(16):1935–41.

Cabrera, J. E, C. Cagliero, S. Quan, C. L. Squires, and D. J. Jin. 2009. “Active Transcription of rRNA Operons Condenses the Nucleoid in Escherichia Coli: Examining the Effect of Transcription on Nucleoid Structure in the Absence of Transertion.” *Journal of Bacteriology* 191(13):4180–85.

Cagliero, C., R. S. Grand, B.M. jones, D. J. Jin, and J. M. O’Sullivan. 2013. “Genome Conformation Capture Reveals That the Escherichia Coli Chromosome Is Organized by Replication and Transcription.” *Nucleic Acids Research* 41(12):6058–71.

Cagliero, C. Y.N. Zhou, and D. J. Jin. 2014. “Spatial Organization of Transcription Machinery and Its Segregation from the Replisome in Fast-Growing Bacterial Cells.” *Nucleic Acids Research* 42(22):13696–705.

Capiaux, H., C. Lesterlin, K. Pérals, J. M. Louarn, and F. Cornet. 2002. “A Dual Role for the FtsK Protein in Escherichia Coli Chromosome Segregation.” *EMBO reports* 3(6):532–36.

Cass, J. A., N.J. Kuwada, B. T. Traxler, and P. A. Wiggins. 2016. “Escherichia Coli Chromosomal Loci Segregate from Midcell with Universal Dynamics.” *Biophysical Journal* 110(12):2597–2609.

Chant, A., C. M. Kraemer-Pecore, R. Watkin, and G. G. Kneale. 2005. “Attachment of a Histidine Tag to the Minimal Zinc Finger Protein of the Aspergillus Nidulans Gene Regulatory Protein AreA Causes a Conformational Change at the DNA-Binding Site.” *Protein Expression and Purification* 39(2):152–59.

Cobbe, N. and M. M. Heck. 2000. “Review: SMCs in the World of Chromosome Biology- from Prokaryotes to Higher Eukaryotes.” *J Struct Biol* 129(2–3):123–43.

Conti, J., M. G. Viola, and J. L. Camberg. 2015. “The Bacterial Cell Division Regulators MinD and MinC Form Polymers in the Presence of Nucleotide.” *FEBS Lett* 589(2):201–6

Cordell, S. C., R. E. Anderson, and J. Löwe. 2001. “Crystal Structure of the Bacterial Cell Division Inhibitor MinC.” *The EMBO journal* 20(10):2454–61.

Corre, J., and J. M. Louarn. 2005. “Extent of the Activity Domain and Possible Roles of FtsK in the Escherichia Coli Chromosome Terminus.” *Molecular Microbiology* 56(6):1539–48.

Cui, Y. Z. M. Petrushenko, and V. V. Rybenkov. 2008. “MukB Acts as a Macromolecular Clamp in DNA Condensation.” *Nature structural & molecular biology* 15(4):411–18.

Dame, R. T. Dame, O. J. Kalmykowa, and D. C. Grainger. 2011. “Chromosomal Macrodomains and Associated Proteins: Implications for DNA Organization and Replication in Gram Negative Bacteria.” *PLoS Genetics* 7(6).

Danilova, O., R. Reyes-Lamothe, M. Pinskaya, D. Sherratt and C. Possoz. 2007. “MukB Colocalizes with the oriC Region and Is Required for Organization of the Two Escherichia Coli Chromosome Arms into Separate Cell Halves.” *Molecular Microbiology* 65(6):1485–92.

Deghorain, M. et al. 2011. “A Defined Terminal Region of the E. Coli Chromosome Shows Late Segregation and High Ftsk Activity.” *PLoS ONE* 6(7).

Deng, S., R. A. Stein, and N. P. Higgins. 2005. “Organization of Supercoil Domains and Their Reorganization by Transcription.” *Molecular Microbiology* 57(6):1511–21.

Dillon, S. C. and C. J. Dorman. 2010. “Bacterial Nucleoid-Associated Proteins, Nucleoid Structure and Gene Expression.” *Nature reviews. Microbiology* 8(3):185–95.

Ebersbach, G. and K. Gerdes. 2004. “Bacterial Mitosis: Partitioning Protein ParA Oscillates in Spiral-Shaped Structures and Positions Plasmids at Mid-Cell.” *Molecular Microbiology* 52(2):385–98.

Egan, A. J. F. and W. Vollmer. 2013. “The Physiology of Bacterial Cell Division.” *Annals of the New York Academy of Sciences* 1277(1):8–28.

Erickson, H. P., D. W. Taylor, K. A. Taylor, and D. Bramhill. 1996. “Bacterial Cell Division Protein FtsZ Assembles into Protofilament Sheets and Minirings, Structural Homologs of Tubulin Polymers.”

Erickson, H. P. 1995. “FtsZ, a Prokaryotic Homolog of Tubulin?” *Cell* 80(3).

Erickson, H. P. 1997. “FtsZ, a Tubulin Homologue in Prokaryote Cell Division.” *Trends in Cell Biology* 7(9):362–67.

Espéli, O., et al. 2012. “A MatP-Divisome Interaction Coordinates Chromosome Segregation with Cell Division in E. Coli.” *The EMBO journal* 31(14):3198–3211.

Espeli, O., R. Mercier and F. Boccard. 2008. “DNA Dynamics Vary according to Macrodomain Topography in the E. Coli Chromosome.” *Molecular Microbiology* 68(6):1418–27.

Fekete, R. A., and D. K. Chattoraj. 2005. “A Cis-Acting Sequence Involved in Chromosome Segregation in Escherichia Coli.” *Molecular Microbiology* 55(1):175–83.

Fisher, J. K., et al. 2013. “Four-Dimensional Imaging of *E. Coli* Nucleoid Organization and Dynamics in Living Cells.” *Cell* 153(4):882–95.

Fogel, M.A., and M.K. Waldor. 2006. “A Dynamic, Mitotic-like Mechanism for Bacterial Chromosome Segregation.” *Genes and Development* 20(23):3269–82.

Fu, Guo, et al. 2010. “In Vivo Structure of the E. Coli FtsZ-Ring Revealed by Photoactivated Localization Microscopy (PALM).” *PLoS ONE* 5(9):1–16.

Funnell, B.E. 2016. “ParB Partition Proteins: Complex Formation and Spreading at Bacterial and Plasmid Centromeres.” *Frontiers in molecular biosciences* 3:44.

Le Gall, A., et al. 2016. “Bacterial Partition Complexes Segregate within the Volume of the Nucleoid.” *Nature Communications* in press(May):1–10.

Ghosal, D., D. Trambaiolo, L. A. Amos, and J. Lowe. 2014. “MinCD Cell Division Proteins Form Alternating Copolymeric Cytomotive Filaments.” *Nat Commun* 5:5341.

Greenfield, N. J. 2007. “Using Circular Dichroism Spectra to Estimate Protein Secondary Structure.” *Nat Protoc.* 1(6):2876–90.

Guzman, L. M., D. Belin, M. J. Carson, and J. Beckwith. 1995. “Tight Regulation, Modulation, and High-Level Expression by Vectors Containing the Arabinose P(BAD) Promoter.” *Journal of Bacteriology* 177(14):4121–30.

H. I. Adler, W. D. Fisher and A. Cohen and A. Hardigree. 1967. “MINIATURE Escherichia Coli CELLS DEFICIENT IN DNA.” *Proceedings of the National Academy of Sciences of the United States of America* 57(2):321.

Han, J. S., S. K. Sung, H. Kim, M. J. Ko, and D. S. Hwang. 2004. “Binding of SeqA Protein to Hemi-Methylated GATC Sequences Enhances Their Interaction and Aggregation Properties.” *Journal of Biological Chemistry* 279(29):30236–43.

Hayashi, I., T. Oyama, and K. Morikawa. 2001. “Structural and Functional Studies of MinD ATPase: Implications for the Molecular Recognition of the Bacterial Cell Division Apparatus.” *Embo J* 20(8):1819–1828.

Hayes, F. and D. Barillà. 2006. “The Bacterial Segrosome: A Dynamic Nucleoprotein Machine for DNA Trafficking and Segregation.” *Nature reviews. Microbiology* 4(2):133–43.

Helgesen, E. S. Fossum-Raunehaug, F. Sætre, K. O. Schink, and K. Skarstad. 2015. “Dynamic Escherichia Coli SeqA Complexes Organize the Newly Replicated DNA at a Considerable Distance from the Replisome.” *Nucleic Acids Research* 43(5):2730–43.

Helgesen, E., S. Fossum-Raunehaug, and K. Skarstad. 2016. “Lack of the H-NS Protein Results in Extended and Aberrantly Positioned DNA during Chromosome Replication and Segregation in Escherichia Coli.” *Journal of Bacteriology* 198(8):1305–16.

Hester, C. M. and J. Lutkenhaus. 2007. “Soj (ParA) DNA Binding Is Mediated by Conserved Arginines and Is Essential for Plasmid Segregation.” *Proceedings of the National Academy of Sciences of the United States of America* 104(51):20326–31.

Hiraga, S. et al. 1991. “Mutants Defective in Chromosome Partitioning in E. Coli.” *Research in Microbiology* 142(2–3):189–94.

Hiraga, S. 2000. “Dynamic Localization of Bacterial and Plasmid Chromosomes.” *Annual review of genetics* 34:21–59.

Hirano, Tatsuya. 2006. “At the Heart of the Chromosome: SMC Proteins in Action.” *Nature Reviews Molecular Cell Biology* 7(5):311–22.

Hsieh, C. W. et al. 2010. “Direct MinE-Membrane Interaction Contributes to the Proper Localization of MinDE in E. Coli.” *Molecular Microbiology* 75(2):499–512.

Hu, Z., E. P. Gogol, and J. Lutkenhaus. 2002. “Dynamic Assembly of MinD on Phospholipid Vesicles Regulated by ATP and MinE.” *Proc Natl Acad Sci U S A* 99(10):6761–66.

Hu, Z. and J. Lutkenhaus. 2000. “Analysis of MinC Reveals Two Independent Domains Involved in Interaction with MinD and FtsZ.” *J Bacteriol* 182(14):3965–71.

Hu, Z. and J. Lutkenhaus. 2003. “A Conserved Sequence at the C-Terminus of MinD Is Required for Binding to the Membrane and Targeting MinC to the Septum.” *Mol Microbiol* 47(2):345–55.

Hu, Z., A. Mukherjee, S. Pichoff, and J. Lutkenhaus. 1999. “The MinC Component of the Division Site Selection System in Escherichia Coli Interacts with FtsZ to Prevent Polymerization.” *Proceedings of the National Academy of Sciences of the United States of America* 96(26):14819–24.

Hu, Z., E. P. Gogol, and J. Lutkenhaus. 2002. “Dynamic Assembly of MinD on Phospholipid Vesicles Regulated by ATP and MinE.” *Proceedings of the National Academy of Sciences of the United States of America* 99(10):6761–66.

Hu, Z., and J. Lutkenhaus. 1999. “Topological Regulation of Cell Division in Escherichia Coli Involves Rapid Pole to Pole Oscillation of the Division Inhibitor MinC under the Control of MinD and MinE.” *Molecular Microbiology* 34(1):82–90.

Hu, Z., and J. Lutkenhaus. 2000. “Analysis of MinC Reveals Two Independent Domains Involved in Interaction with MinD and FtsZ.” *Journal of Bacteriology* 182(14):3965–71.

Hu, Z., and J. Lutkenhaus. 2001. “Topological Regulation of Cell Division in E. Coli: Spatiotemporal Oscillation of MinD Requires Stimulation of Its ATPase by MinE and Phospholipid.” *Molecular Cell* 7(6):1337–43.

Hu, Z., and J. Lutkenhaus. 2003. “A Conserved Sequence at the C-Terminus of MinD Is Required for Binding to the Membrane and Targeting MinC to the Septum.” *Molecular Microbiology* 47(2):345–55.

Hu, Z., C. Saez, and J. Lutkenhaus. 2003. “Recruitment of MinC, an Inhibitor of Z-Ring Formation, to the Membrane in Escherichia Coli: Role of minD and minE.” *Journal of Bacteriology* 185(1):196–203.

Iniesta, A. A. 2014. “ParABS System in Chromosome Partitioning in the Bacterium Myxococcus Xanthus.” *PLoS ONE* 9(1).

Ishikawa, S. et al. 2007. “Distribution of Stable DnaA-Binding Sites on the Bacillus Subtilis Genome Detected Using a Modified ChIP-Chip Method.” *DNA Research* 14(4):155–68.

Jerabek-Willemsen, M. et al. 2014. “MicroScale Thermophoresis: Interaction Analysis and beyond.” *Journal of Molecular Structure* 1077:101–13.

Joshi, M. C. et al. 2011. “Escherichia Coli Sister Chromosome Separation Includes an Abrupt Global Transition with Concomitant Release of Late-Splitting Intersister Snaps.” *Proceedings of the*

National Academy of Sciences of the United States of America 108(7):2765–70.

Jun, S. and B. Mulder. 2006. "Entropy-Driven Spatial Organization of Highly Confined Polymers: Lessons for the Bacterial Chromosome." *Proceedings of the National Academy of Sciences of the United States of America* 103(33):12388–93.

Jun, S. and A. Wright. 2010. "Entropy as the Driver of Chromosome Segregation." *Nature Reviews Microbiology* 8(8):600–607.

Kahramanoglou, C. et al. 2011. "Direct and Indirect Effects of H-NS and Fis on Global Gene Expression Control in Escherichia Coli." *Nucleic Acids Res* 39(6):2073–91.

Kang, S., H. Lee, J. S. Han, and D. S. Hwang. 1999. "Interaction of SeqA and Dam Methylase on the Hemimethylated Origin of Escherichia Coli Chromosomal DNA Replication." *Journal of Biological Chemistry* 274(17):11463–68.

Kar, S., R. Edgar, and S. Adhya. 2005. "Nucleoid Remodeling by an Altered HU Protein: Reorganization of the Transcription Program." *Proceedings of the National Academy of Sciences of the United States of America* 102(45):16397–402.

Kavenoff, R. and O. A. Ryder. 1976. "Electron Microscopy of Membrane-Associated Folded Chromosomes of Escherichia Coli." *Chromosoma* 55(1):13–25.

Kleckner, N., et al. 2004. "A Mechanical Basis for Chromosome Function." *Proceedings of the National Academy of Sciences of the United States of America* 101(34):12592–97.

Kloosterman, T. G. et al. 2016. "Complex Polar Machinery Required for Proper Chromosome Segregation in Vegetative and Sporulating Cells of Bacillus Subtilis." *Molecular Microbiology* 101(2):333–50.

Kornberg, R. D. 1974. "Chromatin Structure: A Repeating Unit of Histones and DNA." *Science (New York, N.Y.)* 184(139):868–71.

Koster, D. A., A Crut, S. Shuman, M. A. Bjornsti, and N. Dekker. 2010. "Cellular Strategies for Regulating DNA Supercoiling: A Single-Molecule Perspective." *Cell* 142(4):519–30.

Kruse, K., M. Howard, and W.Margolin. 2007. "An Experimentalist's Guide to Computational Modelling of the Min System." *Molecular Microbiology* 63(5):1279–84.

Kuwada, N. J., K. C. Cheveralls, B. Traxler, and P. A. Wiggins. 2013. "Mapping the Driving Forces of Chromosome Structure and Segregation in Escherichia Coli." *Nucleic Acids Research* 41(15):7370–77.

Labie, C., F. Bouche, and J. P. Bouche. 1990. "Minicell-Forming Mutants of Escherichia Coli: Suppresion of Both DicB- and minD-Dependent Division Inhibition by Inactivation of the minC Gene Product." *Journal of Bacteriology* 172(10):5852–55.

Lackner, L. L., D. M. Raskin, and P. A. J. De Boer. 2003. "ATP-Dependent Interactions between Escherichia Coli Min Proteins and the Phospholipid Membrane in Vitro." *Journal of Bacteriology* 185(3):735–49.

Lee, P. S. and A. D. Grossman. 2006. "The Chromosome Partitioning Proteins Soj (ParA) and Spo0J (ParB) Contribute to Accurate Chromosome Partitioning, Separation of Replicated Sister Origins, and Regulation of Replication Initiation in Bacillus Subtilis." *Molecular Microbiology* 60(4):853–69.

Lee, P. S., D. C. H. Lin, S. Moriya, and A. D. Grossman. 2003. “Effects of the Chromosome Partitioning Protein Spo0J (ParB) on oriC Positioning and Replication Initiation in Bacillus Subtilis.” *Journal of Bacteriology* 185(4):1326–37.

Leonard, T. A., P. J. Butler, and J. Lowe. 2005. “Bacterial Chromosome Segregation: Structure and DNA Binding of the Soj Dimer--a Conserved Biological Switch.” *Embo Journal* 24(2):270–82.

Li,. G. W., D. Burkhardt, C. Gross, and J. S. Weissman. 2014. “Quantifying Absolute Protein Synthesis Rates Reveals Principles Underlying Allocation of Cellular Resources.” *Cell* 157(3):624–35.

Liu, G., G. C. Draper, and W. D. Donachie. 1998. “FtsK Is a Bifunctional Protein Involved in Cell Division and Chromosome Localization in Escherichia Coli.” *Molecular microbiology* 29:893–903.

Liu, L. F. and J. C. Wang. 1987. “Supercoiling of the DNA Template during Transcription.” *Proceedings of the National Academy of Sciences of the United States of America* 84(20):7024–27.

Livny, J., Y. Yamaichi, and M. K. Waldor. 2007. “Distribution of Centromere-like parS Sites in Bacteria: Insights from Comparative Genomics.” *Journal of Bacteriology* 189(23):8693–8703.

Loose, M., E. Fischer-Friedrich, C. Herold, K. Kruse, and P. Schwille. 2011. “Min Protein Patterns Emerge from Rapid Rebinding and Membrane Interaction of MinE.” *Nature structural & molecular biology* 18(5):577–83.

Lu, C., J. Stricker, and H. P. Erickson. 1998. “FtsZ from Escherichia Coli, Azotobacter Vinelandii, and Thermotoga Maritima--Quantitation, GTP Hydrolysis, and Assembly.” *Cell motility and the cytoskeleton* 40(1):71–86.

Lu, M.,J. L. Campbell, E. boye, and N. Kleckner. 1994. “SeqA: A Negative Modulator of Replication Initiation in E. Coli.” *Cell* 77(3):413–26.

Lutkenhaus, J. and M. Sundaramoorthy. 2003. “MinD and Role of the Deviant Walker A Motif, Dimerization and Membrane Binding in Oscillation.” *Mol Microbiol* 48(2):295–303.

Ma, L. Y., G. King, and L. Rothfield. 2003. “Mapping the MinE Site Involved in Interaction with the MinD Division Site Selection Protein of Escherichia Coli.” *Journal of Bacteriology* 185(16):4948–55.

Männik, J., M. W. Bailey, J. C. O´Neill, and J. Männik. 2017. “Kinetics of Large-Scale Chromosomal Movement during Assymmetric Cell Division in Escherichia Coli.” *PLoS Genetics* 13(2).

Männik, J. and M. W. Bailey. 2015. “Spatial Coordination between Chromosomes and Cell Division Proteins in Escherichia Coli.” *Frontiers in Microbiology* 6(MAR).

Mannik, J., DE Castillo, D. Yang, G. Siopsis, and J. Mannik. 2016. “The Role of MatP, ZapA and ZapB in Chromosomal Organization and Dynamics in Escherichia Coli.” *Nucleic Acids Research* 44(3):1216–26.

Marston, A. L., H. B. Thomaides, D. H. Edwards, M. E. Sharpe, and J. Errington. 1998. “Polar Localization of the MinD Protein of Bacillus Subtilis and Its Role in Selection of the Mid-Cell Division Site.” *Genes and Development* 12(21):3419–30.

Massé, E., and M. Drolet. 1999. “Relaxation of Transcription-Induced Negative Supercoiling Is an Essential Function of Escherichia Coli DNA Topoisomerase I.” *Journal of Biological Chemistry* 274(23):16654–58.

Mazor, S. et al. 2008. “Mutual Effects of MinD-Membrane Interaction: I. Changes in the Membrane Properties Induced by MinD Binding.” *Biochim Biophys Acta* 1778(11):2496–2504.

Mercier, R. et al. 2008. “The MatP/matS Site-Specific System Organizes the Terminus Region of the E. Coli Chromosome into a Macrodomain.” *Cell* 135(3):475–85.

Messerschmidt, J. S. and T. Waldminghaus. 2014. “Dynamic Organization: Chromosome Domains in Escherichia Coli.” *Journal of Molecular Microbiology and Biotechnology* 24(5–6):301–15.

Mohammadi, T. et al. 2009. “The GTPase Activity of Escherichia Coli FtsZ Determines the Magnitude of the FtsZ Polymer Bundling by ZapA in Vitro.” *Biochemistry* 48(46):11056–66.

Nicolas, E. et al. 2014. “The SMC Complex MukBEF Recruits Topoisomerase IV to the Origin of Replication Region in Live Escherichia Coli.” *mBio* 5(1).

Nielsen, H. J., J. R. Ottesen, B. Youngren, S. J. Austin, and F. G. Hansen. 2006. “The Escherichia Coli Chromosome Is Organized with the Left and Right Chromosome Arms in Separate Cell Halves.” *Molecular Microbiology* 62(2):331–38.

Niki, H., A. Jaffe, R. Imamura, T. Ogura, and S. Hiraga. 1991. “The New Gene mukB Codes for a 177 Kd Protein with Coiled-Coil Domains Involved in Chromosome Partitioning of E. Coli.” *The EMBO Journal* 10(1):183–93.

Niki, H., Y. Yamaichi, and S. Hiraga. 2000. “Dynamic Organization of Chromosomal DNA in Escherichia Coli.” *Genes and Development* 14(2):212–23.

Nolivos, S. et al. 2016. “MatP Regulates the Coordinated Action of Topoisomerase IV and MukBEF in Chromosome Segregation.” *Nature communications* 7:10466.

Odijk, T. 1998. “Osmotic Compaction of Supercoiled DNA into a Bacterial Nucleoid.” *Biophysical Chemistry* 73(1–2):23–29.

Okuno, T., M. Ogoh, H. Tanina, N. Funasaki, and K. Kogure. 2009. “Direct Monitoring of Interaction between Escherichia Coli Proteins, MinC and Monomeric FtsZ, in Solution.” *Biological & pharmaceutical bulletin* 32(8):1473–75.

Opel, M. L., et al. 2004. “Activation of Transcription Initiation from a Stable RNA Promoter by a Fis Protein-Mediated DNA Structural Transmission Mechanism.” *Molecular Microbiology* 53(2):665–74.

Ortiz, C., P. Natale, L. Cueto, and M. Vicente. 2015. “The Keepers of the Ring: Regulators of FtsZ Assembly.” *FEMS Microbiology Reviews* 40(1):57–67.

Park, K. T., W. Wu, S. Lovell, and J. Lutkenhaus. 2012. “Mechanism of the Asymmetric Activation of the MinD ATPase by MinE.” *Mol Microbiol* 85(2):271–81.

Park, K. T., et al. 2011. “The Min Oscillator Uses MinD-Dependent Conformational Changes in MinE to Spatially Regulate Cytokinesis.” *Cell* 146(3):396–407.

Park, K. T., S. Du, and J. Lutkenhaus. 2015. “MinC/MinD Copolymers Are Not Required for Min Function.” *Molecular Microbiology* 98(5):895–909.

Patrick, J. E. and D. B. Kearns. 2008. “MinJ (YvjD) Is a Topological Determinant of Cell Division in Bacillus Subtilis.” *Molecular Microbiology* 70(5):1166–79.

Pazos, M. et al. 2014. “FtsZ Placement in Nucleoid-Free Bacteria.” *PLoS One* 9(3):e91984.

De Pereda, J. M., D. Leynadier, J. A. Evangelio, P. Chacón, and J. M. Andreu. 1996. “Tubulin Secondary Structure Analysis, Limited Proteolysis Sites, and Homology to FtsZ.” *Biochemistry* 35(45):14203–15.

Petrushenko, Z. M., Y. Cui, W. She, and V. V. Rybenkov. 2010. “Mechanics of DNA Bridging by Bacterial Condensin MukBEF in Vitro and in Singulo.” *The EMBO journal* 29(6):1126–35.

Petrushenko, Zoya M., Chien Hung Lai, and Valentin V. Rybenkov. 2006. “Antagonistic Interactions of Kleisins and DNA with Bacterial Condensin MukB.” *Journal of Biological Chemistry* 281(45):34208–17.

Pichoff, S., B. Vollrath, C. Touriol, and J.P Bouché. 1995. “Deletion Analysis of Gene minE Which Encodes the Topological Specificity Factor of Cell Division in Escherichia Coli.” *Molecular Microbiology* 18(2):321–29.

Plumbridge, J. 2001. “DNA Binding Sites for the Mlc and NagC Proteins: Regulation of nagE, Encoding the N-Acetylglucosamine-Specific Transporter in Escherichia Coli.” *Nucleic acids research* 29(2):506–14.

Postow, L., C. D. Hardy, J. Arsuaga, and N. R. Cozzarelli. 2004. “Topological Domain Structure of the Escherichia Coli Chromosome.” *Genes & development* 18(14):1766–79.

Prieto, Ana I. et al. 2012. “Genomic Analysis of DNA Binding and Gene Regulation by Homologous Nucleoid-Associated Proteins IHF and HU in Escherichia Coli K12.” *Nucleic Acids Research* 40(8):3524–37.

Ptacin, J. L. et al. 2010. “A Spindle-like Apparatus Guides Bacterial Chromosome Segregation.” *Nature cell biology* 12(8):791–98.

Quisel, J., D. Lin, and A. Grossman. 1999. “Control of Development by Altered Localization of a Transcription Factor in B. Subtilis.” *Mol Cell* 4(5):665–72.

R Core Team. 2014. “R: A Language and Environment for Statistical Computing.” *R Foundation for Statistical Computing* {ISBN} 3-900051-07-0, http://www.R-project.org.

Raskin, D. M. and P. A. de Boer. 1999. “Rapid Pole-to-Pole Oscillation of a Protein Required for Directing Division to the Middle of Escherichia Coli.” *Proceedings of the National Academy of Sciences of the United States of America* 96(9):4971–76.

Raskin, D. M. and P. a de Boer. 1997. “The MinE Ring: An FtsZ-Independent Cell Structure Required for Selection of the Correct Division Site in E. Coli.” *Cell* 91(5):685–94.

Raskin, David M. and Piet a J. De Boer. 1999. “MinDE-Dependent Pole-to-Pole Oscillation of Division Inhibitor MinC in Escherichia Coli.” *Journal Of Bacteriology* 181(20):6419–24.

Renner, L. D. and D. B. Weibel. 2012. “MinD and MinE Interact with Anionic Phospholipids and Regulate Division Plane Formation in Escherichia Coli.” *J Biol Chem* 287(46):38835–44.

Rico, A. I., M. Krupka, and M. Vicente. 2013. “In the Beginning, Escherichia Coli Assembled the Proto-Ring: An Initial Phase of Division.” *Journal of Biological Chemistry* 288(29):20830–36.

Rivas, G. et al. 2000. “Magnesium-Induced Linear Self-Association of the FtsZ Bacterial Cell Division Protein Monomer. The Primary Steps for FtsZ Assembly.” *Journal of Biological Chemistry* 275(16):11740–49.

Rothfield, L., A. Taghbalout, and Yu-Ling Shih. 2005. “Spatial Control of Bacterial Division-Site Placement.” *Nature reviews. Microbiology* 3(12):959–68.

Rybenkov, V. V., V. Herrera, Z. M. Petrushenko, and H. Zhao. 2014. “MukBEF, a Chromosomal Organizer.” *Journal of Molecular Microbiology and Biotechnology* 24(5–6):371–83.

Saint-Dic, Djenann, Brian P. Frushour, Jason H. Kehrl, and Lyn Sue Kahng. 2006. “A parA Homolog Selectively Influences Positioning of the Large Chromosome Origin in Vibrio Cholerae.” *Journal of Bacteriology* 188(15):5626–31.

Sánchez-Romero, María Antonia et al. 2010. “Dynamic Distribution of SeqA Protein across the Chromosome of Escherichia Coli K-12.” *mBio* 1(1).

Sawitzke, J. a and S. Austin. 2000. “Suppression of Chromosome Segregation Defects of Escherichia Coli Muk Mutants by Mutations in Topoisomerase I.” *Proceedings of the National Academy of Sciences of the United States of America* 97(4):1671–76.

Schumacher, M. A. and B. E. Funnell. 2005. “Structures of ParB Bound to DNA Reveal Mechanism of Partition Complex Formation.” *Nature* 438(7067):516–19.

She, W., E. Mordukhova, H. Zhao, Z. M. Petrushenko, and V. V. Rybenkov. 2013. “Mutational Analysis of MukE Reveals Its Role in Focal Subcellular Localization of MukBEF.” *Molecular Microbiology* 87(3):539–52.

She, W., Q. Wang, E. A. Mordukhova, and V. V. Rybenkov. 2007. “MukEF Is Required for Stable Association of MukB with the Chromosome.” *Journal of Bacteriology* 189(19):7062–68.

Shen, B. and J. Lutkenhaus. 2009. “The Conserved C-Terminal Tail of FtsZ Is Required for the Septal Localization and Division Inhibitory Activity of MinCC/MinD.” *Molecular Microbiology* 72(2):410–24.

Shen, B. and Joe Lutkenhaus. 2010. “Examination of the Interaction between FtsZ and MinCN in E. Coli Suggests How MinC Disrupts Z Rings.” *Molecular Microbiology* 75(5):1285–98.

Shiomi, D. and W. Margolin. 2007. “The C-Terminal Domain of MinC Inhibits Assembly of the Z Ring in Escherichia Coli.” *J Bacteriol* 189(1):236–43.

Sinden, R. R. and D. E. Pettijohn. 1981. “Chromosomes in Living Escherichia Coli Cells Are Segregated into Domains of Supercoiling.” *Proceedings of the National Academy of Sciences of the United States of America* 78(1):224–28.

Spahn, Christoph, Ulrike Endesfelder, and Mike Heilemann. 2014. “Super-Resolution Imaging of Escherichia Coli Nucleoids Reveals Highly Structured and Asymmetric Segregation during Fast Growth.” *Journal of Structural Biology* 185(3):243–49.

Stouf, M., J. C. Meile, and F. Cornet. 2013. “FtsK Actively Segregates Sister Chromosomes in Escherichia Coli.” *Proc Natl Acad Sci U S A* 110(27):11157–62.

Stricker, Jesse, Paul Maddox, E. D. Salmon, and Harold P. Erickson. 2002. “Rapid Assembly Dynamics of the Escherichia Coli FtsZ-Ring Demonstrated by Fluorescence Recovery after Photobleaching.” *Proceedings of the National Academy of Sciences of the United States of America* 99(5):3171–75.

Suefuji, Kyoko, Regina Valluzzi, and Debabrata RayChaudhuri. 2002. “Dynamic Assembly of MinD into Filament Bundles Modulated by ATP, Phospholipids, and MinE.” *Proceedings Of The*

National Academy Of Sciences Of The United States Of America 99(26):16776–81.

Szardenings, Florian, David Guymer, and Kenn Gerdes. 2011. "ParA ATPases Can Move and Position DNA and Subcellular Structures." *Current Opinion in Microbiology* 14(6):712–18.

Szeto, T. H., S. L. Rowland, and G. F. King. 2001. "The Dimerization Function of MinC Resides in a Structurally Autonomous C-Terminal Domain." *Journal of Bacteriology* 183(22):6684–87.

Szeto, Tim H., Susan L. Rowland, Cheryl L. Habrukowich, and Glenn F. King. 2003. "The MinD Membrane Targeting Sequence Is a Transplantable Lipid-Binding Helix." *Journal of Biological Chemistry* 278(41):40050–56.

Taghbalout, Aziz, Luyan Ma, and Lawrence Rothfield. 2006. "Role of MinD-Membrane Association in Min Protein Interactions." *Journal of Bacteriology* 188(8):2993–3001.

Talukder, AliAzam and Akira Ishihama. 2015. "Growth Phase Dependent Changes in the Structure and Protein Composition of Nucleoid in Escherichia Coli." *Science China. Life sciences* 58(9):902–11.

Thiel, Axel, Michèle Valens, Isabelle Vallet-Gely, Olivier Espéli, and Frédéric Boccard. 2012. "Long-Range Chromosome Organization in E. Coli: A Site-Specific System Isolates the Ter Macrodomain." *PLoS Genetics* 8(4).

Tonthat, Nam Ky et al. 2011. "Molecular Mechanism by Which the Nucleoid Occlusion Factor, SlmA, Keeps Cytokinesis in Check." *The EMBO journal* 30(1):154–64.

Tusher, V. G., R. Tibshirani, and G. Chu. 2001. "Significance Analysis of Microarrays Applied to the Ionizing Radiation Response." *Proceedings of the National Academy of Sciences of the United States of America* 98(9):5116–21.

Valens, M., S. Penaud, M. Rossignol, F. Cornet, and F. Boccard. 2004. "Macrodomain Organization of the Escherichia Coli Chromosome." *The EMBO journal* 23(21):4330–41.

Valens, M., A. Thiel, and F. Broccard. 2016. "The MaoP/maoS Site-Specific System Organizes the Ori Region of the E. Coli Chromosome into a Macrodomain." *PLoS Genetics* 12(9).

Vecchiarelli, A. G., K. Mizuuchi, and B. E. Funnell. 2012. "Surfing Biological Surfaces: Exploiting the Nucleoid for Partition and Transport in Bacteria." *Molecular Microbiology* 86(3):513–23.

Di Ventura, B. et al. 2013. "Chromosome Segregation by the Escherichia Coli Min System." *Molecular Systems Biology* 9(1):686–686.

Di Ventura, B., and V. Sourjik. 2011. "Self-Organized Partitioning of Dynamically Localized Proteins in Bacterial Cell Division." *Molecular systems biology* 7(457):457.

Vos, S. M., E. M. Tretter, B. H. Schmidt, and J. M. Berger. 2011. "All Tangled up: How Cells Direct, Manage and Exploit Topoisomerase Function." *Nature reviews. Molecular cell biology* 12(12):827–41.

Waldminghaus, T., C. Weigel, and K. Skarstad. 2012. "Replication Fork Movement and Methylation Govern SeqA Binding to the Escherichia Coli Chromosome." *Nucleic Acids Research* 40(12):5465–76.

Wang, J. D. and P. A. Levin. 2009. "Metabolism, Cell Growth and the Bacterial Cell Cycle." *Nature microbiology reviews* 7(11):822–27.

Wang, J. C. 2002. “Cellular Roles of DNA Topoisomerases: A Molecular Perspective.” *Nature reviews. Molecular cell biology* 3(6):430–40.

Wang, Q., E. A. Mordukhova, A. L. Edwards, and V. V. Rybenkov. 2006. “Chromosome Condensation in the Absence of the Non-SMC Subunits of MukBEF.” *Journal of Bacteriology* 188(12):4431–41.

Wang, W., G. W. Li, C. Chen, X. S. Xie, and X. Zhuang. 2011. “Chromosome Organization by a Nucleoid-Associated Protein in Live Bacteria.” *Science* 333(6048):1445–49.

Wang, X., P. Montero Llopis, and D. Z. Rudner. 2013. “Organization and Segregation of Bacterial Chromosomes.” *Nat Rev Genet* 14(3):191–203.

Wang, X., C. Lesterlin, R. Reyes-Lamothe, G. Ball, and D. J. Sherratt. 2011. “Replication and Segregation of an Escherichia Coli Chromosome with Two Replication Origins.” *Proceedings of the National Academy of Sciences of the United States of America* 108(26):E243-50.

Wang, X., X. Liu, C. Possoz, and D. J. Sherratt. 2006. “The Two Escherichia Coli Chromosome Arms Locate to Separate Cell Halves.” *Genes and Development* 20(13):1727–31.

Wang, X., C. Possoz, and D. J. Sherratt. 2005. “Dancing around the Divisome: Asymmetric Chromosome Segregation in Escherichia Coli.” *Genes and Development* 19(19):2367–77.

Wang, X. and D. Z. Rudner. 2014. “Spatial Organization of Bacterial Chromosomes.” *Current Opinion in Microbiology* 22:66–72.

Wang, X. and D. J. Sherratt. 2010. “Independent Segregation of the Two Arms of the Escherichia Coli Ori Region Requires Neither RNA Synthesis nor MreB Dynamics.” *Journal of Bacteriology* 192(23):6143–53.

Wang, X., J. Huang, A. Mukherjee, C. Cao, and J. Lutkenhaus. 1997. “Analysis of the Interaction of FtsZ with Itself, GTP, and FtsA.” *Journal of Bacteriology* 179(17):5551–59.

Woldringh, C. L., F. G. Hansen, N. O. E. Vischer, and T. Atlung. 2015. “Segregation of Chromosome Arms in Growing and Non-Growing Escherichia Coli Cells.” *Frontiers in Microbiology* 6(MAY).

Wu, W., K. T. Park, T. Holyoak, and J. Lutkenhaus. 2011. “Determination of the Structure of the MinD-ATP Complex Reveals the Orientation of MinD on the Membrane and the Relative Location of the Binding Sites for MinE and MinC.” *Mol Microbiol* 79(6):1515–28.

Yamaichi, Y. and H. Niki. 2004. “migS, a Cis-Acting Site That Affects Bipolar Positioning of oriC on the Escherichia Coli Chromosome.” *Embo Journal* 23(1):221–33.

Youngren, B., H. J. Nielsen, S. Jun, and S. Austin. 2014. “The Multifork Escherichia Coli Chromosome Is a Self-Duplicating and Self-Segregating Thermodynamic Ring Polymer.” *Genes and Development* 28(1):71–84.

Zhang, X. and H. Bremer. 1995. “Control of the Escherichia Coli rrnB P1 Promoter Strength by ppGpp.” *Journal of Biological Chemistry* 270(19):11181–89.

Zhao, C. R., P. a de Boer, and L. I. Rothfield. 1995. “Proper Placement of the Escherichia Coli Division Site Requires Two Functions That Are Associated with Different Domains of the MinE Protein.” *Proceedings of the National Academy of Sciences of the United States of America* 92(10):4313–17.

Zheng, M. et al. 2014. “Self-Assembly of MinE on the Membrane Underlies Formation of the MinE Ring to Sustain Function of the Escherichia Coli Min System.” *Journal of Biological Chemistry* 289(31):21252–66.

Zhou, H. et al. 2005. “Analysis of MinD Mutations Reveals Residues Required for MinE Stimulation of the MinD ATPase and Residues Required for MinC Interaction.” *J Bacteriol* 187(2):629–38. R).

Zhou, H. et al. 2005. “Analysis of MinD Mutations Reveals Residues Required for MinE Stimulation of n the MinD ATPase and Residues Required for MinC Interaction.” *Journal of Bacteriology* 187(2):629–38.

Zhou, H. and J.Lutkenhaus. 2004. “The Switch I and II Regions of MinD Are Required for Binding and Activating MinC.” *Journal of Bacteriology* 186(5):1546–55.

Zhou, H., and J. Lutkenhaus, “ MinC Mutants Deficient in MinD- and DicB-Mediated Cell Division Inhibition due to Loss of Interaction with MinD, DicB, or a Septal Component. ” *J. Bacteriol* 187:2846–2857.